Renewable Energy

Prototype of a novel hybrid concentrator photovoltaic/thermal and solar thermoelectric generator system for outdoor study

--Manuscript Draft--

Manuscript Number:	RENE-D-22-04154R1
Article Type:	Research Paper
Keywords:	Thermoelectric generator; Concentrator photovoltaic/thermal; Hybrid System; Prototype development; experimental analysis; Transient simulation
Corresponding Author:	Chockalingam Aravind Vaithilingam MALAYSIA
First Author:	Sridhar Sripadmanabhan Indira
Order of Authors:	Sridhar Sripadmanabhan Indira
	Chockalingam Aravind Vaithilingam
	Ramsundar Sivasubramanian
	Kok-Keong Chong
	Kulasekharan Narasingamurthi
	Saidur Rahman
Abstract:	In this study, a novel prototype of a hybrid concentrator photovoltaic/thermal and solar thermoelectric generator system has been designed and constructed for combined heat and power production. In the developed hybrid system, both the solar cells and thermoelectric modules that share a common heat transfer medium are exposed to concentrated irradiance via a compound parabolic concentrator and a parabolic trough concentrator, respectively. To assess the performance of the hybrid system, a prototype of the hybrid system was built and tested under outdoor operating conditions, and the findings were compared with those of a transient numerical simulation conducted using ANSYS Fluent. The average PV temperature obtained during the test period at a flow rate of 3.8 L/min is 318.19 K which is ~5.6 % lesser compared with a conventional hybrid CPVT-TEG system. The outdoor trials show maximum electrical efficiency of 4.86 % and thermal efficiency of 40% when the solar irradiance is greater than or equal to 1000 W/m2. The overall power conversion efficiency of the developed prototype is 3 times higher compared to a standalone PV system. The hybrid system helps to reduce carbon emission by 0.5 kg/h, with an associated environmental cost of 0.025 €/h.
Suggested Reviewers:	Tzivanidis Christos Professor, National Technical University of Athens ctzivan@central.ntua.gr
	Lasse Rossendahl Professor, Aalborg University lar@et.aau.dk

Prototype of a novel hybrid concentrator photovoltaic/thermal and solar thermoelectric generator system for outdoor study

Sridhar Sripadmanabhan Indira[1*], Chockalingam Aravind Vaithilingam[1*], Ramsundar Sivasubramanian[1], Kok-Keong Chong[2], Kulasekharan Narasingamurthi[3], R. Saidur [4,5]

[1] School of Engineering, Faculty of Innovation and Technology, Taylor's University Lakeside Campus, No. 1, Jalan Taylor's, 47500 Subang Jaya, Selangor, Malaysia.
[2] Lee Kong Chian Faculty of Engineering and Science, Universiti Tunku Abdul Rahman, Bandar Sungai Long, 43000 Kajang, Selangor, Malaysia.
[3] Metier Technical Leader, Valeo India Private Limited, No. 63, Rajiv Gandhi Salai, Navallur, Chennai – 600130, India.
[4] Research Centre for Nano-Materials and Energy Technology (RCNMET), School of Engineering and Technology, Sunway University, 47500 Subang Jaya, Malaysia.
[5] Department of Engineering, Lancaster University, Lancaster LA1 4YW, UK.

*Corresponding authors.

E-mail addresses: sridharsripadmanabhannadarindira@sd.taylors.edu.my, sibisri819@gmail.com (S. S Indira), chockalingamaravind.vaithilingam@taylors.edu.my, aravindcv@ieee.org (C.A. Vaithilingam).

From 24 September 2022

Dr Chockalingam Aravind Vaithilingam
School of Engineering,
Faculty of Innovation and Technology,
Taylor's University Lakeside Campus,
Jalan Taylor's 47500, Subang Jaya,
Selangor, Malaysia.

To
The Editor-in-Chief
Renewable Energy
Elsevier.

Dear Sir,

We wish to resubmit our revised manuscript entitled "Prototype of a novel hybrid concentrator photovoltaic/thermal and solar thermoelectric generator system for outdoor study" for consideration by the "Renewable Energy" journal (Ref. No.: RENE-D-22-04154). Thank you for the constructive feedback you provided regarding our manuscript.

We appreciate the interest that the editors and reviewers have taken in our manuscript and the constructive criticism. We agree with the reviewers' comments and criticisms, and we have amended the reviewers' primary concerns in the revised manuscript. More specifically, we have compared the performance of the proposed hybrid CPVT-STEG system to that of the standalone PV system. There is also a separate section discussing the challenges and future outlook of the hybrid prototype. A point-by-point response to the reviewer's comments is also attached for your perusal. We are certain that you will find that this most recent version of our manuscript clears up the main issues indicated by the reviewers.

With these changes to our final manuscript, we hereby resubmit our manuscript for a secondary evaluation. Thank you once again for your consideration of our research paper.

Sincerely,
Dr Chockalingam Aravind Vaithilingam

Email id: chockalingamaravind.vaithilingam@taylors.edu.my
Tel: +60 12-354 3891

Response to Reviewer 1 Comments

Comment 1:

The idea of using CPC and PTC for the solar concentration on the PV and TEG is brilliant. The cooling channel was used to cool the temperature of PV and cold side plate of TEG so that the PV and TEG efficiencies can be maintained at the highest point. However, the overall electrical efficiency of the prototype is not so promising, as the result shows the peak electrical efficiency around 4.86%, which is quite low compared to typical PV cells. I understand that the overall electric efficiency was calculated by equation (2). This small efficiency value is caused by the large aperture area of the PTC. Hence, what do you think if a single PV module with the same aperture area is used instead of your prototype? Do you think that the electric efficiency of the current prototype is better than the single PV or CPV systems? It is always good to discuss the advantages of your prototype over typical PV systems.

Response:

This is an interesting and valuable perspective. The purpose of the proposed hybrid system is to maximise power production per unit area by capturing both electrical and thermal energy from solar irradiation. The proposed new structure is intended to adapt the current parabolic trough plants so that in addition to thermal energy, extra electricity may be generated. Since parabolic trough power plants require a larger land area, it would be advantageous to produce more energy on the same area of land. We cannot assert that the hybrid system described can entirely outperform PV or CPV systems. The decision between a standalone PV system and a hybrid concentrator system is determined by the application's unique requirements. If better electrical efficiency is desired, PV or CPV with passive cooling methods are chosen. However, as per the reviewer's suggestion we have included a comparison with standalone PV to describe the advantages of the proposed hybrid system.

(Refer: Section 6.4, Page 36, Line 597 – 620)

A performance comparison between the hybrid CPVT-STEG system and a standalone PV system was performed by considering a 0.51 m^2 mono-crystalline PV module (approx. 32 PV cells) comparable to the aperture area of the hybrid CPVT-STEG prototype. For a 1000 W/m^2 solar irradiance, a standalone PV of 0.51 m^2 area can provide a maximum electric power output of 78.69 W at an efficiency of 15.43% and reach a temperature of 334.4 K (assume: $NOCT = 318.15\ K$; $T_{amb} = 303.15\ K$). On the other hand, the overall power conversion efficiency of the developed hybrid prototype, including electrical and thermal output, is about 4.86% + 40%, which is 3 times higher compared to standalone PV.

The electrical efficiency of the hybrid CPVT-STEG system is 68.5% lower than the standalone PV system. The lower power conversion efficiency of the TEG (3.69%) and the PTC area that is used to focus the sunlight onto the TEG has greatly discounted the overall electrical efficiency of the hybrid system. Nevertheless, the benefits of the hybrid CPVT-STEG system over the standalone PV system are to provide an additional recovery of thermal energy and lower the PV temperature. Besides the direct focused sunlight, the TEG can also harvest the radiative heat from the surrounding environment. The choice between a standalone PV system and a hybrid CPVT-STEG system is determined completely by the specific needs of the application.

A comparison analysis between the developed CPVT-STEG prototype and a similar CPVT-TEG hybrid solar system that uses PTC and mono-crystalline silicon PV cells was performed. The hybrid CPVT-TEG system studied in [22] uses a PTC with a reflectivity 0.89, and the electrical efficiency is estimated as 7.27% if only DNI is considered in the input power. The maximum electrical output of the developed CPVT-STEG prototype can be normalized to 35.5 W at 0.89 reflectivity. The maximum electrical efficiency of the prototype by considering only the DNI (765 W/m^2) in the input is about 9.1% which shows the superiority of the developed CPVT-STEG hybrid system.

Comment 2:

In the experiment study, commercial mono-crystalline PV cells were used. Please mention specifications of the PV cell used including efficiency.

Response:

Thank you for the suggestion. We have included the specification of the commercial mono-crystalline PV cells and TEG module in the revised version of the manuscript.

(Refer: Table 1-3, Page 9-10).

Table 1. Geometrical parameters of different components in the hybrid CPVT-STEG prototype [26].

Components	Width, mm	Length, mm	Thickness, mm
		PV panel	
Glass layer	130	540	5
EVA layer	130	540	0.5
Silicon wafer	125	540	0.2
Thermal pad	130	540	0.5
		TEG module	
Graphite layer	30	30	0.13
Ceramic layer	30	30	0.8
Copper strips	1.08	2.7	0.15
P-N legs	1.08	1.08	1.5
Aluminium absorber clamp	30	540	2
		Rectangular Channel	
Fluid domain	124	540	30
Wall thickness	-	-	3
Full channel	130	540	36

Table 2. The characteristics of the PV module in the hybrid CPVT-STEG prototype [26].

Parameters	Value
Optical parameters	
Absorptivity of glass	0.018
Transmissivity of glass	0.92
Emissivity of glass	0.85
Absorptivity of EVA	0.08
Emissivity of EVA	0.9
Transmissivity of EVA	0.9
Absorptivity of silicon wafer	0.9
Absorptivity of thermal pad	0.5
Thermal parameters	
Thermal conductivity of glass	2 W/m.K
Thermal conductivity of EVA	0.35 W/m.K
Thermal conductivity of silicon wafer	148 W/m.K
Thermal conductivity of thermal pad	2.8 W/m.K
Electrical parameters	
No. of PV cells connected in series (mono-Si)	4 cells (125 mm x 125 mm each)
Open circuit voltage of a cell	0.635 V
Short circuit current of a cell	5.744 A
Maximum voltage of a cell	0.530 V
Maximum current of a cell	5.401 A
PV efficiency at STC	18.6 %
Temperature coefficient of power	-0.47 % / °C

Table 3. The characteristics of the TEG module in the hybrid CPVT-STEG prototype [26].

Parameters	Value
Pairs of PN legs	126
Max. TEG hot side temperature limit	613.15 K
Max. TEG cold side temperature limit	463.15 K
Thermal conductivity of graphite	10 W/m.K
Thermal conductivity of ceramic	18 W/m.K
Seebeck coefficient of p leg	$\alpha_p(T)$ = -8.105 x 10^{-14} T^3 -1.45838 x 10^{-9} T^2 + 9.2444677 x 10^{-7} T + 7.417 x 10^{-5}
Seebeck coefficient of n leg	$\alpha_n(T)$ = 1.7324623 x 10^{-13} T^3 – 1.147783 x 10^{-9} T^2 + 5.90568332 x 10^{-7} T + 1.4392165 x 10^{-4}
Electrical resistivity of p leg	$\rho_p(T)$ = 6.21731 x 10^{-15} T^4 – 1.085722 x 10^{-11} T^3 + 6.857354 x 10^{-9} T^2 – 1.797597 x 10^{-6} T + 1.73549 x 10^{-4}
Electrical resistivity of n leg	$\rho_n(T)$ = 1.18538 x 10^{-15} T^4 - 2.301947 x 10^{-12} T^3 + 1.5708605 x 10^{-9} T^2 – 4.125723 x 10^{-7} T + 4.42835937 x 10^{-5}
Thermal conductivity of p leg	$k_p(T)$ = - 6.0097596 x 10^{-8} T^3 + 9.0134323 x 10^{-5} T^2 - 3.7380241 x 10^{-2} T + 6.1921321
Thermal conductivity of n leg	$k_n(T)$ = - 3.38062 x 10^{-8} T^3 + 6.22422 x 10^{-5} T^2 - 2.95477835 x 10^{-2} T + 5.7041796
Figure of merit of p leg	$ZT_p(T)$ = -1.68766 x 10^{-8} T^3 + 3.2614 x 10^{-5} T^2 - 2.2459 x 10^{-2} T + 5.424505
Figure of merit of n leg	$ZT_n(T)$ = 2.85296 x 10^{-8} T^{-3} - 3.5168 x 10^{-5} T^2 + 1.0560 x 10^{-2} T + 0.3213
Thermal conductivity of Copper strips	385 W/m.K
Thermal conductivity of Aluminium	202.4 W/m.K
Absorptivity of aluminium absorber clamp	0.9
Emissivity of aluminium absorber clamp	0.15

Comment 3:

1:30 hours of experiment testing in a single day is not enough. Although the result quality is good, more results are needed for the validation. The authors included the repeatability test results, but no comparison with the simulation. It is good to conduct multiple experimental tests for several extreme cases (such as various ambient conditions, solar positions or incident angles, etc.).

Response:

Thank you for the suggestion. You have raised an important point regarding the experiment duration. The outdoor experimental duration in the present study is limited due to the copious and frequent rainfall in the test location. The current research is constrained in its ability to conduct extensive outdoor experiments since neither the prototype nor the data acquisition system employed were designed to withstand the rigours of wet conditions. However, we have managed to capture the transient effects of varying ambient conditions (ambient temperature, wind speed, solar irradiance) on the performance of the developed prototype during these 1 hour and 30 minutes periods. The concentrator solar systems are feasible only in regions with high direct normal irradiance; hence, the period between 11.15 am and 12.45 pm was preferred in the current study for peak solar irradiance. In addition, since the prototype is designed to track the sun's position in dual axis, the solar concentrators and PV module are facing the sun all the time, and hence the effect of different incident angles does not exist. However, the future scope of the current investigation using a large-scale prototype can be extended to include long-term effects under extreme conditions such as the soiling effect and durability. In the present investigation, the transient experimental results are conducted to verify the numerical simulation results, and it is found that they validate each other well. Hence, for the repeatability test, only the experimental results are considered.

(Refer: Section 6.6, Page 37)

In order to ensure the performance repeatability of the developed prototype, the experiments have been repeated five times on different days during the noon time with good DNI and GHI values.

Comment 4:

In Figure 9, what is the specific acceptable agreement range for experiment and simulation validation? Since it is a conditional box, I am assuming that the authors have set a certain range of agreements to complete or redo the test.

Response:

Thank you for highlighting this issue. The specific acceptable agreement range for experiment and simulation validation is $\leq$ 10%. We have included the correction in the Figure 9 in the updated version of the manuscript.

(Refer: Figure 9, Page 19)

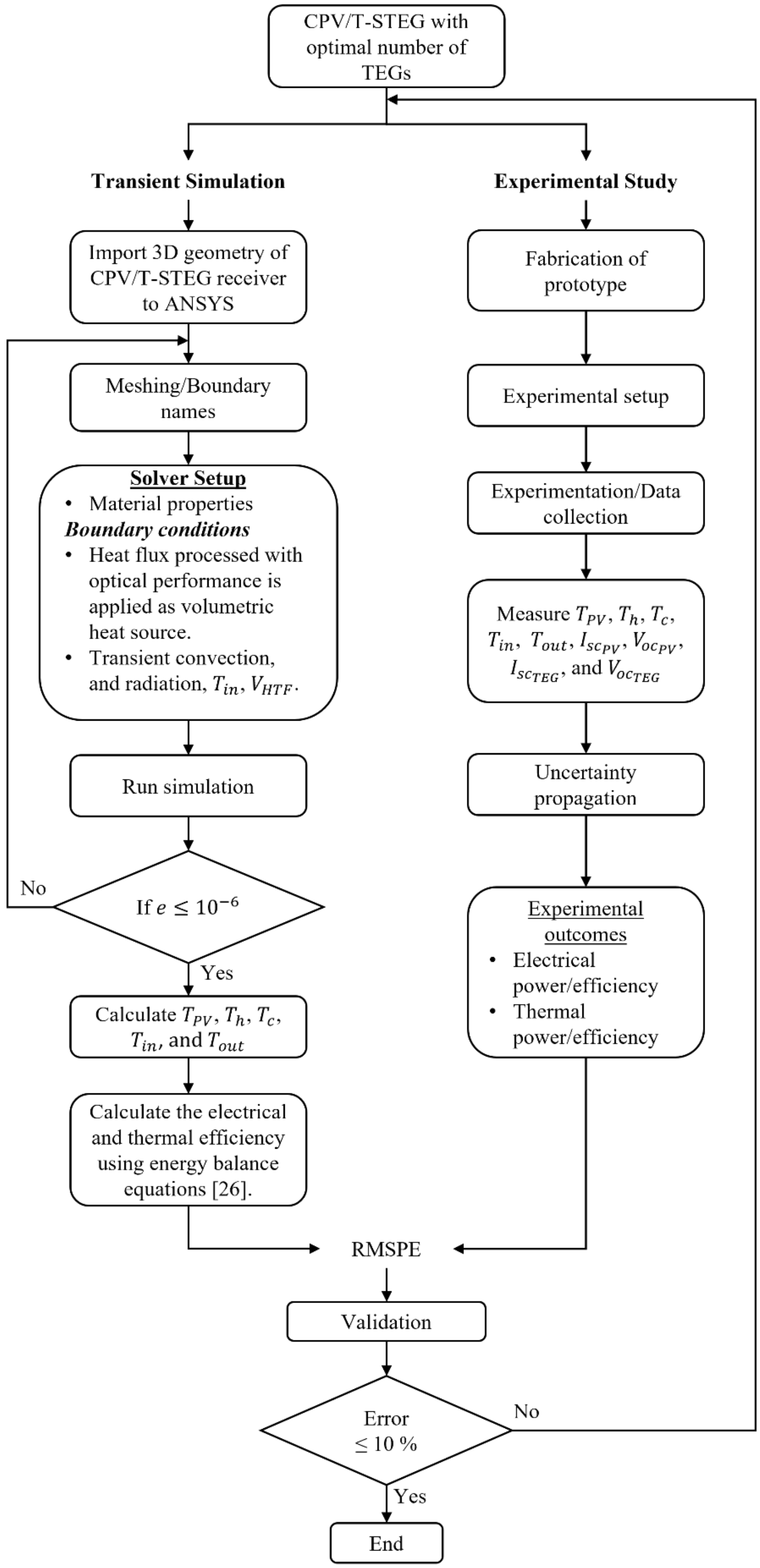

Figure 1. Flowchart of transient numerical simulation and experimental study

Comment 5:

For the validation analysis, equation (12), the definition is confusing. Which is correct? Should the simulation results be used to verify the experimental results, or should the experimental results be used to verify the simulation results?

Response:

We agree with your comment that the definition is not sufficiently clear. The experimental results were used to validate the transient numerical simulation results. We have revised the definition in the manuscript. We hope that the updated version solves the issue.

(Refer: Section 5.6, Page 23, Line 417 - 418)

To identify the percentage error between the simulation results (x_i) and the experimental results (y_i), the root mean square percentage error (RMSPE) method is applied as follows [35]:

$$RMSPE = \sqrt{\frac{\sum_{i=1}^{N}\left(\left[\frac{y_i - x_i}{x_i}\right]\right)^2}{N}} \times 100 \tag{12}$$

Comment 6:

The authors should explain the reasons for the discrepancies between experiments and simulations, especially the PV and TEG temperature results. More discussion of comparison errors should be included.

Response:

Thank you for the suggestion. We have included the reasons for the discrepancies between the experiment and simulation results in the revised manuscript.

(Refer: Page 27, Line 472 – 474)

The experimental PV temperature is found to be greater than the simulation findings mostly owing to the thermal contact resistance existed between the fluid channel and the PV module, which is caused by the manufacturing faults.

(Refer: Page 31, Line 533 – 538)

The thermal contact resistance generated by the presence of thermocouples in both between the TEG cold side and fluid channel, as well as between the TEG hot side and absorber clamp accounts for the differences between the experimental and simulated TEG temperatures. The optical losses caused by misalignment of the PTC can result in a lower temperature of TEG hot side in the measured results as compared to that of simulation results.

Response to Reviewer 2 Comments

Comment 1:

Do not describe the reference by the lumped manner in the Introduction section.

Response:

Thank you for highlighting this issue. It has been rectified in the revised version of the manuscript.

Comment 2:

In the first paragraph of the Introduction section, it is suggested the CPVT-TEG technology should be introduced as the standpoint of performance enhancement instead of lowering the PV cell temperature, since the PV cell temperature is the CPVT module is relatively high.

Response:

Thank you for the suggestion. For clarification, we didn’t mean to introduce the CPVT-TEG technology as lowering the PV cell temperature. Instead, the main objective of CPVT-TEG technology is to improve the overall power generation, and hence we have modified the sentence in the revised manuscript to further elaborate on the actual meaning.

(Refer: Section 1, Page 4, Line 113 – 117)

Therefore, various hybrid systems, including PV-TEG, CPVT, CPV-TEG, and CPVT-TEG have been proposed to increase the performance by boosting the power production via converting the excess heat into electricity and useful thermal energy. The CPVT system can resolve the inherent drawbacks of high temperature issue in CPVs and low thermal energy in PVTs by harnessing the unutilized excess heat [4].

Comment 3:

The main difference of the paper and the author's previous work [27,28] should be stated exactly.

Response:

Thank you for the comment. We have highlighted the differences between the previous works and the present work in the revised manuscript.

(Refer: Page 7, Line 193 – 207)

Although several hybrid CPV-TEG and CPVT-TEG experiments have been reported, the studies on the outdoor performance of such hybrid systems are limited. Hence, the outdoor performance of a prototype of our proposed hybrid CPVT and STEG system is presented in this study. In our prior work the optical and mathematical modelling have been carried out to analyse the electrical and thermal performance of the CPVT-STEG system under steady-state conditions [25,26]. Using the steady-state model developed in our previous study [26], the final design of a CPVT-STEG prototype with the optimal number of TEGs have been determined and fabricated for field testing to evaluate the transient effects of environmental parameters on its performance. Since the TEGs are not thermally connected to the PV cells in the developed CPVT-STEG system, the number of TEGs is optimised for obtaining a maximum TEG output power. In the present study, a transient 3-D numerical simulation of the CPVT-STEG system was conducted using ANSYS Fluent, and the results are compared with the experimental results obtained from the prototype. Despite the limitations and challenges in evaluating the effectiveness of the CPVT-STEG prototype, this study seeks to be a significant benchmark in investigating the CPVT-STEG system under outdoor operating conditions.

Comment 4:

The original of the paper should be supplemented.

Response:

Thank you for the comment. The originality of the paper is discussed in the Introduction section 6th paragraph, line 180 – 192, page 6 – 7. The important points were highlighted in the revised manuscript.

Most of the CPV-TEG and CPVT-TEG studies in the existing literature are limited to either conceptual models without any practical prototype or small-scale setups tested under laboratory conditions. Although the idea of combining CPV and TEG has been explored in many studies, this type of hybrid system is still far from reaching a commercialization stage due to a lack of field testing under transient environmental conditions. In the majority of the hybrid CPV and TEG experimental investigations, the TECs are employed instead of TEGs, despite the fact that the TEC's working temperature limit is not suitable to work under high concentration solar collectors such as PTC and Fresnel lenses. Furthermore, the effect of the working temperature limit and the quantity of TEG modules on the electrical output of the hybrid system are often overlooked in the modelling and experimental studies. Increasing the number of TEG modules in a hybrid system where TEGs are thermally coupled to PV cells may reduce the thermal gradient and electrical output of TEG. Hence, the required quantity of TEG modules should be optimised based on the PV temperature as well as the overall output power of the PV and TEG modules.

Comment 5:

The size of the proposed CPVT-TEG seems very large. I think the PV cell area of such collector is less than that of traditional PV panel in the case of the same land area, which is contradictory for the sentence in the line 108-109.

Response:

This is a valuable perspective for us. However, the sentence in the lines 108-109 is based on the literature findings that the use of concentrators in PV increases the power generation per unit area by increasing the incident intensity of solar irradiance. In the present study a hybrid CPVT-STEG system was developed for higher power generation (electric + thermal) per unit area. At lower concentration the electrical efficiency might be lower than the PV standalone system but the overall power conversion efficiency of the hybrid system including both electrical and thermal output is higher compared to the PV alone system. In this the revised manuscript we have included a section discussing on the performance enhancements of the developed prototype over the PV standalone system.

(Refer: Section 6.4, Page 36, Line 597 - 620).

Comment 6:

The method to achieve the stable test condition should be supplemented.

Response:

Thank you for the comment. Since the present study is on transient effects the only stable condition for the experiment is the water flow inside the channel. The methodology to achieve a stable water flow is included in the revised version of the manuscript.

(Refer: Page 16, Line 328 – 331)

To achieve a stable test condition, the fluid outlet is closed so that the water fills the channel without any air gaps and achieves a uniform flow. Once the water flow in the channel is uniform, the outlet is opened and the system is exposed to direct sunlight for power production.

Comment 7:

The conclusion is lengthy. Please make it concise.

Response:

Thank you for this comment. We have reduced the length of the conclusion in the revised version of the manuscript.

(Refer: Section 7, Page 40)

Comment 8:

The challenge and outlook of the proposed PVT collector should be discussed.

Response:

Thank you for this valuable suggestion. We agree with this suggestion, and we have included a separate section in the revised manuscript regarding the challenges and future outlook of the developed prototype.

(Refer: Section 6.8, Page 39 - 40)

6.8 Challenges and Outlook

The efficiency of the developed CPVT-STEG hybrid system is limited by the reflectivity (67%) of the concentrator material used. The electrical and thermal efficiency can be further improved if a reflective material with a reflectivity of more than 90% is used. The electrical efficiency of the CPVT-STEG is also restricted by the number of TEG modules used and its lower efficiency. The optimal number of TEGs used for a maximum power output in a 540 mm long channel is two, and the remaining space is left insulated and unutilised. Hence, solar cells with higher efficiency can replace the TEGs on the rear side of the channel in the prototype to achieve higher overall electrical efficiency. The performance of the CPVT-STEG system can be further enhanced by optimising the design of fluid channels and using highly conductive heat transfer fluids.

In addition to the direct sunlight reflected by PTC, the TEG modules in the prototype can also harvest waste heat from other energy sources through radiation. It is possible if the prototype system is positioned at a geothermal site with hot steam from hot spring water, which can be explored in future work. The developed hybrid structure has the potential to remodel the existing PTC-based solar power plants as CPVT or hybrid CPVT-STEG systems to increase the power production per unit area. Finally, economic and environmental studies can be conducted to evaluate the commercial feasibility of the hybrid prototype. The viability of redesigning existing PTC-based solar power plants requires a comprehensive optimization and techno-economic study of the hybrid prototype.

Highlights

- A new prototype for a hybrid CPVT-STEG system has been developed and experimentally tested.
- The transient numerical simulation results are validated with the experimental results.
- The TEG efficiency is 1.23 times higher compared to an existing hybrid CPVT-STEG system.
- The overall electrical efficiency of the hybrid CPVT-STEG prototype is 25% higher compared to the existing hybrid CPVT-TEG system.

Prototype of a novel hybrid concentrator photovoltaic/thermal and solar thermoelectric generator system for outdoor study

Sridhar Sripadmanabhan Indira[1*], Chockalingam Aravind Vaithilingam[1*], Ramsundar Sivasubramanian[1], Kok-Keong Chong[2], Kulasekharan Narasingamurthi[3], R. Saidur [4,5]

[1] School of Engineering, Faculty of Innovation and Technology, Taylor's University Lakeside Campus, No. 1, Jalan Taylor's, 47500 Subang Jaya, Selangor, Malaysia.
[2] Lee Kong Chian Faculty of Engineering and Science, Universiti Tunku Abdul Rahman, Bandar Sungai Long, 43000 Kajang, Selangor, Malaysia.
[3] Metier Technical Leader, Valeo India Private Limited, No. 63, Rajiv Gandhi Salai, Navallur, Chennai – 600130, India.
[4] Research Centre for Nano-Materials and Energy Technology (RCNMET), School of Engineering and Technology, Sunway University, 47500 Subang Jaya, Malaysia.
[5] Department of Engineering, Lancaster University, Lancaster LA1 4YW, UK.

*Corresponding authors.

E-mail addresses: sridharsripadmanabhannadarindira@sd.taylors.edu.my, sibisri819@gmail.com (S. S Indira), chockalingamaravind.vaithilingam@taylors.edu.my, aravindcv@ieee.org (C.A. Vaithilingam).

Abstract

In this study, a novel prototype of a hybrid concentrator photovoltaic/thermal and solar thermoelectric generator system has been designed and constructed for combined heat and power production. In the developed hybrid system, both the solar cells and thermoelectric modules that share a common heat transfer medium are exposed to concentrated irradiance via a compound parabolic concentrator and a parabolic trough concentrator, respectively. To assess the performance of the hybrid system, a prototype of the hybrid system was built and tested under outdoor operating conditions, and the findings were compared with those of a transient numerical simulation conducted using ANSYS Fluent. The average PV temperature obtained during the test period at a flow rate of 3.8 L/min is 318.19 K which is ~5.6 % lesser compared with a conventional hybrid CPVT-TEG system. The outdoor trials show maximum electrical efficiency of 4.86 % and thermal efficiency of 40% when the solar irradiance is greater than or equal to 1000 W/m^2. The overall power conversion efficiency of the developed prototype is 3 times higher compared to a standalone PV system. The hybrid system helps to reduce carbon emission by 0.5 kg/h, with an associated environmental cost of 0.025 €/h.

Keywords: Thermoelectric generator; Concentrator photovoltaic/thermal; Hybrid system; Prototype development; Experimental analysis; Transient simulation

Nomenclature

A	area
C_p	specific heat capacity
D_h	hydraulic diameter
E	thermal energy (W)
EC	environmental cost
$\dot{E}x$	Exergy rate
f	friction coefficient
G	solar radiation
I	current
L	length
m	mass flow rate
N	sample size
P_{CO_2}	carbon price
Re	Reynolds number
T	temperature
T_h	hot side temperature of TEG
T_c	cold side temperature of TEG
T_{Sun}	surface temperature of sun
V	velocity / voltage

Greek Symbols

η	efficiency
ϱ_f	density of HTF
ψ_{CO_2}	average CO_2 emission

Subscripts

amb	ambient
DNI	direct normal irradiance
ex	exergy
el	electrical
GHI	global horizontal irradiance
in	inlet/input
m	maximum
oc	open-circuit
out	outlet/output

sc	short-circuit
th	thermal

Abbreviations

CPV	Concentrator Photovoltaics
CPVT	Concentrator Photovoltaic/Thermal
EMR	Eliminating Multiple Reflections
HTF	Heat Transfer Fluid
NOCT	Nominal Operating Cell Temperature
PV	Photovoltaic
PCM	Phase Changing Material
STEG	Solar Thermoelectric Generator
TEC	Thermoelectric Cooler
TEG	Thermoelectric Generator

1. Introduction

Solar photovoltaic (PV) technology has advanced rapidly in recent decades due to the increased global demand for renewable energy to reduce greenhouse gas emissions. The PV technology requires a large land area to compensate for the moderate power conversion efficiency of the commercial silicon solar cells. Concentrator photovoltaics (CPV) is a new generation of PV technology with the idea of using cost-effective reflective mirrors or concentrating lenses to enhance the yield intensity of commercial solar cells [1]. The solar cell's efficiency drops by 0.2 % to 0.5 % for every 1°C rise in temperature, making CPV technology vulnerable to high temperatures [2]. A temperature gradient in the CPV cell can lead to hotspots which degrade the performance of the CPV at high rates [3]. Therefore, various hybrid systems, including PV-TEG, CPVT, CPV-TEG, and CPVT-TEG have been proposed to increase the performance by boosting the power production via converting the excess heat into electricity and useful thermal energy. The CPVT system can resolve the inherent drawbacks of high temperature issue in CPVs and low thermal energy in PVTs by harnessing the unutilized excess heat [4]. In hybrid CPV-TEG and CPV/T-TEG systems, the TEGs are introduced to transform the surplus heat from the PV into electric power. Several studies suggest that the overall power output of PV-TEG, CPV-TEG, and CPVT-TEG systems have increased in comparison to a standalone PV system [5].

The purpose of introducing the TEG on the rear side of the PV is to compensate the power loss in PV attributed to high operating temperature [6]. In comparison to standalone PV, solar TEG, and PV/T systems, the amount of power produced by hybrid PV-TEG systems is much greater [7]. However, there are a few studies that have reported negative results in a combination of TEG and PV. With the poor conversion efficiency of TEG, the reduction of PV performance with increasing temperature was reported to be faster than the increase in power generated by TEG [8]. It was discovered that the overall efficiency of hybrid CPV-TEG decreases with an increase in temperature, regardless of the ZT of TEG [9]. In most of the existing hybrid systems, the TEG is positioned between the PV and the heat sink, which leads to a competing relationship between the PV cells and TEGs because the PV cell requires a lower temperature for a better efficiency, whereas the hot side of the TEGs requires a higher temperature for a higher temperature gradient [10]. According to Lin et al. [11], a higher efficiency of PV-TEG is only possible if TEG has a low thermal conductivity and a high Seebeck coefficient. Yin et al. [12] included the thermal resistance concept into the theoretical model of a CPV-TEG hybrid system with different types of PV cells and cooling technologies to optimise the performance of the hybrid system. The results demonstrated that the water-cooled hybrid system consisting of an amorphous silicon PV cell or a polymer PV cell and a TEG with increased thermal resistance is superior in performance.

Su et al. [13] and Cui et al. [9] discovered an ideal operating temperature at which the TEG output equals the reduced power output of the PV and thus it can lead to the improved overall efficiency of the hybrid system. Later, Cui et al. [14] introduced PCM in between the PV and TEG in a hybrid CPV-TEG system to maintain the optimal working temperature for improving efficiency. Nevertheless, the thermal contact resistance at the interface and the low thermal conductivity of the PCM can result in large temperature differences between the PV, the PCM, and the TEG, which impacts the efficiency of the hybrid system. In another work, Yin et al. [15] employed PCM to manage the operational temperature of a CPV-TEG hybrid system and reported a 23.52 % increase in output power. Zhang et al. [16] employed thermal interface materials between PV and TEG to reduce the thermal contact resistance, resulting in a 14 % increase in PV production and a 60 % increase in TEG output.

Lekbir et al. [17] in their theoretical study of the hybrid CPVT-TEG system suggest that using nanofluid as a heat transfer medium can improve the electrical and thermal efficiency in comparison to conventional cooling methods. The effects of thermal contact resistance and thermal resistance of the TEG were not considered in their study. Soltani et al. [18] modelled a PTC based CPVT-TEG in which the PV cells are arranged on the lateral side of the absorber tube with the TEGs on their back side. In their analysis, the non-uniform PV illumination induced by PTC, as well as the impacts of thermal contact resistance and thermal resistance of TEG, were not considered. Mohsenzadeh et al. [19] designed an experimental prototype of a PTC-based CPVT-TEG system with a triangular channel covered with PV cells and TEGs at the back of the PV to generate both electrical and thermal energy. It was discovered that the hybrid system performed better than that of the PV alone system. Yin et al. [20] optimised the effects of PV voltage and TEG load resistance on the temperature and output power of a water-cooled CPV-TEG hybrid system in their experimental study. The optimised output performance of the CPV-TEG outperforms the CPV alone system.

Abdo et al. [21] developed a new configuration of PV and TEG hybrid systems that are not thermally connected. Both the PV and TEG are combined with a microchannel heat sink between them, and they are exposed to high intensity solar irradiance using a Fresnel lens. Numerical evaluation reveals that the efficiency of the hybrid concentrator photovoltaic/thermal-solar thermoelectric generator (CPVT-STEG) system configuration is more efficient than the traditional hybrid CPVT-TEG system configuration. An experimental prototype of a PTC-based hybrid CPVT-TEG system was described by Riahi et al. [22]. The findings revealed that the CPVT-TEG performed better than a CPVT system. Nevertheless, the PV temperature in the CPV/T-TEG system was found to be higher when compared to the CPVT system, and this is due to the higher thermal resistance of the TEG. Shittu et al. [23] carried out a three-dimensional (3-D) numerical simulation of a hybrid CPV-TEG system by considering all the contact resistances and discovered that ignoring the contact resistances causes the total power output and efficiency to be overestimated by 7.6 % and 7.4 % respectively. In the study conducted by Rejeb et al. [24], the numerical simulation results of the CPV-TEG system were analysed using a statistical tool to determine the significance of solar radiation, solar concentration ratio, ambient temperature, height of TEG leg, and external load resistance on the electrical efficiency, as well as how to optimise these parameters for maximum electrical efficiency.

Most of the CPV-TEG and CPVT-TEG studies in the existing literature are limited to either conceptual models without any practical prototype or small-scale setups tested under laboratory conditions. Although the idea of combining CPV and TEG has been explored in many studies, this type of hybrid system is still far from reaching a commercialization stage due to a lack of field testing under transient environmental conditions. In the majority of the hybrid CPV and TEG experimental investigations, the TECs are employed instead of TEGs, despite the fact that the TEC's working temperature limit is not suitable to work under high concentration solar collectors such as PTC and Fresnel lenses. Furthermore, the effect of the working temperature limit and the quantity of TEG modules on the electrical output of the hybrid system are often overlooked in the modelling and experimental studies. Increasing the number of TEG modules in a hybrid system where TEGs are thermally coupled to PV cells may reduce the thermal gradient and electrical output of TEG. Hence, the required quantity of TEG modules should be optimised based on the PV temperature as well as the overall output power of the PV and TEG modules.

Although several hybrid CPV-TEG and CPVT-TEG experiments have been reported, the studies on the outdoor performance of such hybrid systems are limited. Hence, the outdoor performance of a prototype of our proposed hybrid CPVT and STEG system is presented in this study. In our prior work the optical and mathematical modelling have been carried out to analyse the electrical and thermal performance of the CPVT-STEG system under steady-state conditions [25,26]. Using the steady-state model developed in our previous study [26], the final design of a CPVT-STEG prototype with the optimal number of TEGs have been determined and fabricated for field testing to evaluate the transient effects of environmental parameters on its performance. Since the TEGs are not thermally connected to the PV cells in the developed CPVT-STEG system, the number of TEGs is optimised for obtaining a maximum TEG output power. In the present study, a transient 3-D numerical simulation of the CPVT-STEG system was conducted using ANSYS Fluent, and the results are compared with the experimental results obtained from the prototype. Despite the limitations and challenges in evaluating the effectiveness of the CPVT-STEG prototype, this study seeks to be a significant benchmark in investigating the CPVT-STEG system under outdoor operating conditions.

2. Prototype description

In the present study, a hybrid CPVT-STEG receiver is integrated between the solar concentrators of CPC and PTC as shown in Fig. 1. Both the PV cells and TEG modules share a common cooling channel, which is designed for harnessing thermal energy from excess heat. The working principle of the hybrid CPVT-STEG receiver is clearly illustrated in the schematic diagram as shown in Fig. 1. In the proposed hybrid system, commercial mono-crystalline PV cells with a dimension of 125 mm × 125 mm each from Allmejores and a high temperature graphite plated TEG (TEG1-1263-4.3) composed of bismuth telluride with a dimension of 30 mm × 30 mm are used in the hybrid receiver for energy conversion. TEGs with high thermal conductive graphite coatings are preferred to minimize the thermal contact resistance. The geometrical parameters of the hybrid CPVT-STEG prototype are listed in Table 1. The characteristics of both the PV and TEG modules used in the prototype are listed in Table 2 and Table 3, respectively.

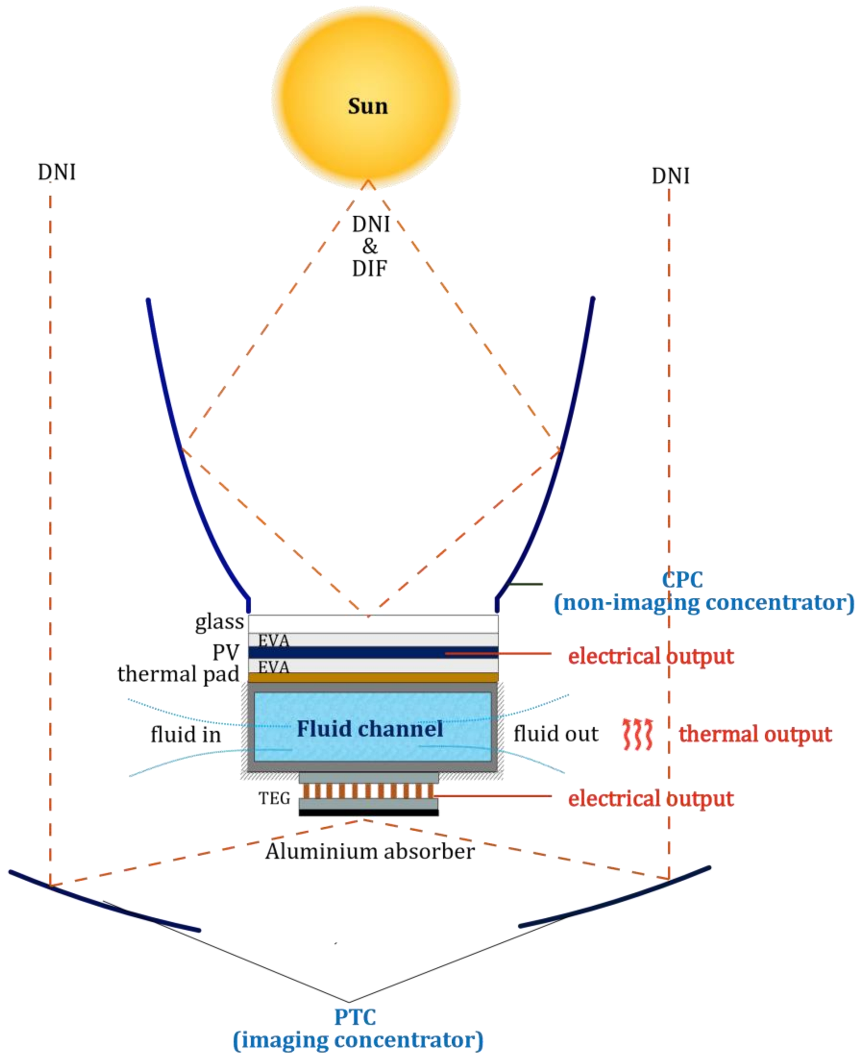

Fig. 1. Schematic diagram of the working principle of hybrid CPVT-STEG prototype.

Table 1. Geometrical parameters of different components in the hybrid CPVT-STEG prototype [26].

Components	Width, mm	Length, mm	Thickness, mm
PV panel			
Glass layer	130	540	5
EVA layer	130	540	0.5
Silicon wafer	125	540	0.2
Thermal pad	130	540	0.5
TEG module			
Graphite layer	30	30	0.13
Ceramic layer	30	30	0.8
Copper strips	1.08	2.7	0.15
P-N legs	1.08	1.08	1.5
Aluminium absorber clamp	30	540	2
Rectangular Channel			
Fluid domain	124	540	30
Wall thickness	-	-	3
Full channel	130	540	36

Table 2. The characteristics of the PV module in the hybrid CPVT-STEG prototype [26].

Parameters	Value
Optical parameters	
Absorptivity of glass	0.018
Transmissivity of glass	0.92
Emissivity of glass	0.85
Absorptivity of EVA	0.08
Emissivity of EVA	0.9
Transmissivity of EVA	0.9
Absorptivity of silicon wafer	0.9
Absorptivity of thermal pad	0.5
Thermal parameters	
Thermal conductivity of glass	2 W/m.K
Thermal conductivity of EVA	0.35 W/m.K
Thermal conductivity of silicon wafer	148 W/m.K
Thermal conductivity of thermal pad	2.8 W/m.K
Electrical parameters	
No. of PV cells connected in series (mono-Si)	4 cells (125 mm x 125 mm each)
Open circuit voltage of a cell	0.635 V
Short circuit current of a cell	5.744 A
Maximum voltage of a cell	0.530 V
Maximum current of a cell	5.401 A
PV efficiency at STC	18.6 %
Temperature coefficient of power	-0.47 % / °C

Table 3. The characteristics of the TEG module in the hybrid CPVT-STEG prototype [26].

Parameters	Value
Pairs of PN legs	126
Max. TEG hot side temperature limit	613.15 K
Max. TEG cold side temperature limit	463.15 K
Thermal conductivity of graphite	10 W/m.K
Thermal conductivity of ceramic	18 W/m.K
Seebeck coefficient of p leg	$\alpha_p(T)$ = -8.105 x 10^{-14} T^3 -1.45838 x 10^{-9} T^2 + 9.2444677 x 10^{-7} T + 7.417 x 10^{-5}
Seebeck coefficient of n leg	$\alpha_n(T)$ = 1.7324623 x 10^{-13} T^3 – 1.147783 x 10^{-9} T^2 + 5.90568332 x 10^{-7} T + 1.4392165 x 10^{-4}
Electrical resistivity of p leg	$\rho_p(T)$ = 6.21731 x 10^{-15} T^4 – 1.085722 x 10^{-11} T^3 + 6.857354 x 10^{-9} T^2 – 1.797597 x 10^{-6} T + 1.73549 x 10^{-4}
Electrical resistivity of n leg	$\rho_n(T)$ = 1.18538 x 10^{-15} T^4 - 2.301947 x 10^{-12} T^3 + 1.5708605 x 10^{-9} T^2 – 4.125723 x 10^{-7} T + 4.42835937 x 10^{-5}
Thermal conductivity of p leg	$k_p(T)$ = - 6.0097596 x 10^{-8} T^3 + 9.0134323 x 10^{-5} T^2 - 3.7380241 x 10^{-2} T + 6.1921321
Thermal conductivity of n leg	$k_n(T)$ = - 3.38062 x 10^{-8} T^3 + 6.22422 x 10^{-5} T^2 - 2.95477835 x 10^{-2} T + 5.7041796
Figure of merit of p leg	$ZT_p(T)$ = -1.68766 x 10^{-8} T^3 + 3.2614 x 10^{-5} T^2 - 2.2459 x 10^{-2} T + 5.424505
Figure of merit of n leg	$ZT_n(T)$ = 2.85296 x 10^{-8} T^{-3} - 3.5168 x 10^{-5} T^2 + 1.0560 x 10^{-2} T + 0.3213
Thermal conductivity of Copper strips	385 W/m.K
Thermal conductivity of Aluminium	202.4 W/m.K
Absorptivity of aluminium absorber clamp	0.9
Emissivity of aluminium absorber clamp	0.15

The supporting frame of the prototype was fabricated as illustrated in Fig. 2, where the size of the primary base structure is 1.10 m × 1.12 m. The primary base structure has a single vertical shaft at the centre that joins the base structure to the secondary base structure. The main shaft has two upper hinges and a lower hinge. The upper hinges allow pivoting movement of the entire secondary base in the east-west direction, while the lower hinge allows pivoting movement of the entire secondary base in the north-south direction. Both the CPC and PTC are mounted on the secondary base, and the upper and lower hinges in the primary shaft are actuated by a pair of linear actuators as shown in Fig. 2(a) to adjust the cardinal orientation of the secondary base based on the direction of solar irradiance from the sun as detected by the light sensor. The width of the secondary base is equivalent to or larger than the aperture width of the CPC. The secondary base has four pairs of vertical shafts to hold the receiver of the hybrid system. The vertical shafts include linear guide rails and rollers to adjust the focal position of the receiver (see Fig. 2(b)). The second set of linear actuators is used to actuate the rollers to adjust the position of the receiver to its focal point.

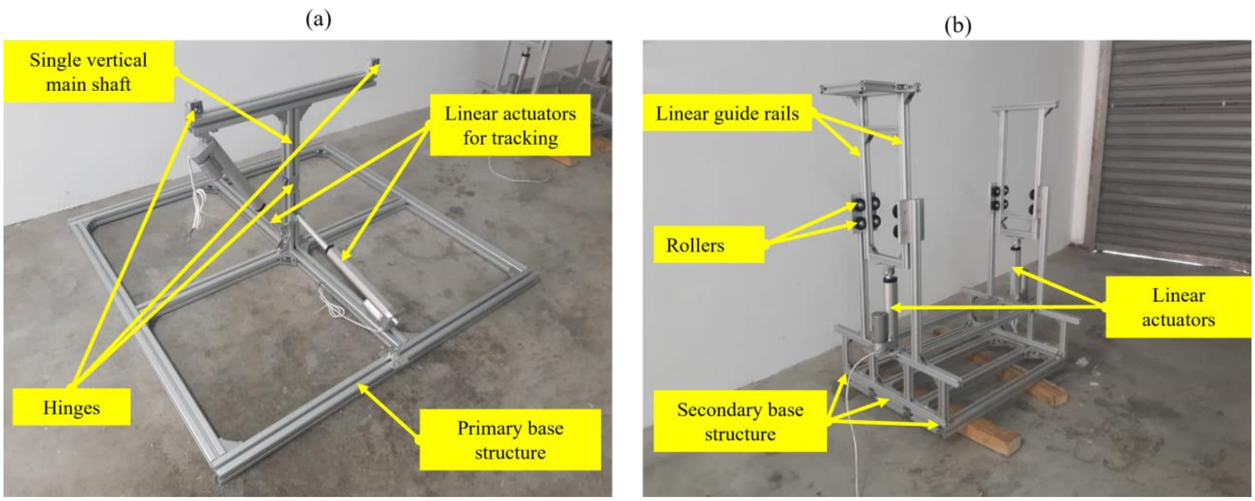

Fig. 2. Fabrication of support structure: (a) primary base and (b) secondary base

Based on our previous optical study, our design for the hybrid CPVT-STEG prototype includes a HEMR CPC ($CR = 4\,suns$, $\theta_c = 10.61°$) paired with a PTC ($CR = 16.6\,suns$, $\varphi_r = 45°$) [25]. The CPC and PTC profiles were built using laser-cut aluminium ribs. Mirror-polished stainless-steel sheets with a reflectivity of 67 % were screwed onto aluminium ribs to construct the HEMR CPC and PTC, as shown in Fig. 3. Flat reflectors are added on the bottom side of the CPC to characterize it as a HEMR CPC, resulting in uniform illumination on the CPC receiver. In Fig. 4, four pieces of mono-crystalline silicon cells are connected in series and sandwiched between the glass cover and EVA layers in an aluminium frame to form a complete PV module. The rear side of the PV module is backed with a 0.5 mm thick silicone thermal pad that acts as a thermal interface material between the PV module and the fluid channel, which allows for efficient heat transfer.

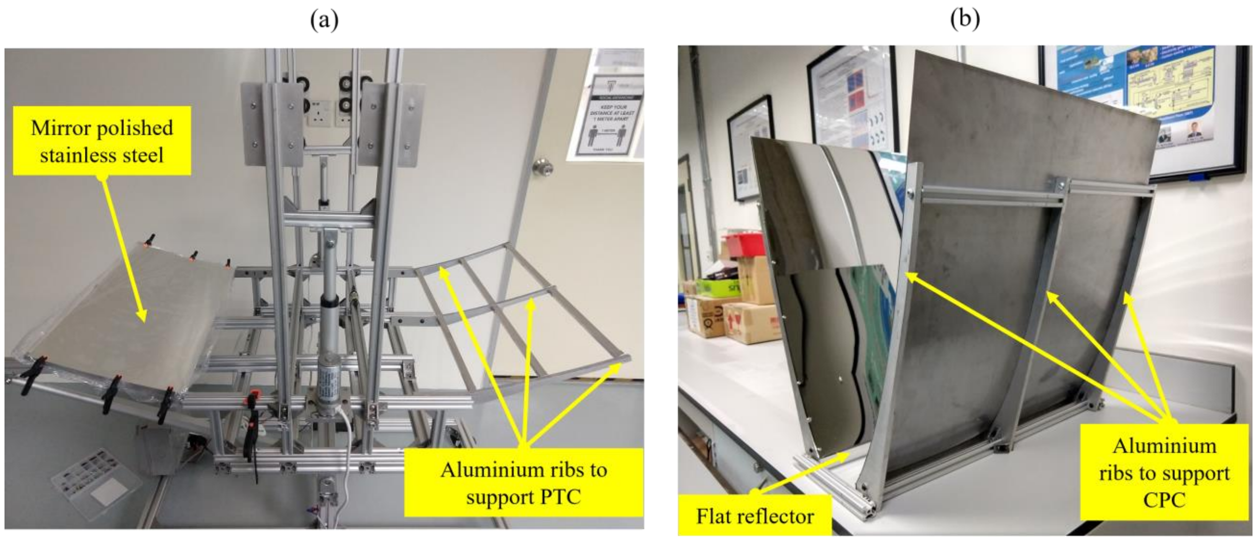

Fig. 3. Fabrication of solar concentrators: (a) PTC, and (b) CPC

As seen in Fig. 5(a), the fluid channel is an enclosed rectangular aluminium tube with an inlet and outlet pipe. The channel is manufactured with thermowell at the inlet and outlet to accommodate thermocouples for measuring the temperature of the water at the inlet and outlet (see Fig. 5(b)). To avoid any fluid channel leakage, the thermowells were sealed with an anti-leakage sealant. On the backside of the fluid channel TEGs are installed and fastened together using an aluminium absorber clamp. Fibreglass was used to insulate the empty area outside of the contact zone between the channel and the TEGs. Additionally, the sidewalls and non-contact parts of the fluid channel were insulated with fibreglass to prevent heat loss (see Fig. 6). In order to increase the absorptivity of the aluminium clamp, it is coated with candle soot [27]. The average absorbance of the candle soot in the spectral range of 150 – 1500 nm is 0.86 [28].

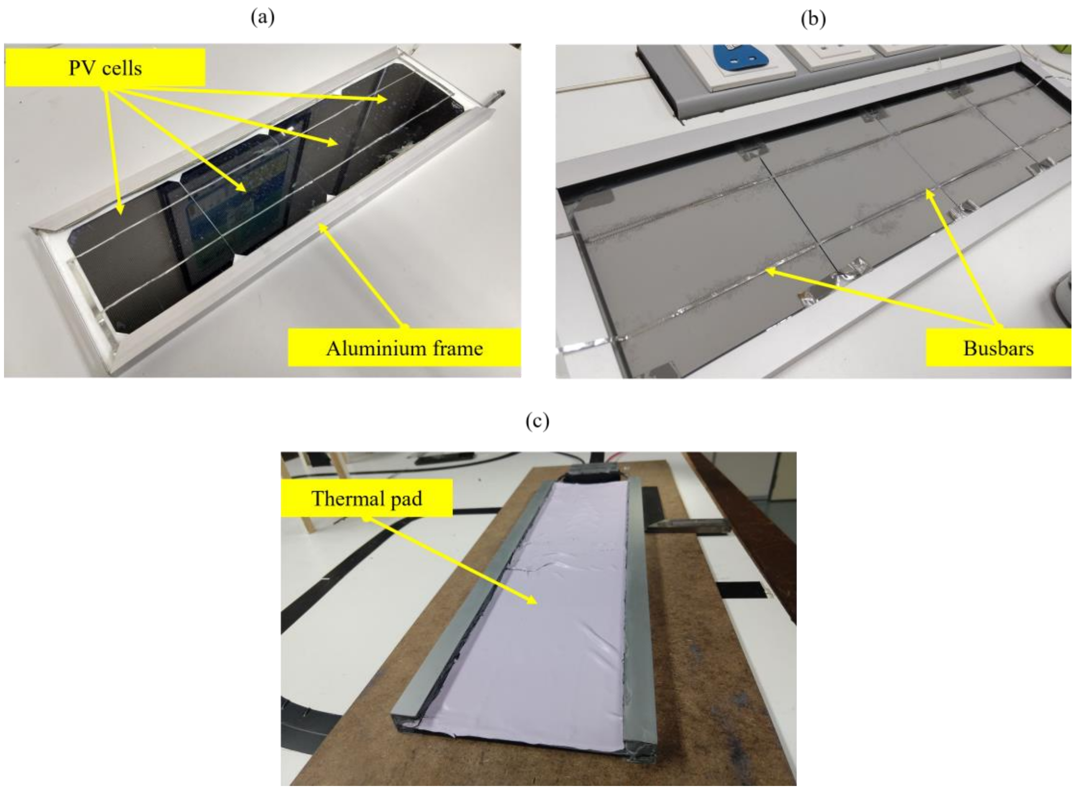

Fig. 4. Fabrication of PV module: (a) PV front side, (b) PV rear side, and (c) PV rear side with thermal pad.

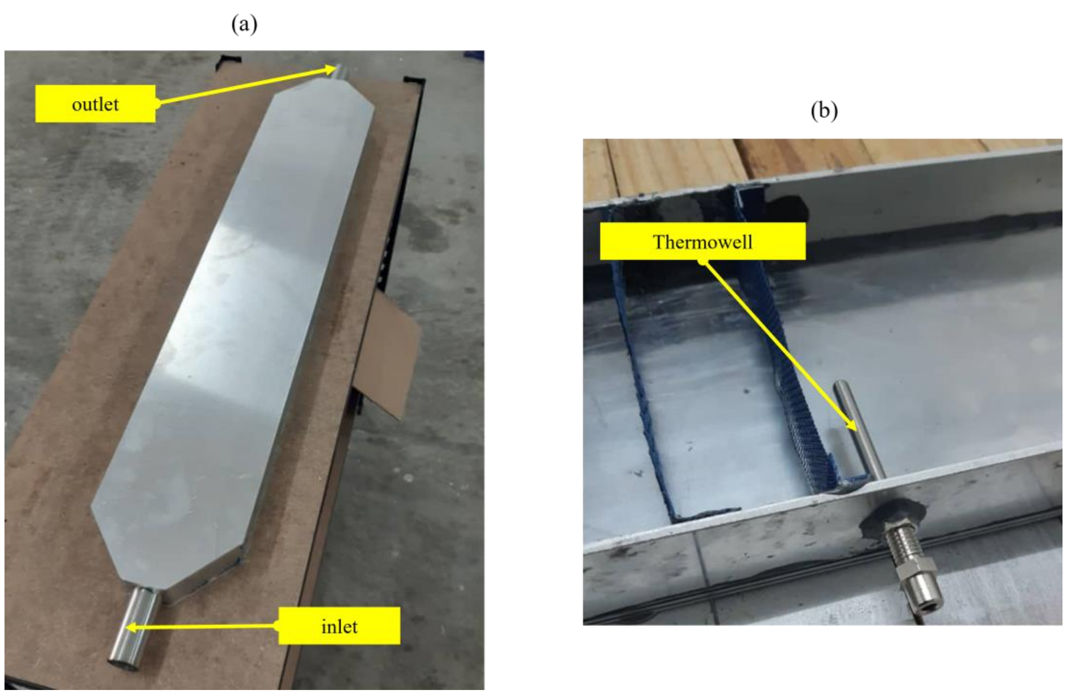

Fig. 5. Fabrication of fluid channel.

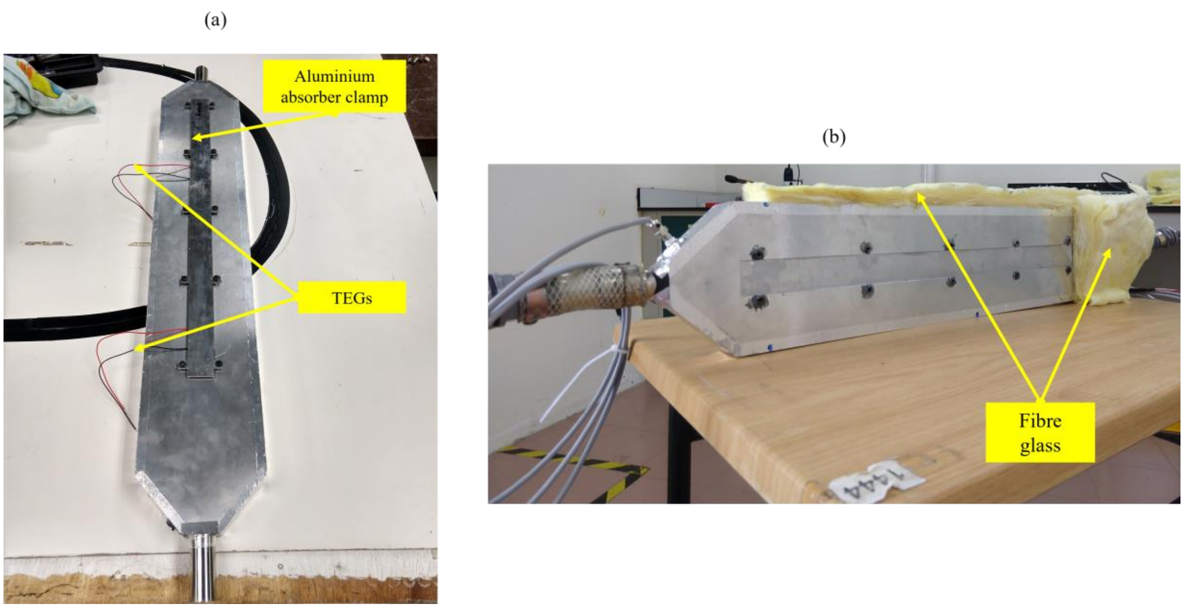

Fig. 6. (a) Integration of TEG modules with fluid channel (b) insulation of fluid channel with fiberglass.

3. Experimental setup and measuring equipment

The experimental prototype was built at the Taylor's University campus, Malaysia (3.0626° 101.6168° E). The constructed prototype was evaluated to assess its electrical and thermal performance under transient outdoor conditions. The schematic diagram of the prototype to show numerous components and thermocouple locations is illustrated in Fig. 7. Table 4 shows the specifications of the measurement devices used throughout the experiment, including their respective measurement ranges and accuracies. The constructed hybrid concentrator structure is equipped with a sun tracking mechanism in both east-west and north-south directions. The receiver of the hybrid system is aligned along the polar north-south axis with the latitude-dependent tilt angle, and a microcontroller with an LED sensor-based sun-tracking system is used to track the aperture of the hybrid system from east to west. The receiver of the hybrid system is fixed at the focal point by adjusting the linear guide rails using the linear actuators. Two units of K-type thermocouples were installed on both sides of the PV module without casting any shadow on the PV cells, which were then connected to the datalogger for monitoring the surface temperatures of the PV module.

Table 4. List of measuring instruments used for the experimental study.

Instruments	Measuring range	Accuracy
Pyranometer (Hukseflux SR05-D1A3	0 – 2000 W/m^2	+/- 1.8 %
Pyrheliometer (Delta Ohm LP Pyrhe 16)	0 – 2000 W/m^2	+/- 2 %
Basic wind speed sensor (Lambrecht meteo)	0.7 – 50 m/s	+/- 2 %
PT 1000 RTD	-20 to 100 ° C	0.15 + 0.002 (° C)
RS PRO Type K Thermocouple	-50 to 1000 ° C	+/- 1.5 ° C
Kimo Type-T thermocouple	-40 to 350 ° C	+/- 0.5 ° C
Proskit multimeter for current measurement	20 Amps Max.	+/- 0.5 %
Techgear multimeter for current measurement	60 mV – 1000 V	+/- 0.2 %
Flow meter hall effect sensor (YF-S201)	1 – 30 L/min	+/- 10 %
INA 219	26 V / 3.2 Amps Max.	1 %

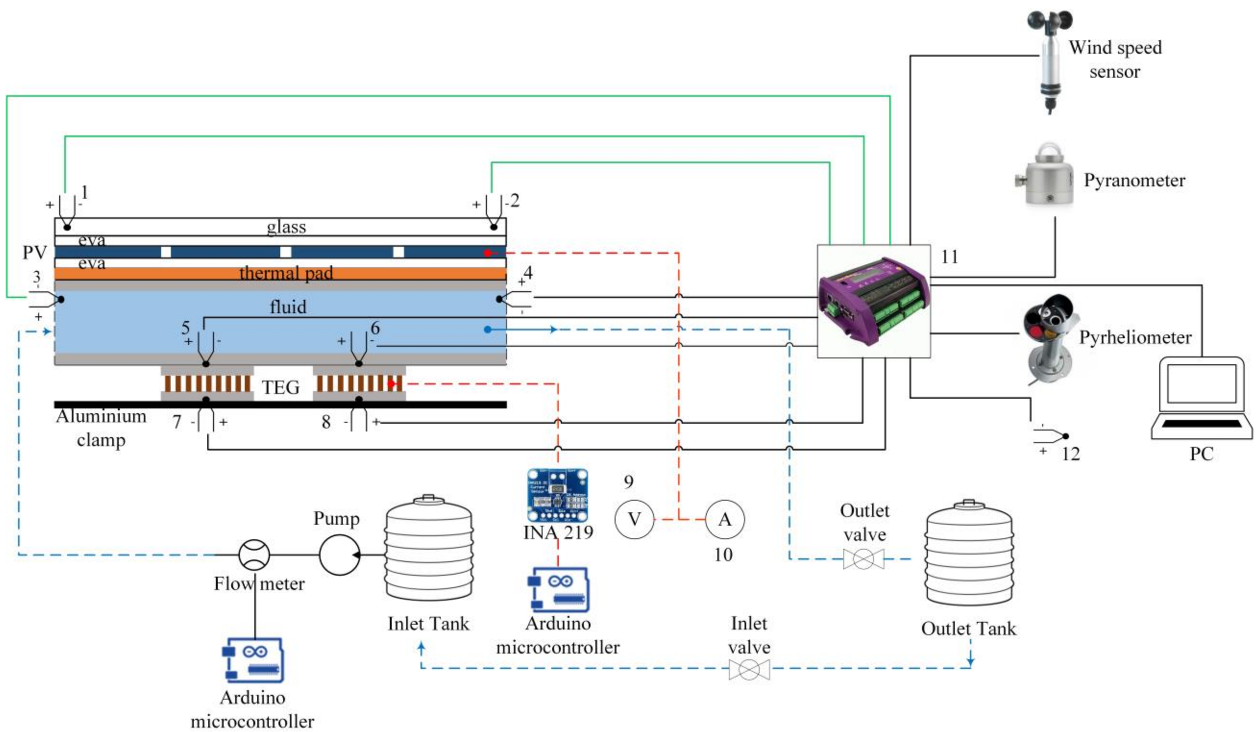

Fig. 7. Schematic of hybrid CPVT-STEG experimental setup: (1 & 2) PV temperature sensor location, (3) and (4) fluid inlet and outlet temperature sensor location, (5) and (6) TEG cold side temperature sensor location, (7) & (8) TEG hot side temperature sensor location, (9 & 10) Multimeter, (11) data logger and (12) ambient temperature sensor location.

Two units of K-type thermocouples were attached between the bottom part of the fluid channel and the cold side of TEGs to measure the cold side temperature of the TEGs. Another two units of K-type thermocouples were attached between the aluminium absorber clamp and the hot side of the TEGs to measure the hot side temperature of the TEGs. The four thermocouples from the TEGs were routed along the fluid channel walls without casting any shade on the bottom part of the PTC, in which all the thermocouples were linked to the data-logger for continuous recording of temperatures throughout the experiment. Additionally, a T-type thermocouple was used to record the ambient temperature during the experiment. Moreover, instruments such as a pyranometer, pyrheliometer, and wind speed sensor were connected to the data-logger for monitoring and recording direct normal irradiance, global horizontal irradiance, and wind speed, respectively, during the field testing. Two units of platinum resistance temperature detectors were fixed in the fluid channel via a tiny hole in the thermowell to monitor the water temperature at the inlet and outlet of the fluid channel. The experimental setup consisted of one inlet tank connected to the inlet of the fluid channel and one outlet tank connected to the outlet of the fluid channel. The water was pumped from the inlet tank using a diaphragm water pump at a constant flow rate. The fluid channel and the inlet pipe from the inlet tank were completely insulated by using fibreglass to avoid the heat losses from the hybrid system.

The CPVT-STEG system was tested on the rooftop of a building on the campus of Taylor's University on a sunny day, October 26, 2021, as depicted in Fig. 8. The water flow rate inside the fluid channel is tuned to achieve a constant rate of 3.8 L/min. To obtain a stable test condition, the fluid outlet was closed so that the water filled the channel without any air gaps and achieved a uniform flow. Once the water flow in the channel was uniform, the outlet was opened so that the prototype was exposed to direct sunlight for power production. The wind speed, ambient temperature, GHI, DNI, PV temperature, TEG temperature, fluid inlet and outlet temperature, voltage, and current were recorded for a period of 1 hour and 30 minutes, from 11:15 am to 12:45 pm (peak sun hours). Due to the frequent rainfall in the test location, the period of data collection was constrained since neither the prototype nor the data acquisition system employed were designed to withstand the rigours of wet conditions. The environmental and operating parameters were recorded every second via an automated data acquisition system. The open-circuit and short-circuit current of both the PV and TEGs were monitored and recorded every 5 minutes using digital multimeters and INA 219 sensor, respectively.

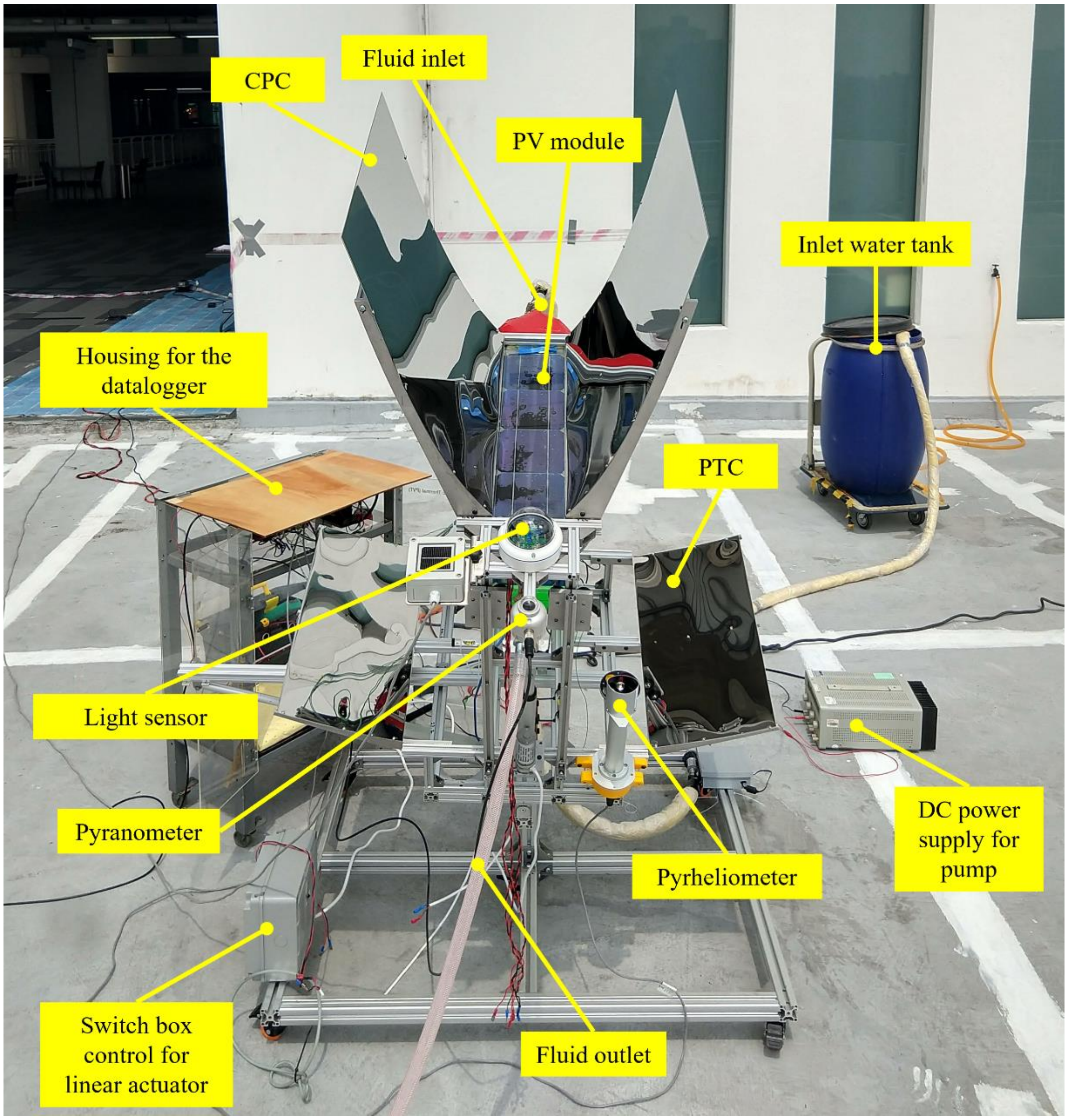

Fig. 8. Outdoor experimental setup for testing the prototype.

4. Numerical simulation

Real-time transient simulation is critical because real-time transient situations can happen in an unpredictable and fast manner in the real world. The intermittency of weather conditions, particularly in partially cloudy climes, can influence the output power and conversion efficiency of the hybrid system, which are significant factors in stabilising the electrical response of hybrid system. The ideal quantity of TEG modules for producing a maximum TEG output in the hybrid system was determined using the steady-state heat transfer model from our previous work [26]. For the transient simulation, the numerical model of the CPVT-STEG system with the optimal number of TEGs (2 units of TEG) is considered. The transient response of the hybrid system was modelled using ANSYS Fluent.

The flowchart to show the methodology of transient numerical simulation and experimental study is indicated in Fig. 9. Based on our previous study, the number mesh elements used is 8.386×10^6 [26]. For transient simulation, the input boundary conditions are based on the measured solar radiation and ambient conditions on the day of measurement. The input solar irradiance is processed based on the optical efficiency, and it is imported to ANSYS Fluent as a volumetric heat source.

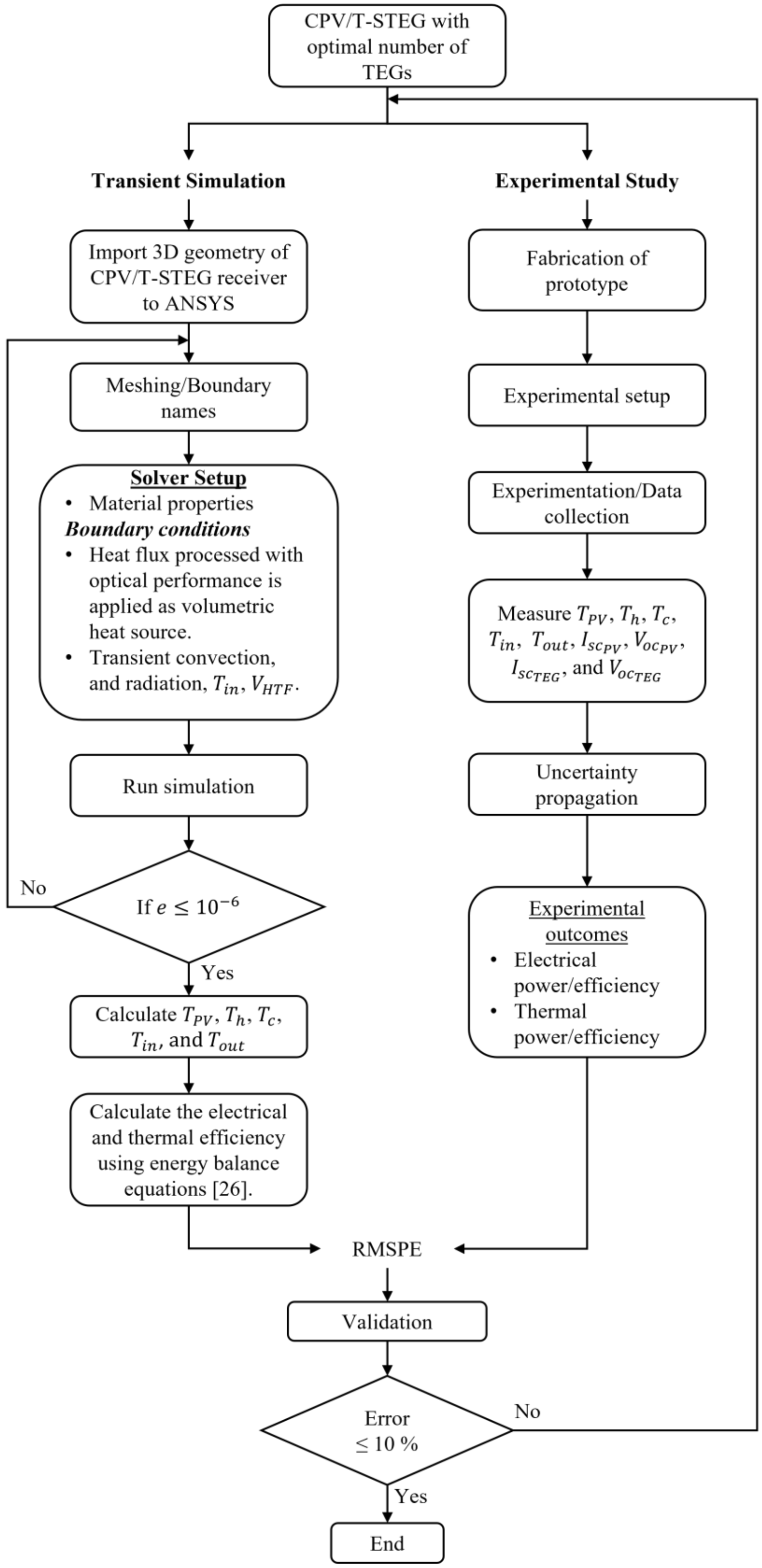

Figure 9. Flowchart of transient numerical simulation and experimental study

5. Computational method

5.1 Photovoltaic module measurements

Since the experimental prototype employs only four silicon PV cells in series, the overall open-circuit voltage is around 2.54 V, which is too low to be measured directly using any commercially available I-V tracer. Electric power generated by any PV module can be estimated using Simulink provided that open-circuit voltage and short-circuit current are added to the modelled circuit [29]. In this investigation, the I-V and P-V curves of the PV module in the hybrid system were simulated using Simulink in MATLAB (see Fig. 10) based on the open-circuit and short-circuit current measured via multimeters. Given the open-circuit voltage, short-circuit current, and temperature of PV module, we can compute the maximum PV voltage, maximum PV current, and the maximum power of the PV module.

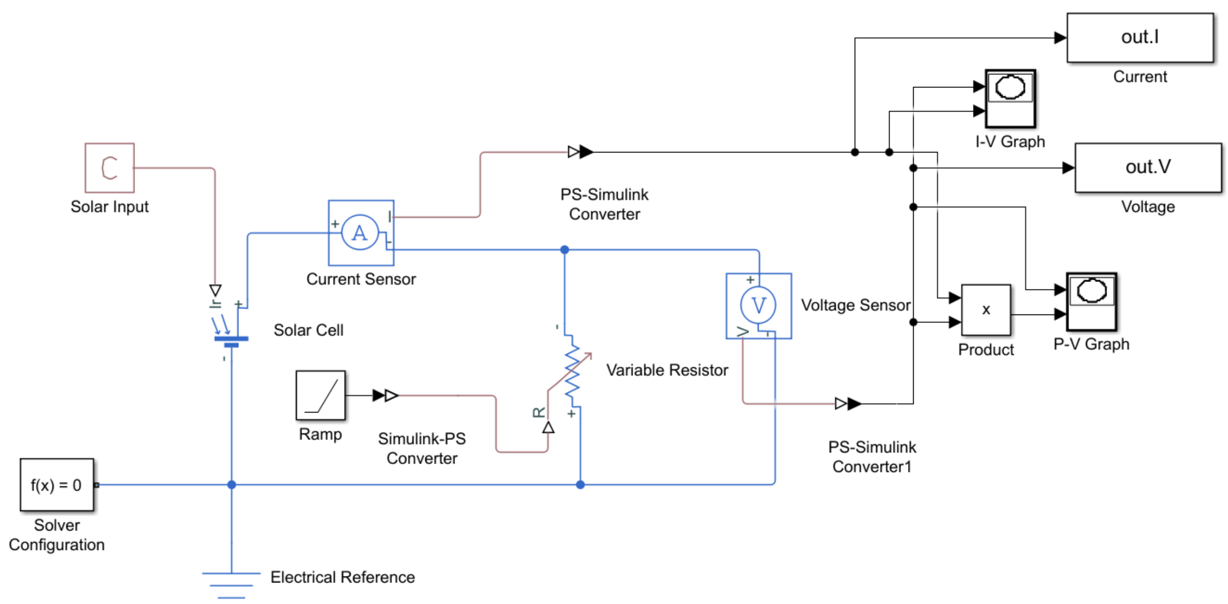

Fig. 10 Simulink circuit model used for I-V and P-V curve calculation.

5.2 Thermoelectric generator measurements

The prototype has two TEGs connected in series, where the output terminals are connected to an INA 219 sensor and an Arduino microcontroller for monitoring the short-circuit current ($I_{sc_{TEG}}$) and open-circuit voltage ($V_{oc_{TEG}}$). The maximum power point (MPP), at which the TEG provides the highest feasible power ($P_{m_{TEG}}$) to the external load at a given temperature, is expressed as the following [30] [31]:

$$P_{m_{TEG}} = \frac{V_{oc_{TEG}}}{2} \times \frac{I_{sc_{TEG}}}{2} \tag{1}$$

5.3 Net efficiency of CPVT-STEG prototype

The net electrical efficiency of the developed CPVT-STEG prototype can be calculated as [26]:

$$\eta_{el} = \frac{P_{m_{PV}} + P_{m_{TEG}} - P_{pump}}{A_{PTC} G_{GHI}} = \frac{P_{total}}{A_{PTC} G_{GHI}} \tag{2}$$

where P_{pump} is the required pump power, A_{PTC} is the aperture area of the PTC, and G_{GHI} is the total solar irradiance falling on the hybrid system. The following equation is used to figure out how much power the pump needs:

$$P_{pump} = \dot{V}_{HTF} f \frac{L}{D_h} \frac{\varrho_{HTF} V_{HTF}^2}{2} \tag{3}$$

where $\dot{V}_{HTF}$ is the volumetric flow rate, f is the friction coefficient, L is the length of the channel, D_h is the hydraulic diameter, ϱ_{HTF} is the density of the HTF, and V_{HTF} is the velocity of the HTF, which can be calculated using Eq. (4):

$$\dot{V}_{HTF} = V_{HTF} A_{cross} \tag{4}$$

$$f = \frac{72.92}{Re} \tag{5}$$

where A_{cross} is the cross-sectional area of the fluid channel and Re is the Reynold's number.

The net thermal efficiency of the hybrid system is computed using the following equation (6):

$$\eta_{th} = \frac{E_{HTF}}{A_{PTC} G_{GHI}} \quad (6)$$

where E_{HTF} is the excess heat transmitted to the HTF from PV cells and TEGs which can be determined by the following equation (7) [32]:

$$E_{HTF} = m_{HTF} C_p (T_{out} - T_{in}) \quad (7)$$

where m_{HTF} is the mass flow rate of HTF, C_p is the specific heat capacity of HTF, T_{in} and T_{out} are the inlet and outlet temperatures of HTF, respectively.

The exergy efficiency (η_{ex}) of the developed prototype is calculated using the following equation [33]:

$$\eta_{ex} = \frac{\dot{E}x_{out}}{\dot{E}x_{in}} \quad (8)$$

where exergy output $\dot{E}x_{out}$ is the total of thermal and electrical exergies. The exergy of incident solar irradiance ($\dot{E}x_{in}$) is calculated using Petela model [34], as given in Eq. (10):

$$\dot{E}x_{out} = \dot{E}x_{th} + \dot{E}x_{el} \quad (9)$$

$$\dot{E}x_{in} = G_{GHI} A_{PTC} \left[1 - \frac{4}{3}\frac{T_{amb}}{T_{Sun}} + \frac{1}{3}\left(\frac{T_{amb}}{T_{Sun}}\right)^4\right] \quad (10)$$

where $\dot{E}x_{el}$ is the total electrical output of the hybrid system. The thermal exergy ($\dot{E}x_{th}$) is determined using the Eq. (11) [33]:

$$\dot{E}x_{th} = mC_p(T_{out} - T_{in}) - mC_p T_{amb} \ln\left[\frac{T_{out}}{T_{in}}\right] \quad (11)$$

5.4 Uncertainty analysis of experimental results

The experimental data are variables measured through equipment with some uncertainties. The uncertainty of experimental measurements can be readily calculated by collecting a sample and acquiring the error percentage of the instruments from the datasheets. The Engineering

Equation Solver (EES) automates the process of uncertainty analysis internally using the root sum square (RSS) method [33]. Based on the energy balance concept, the uncertainty assessment was conducted on both thermal and electrical efficiencies using EES. The error percentage values can be assigned to measured variables such as G_{GHI}, G_{DNI}, V_{air}, T_{amb}, T_{PV}, T_h, T_c, V_{HTF}, T_{in}, T_{out}, $I_{sc_{PV}}$, $V_{oc_{PV}}$, $I_{sc_{TEG}}$, and $V_{oc_{TEG}}$. EES uses these values of uncertainty to automatically compute the associated uncertainty in the thermal and electrical efficiencies of the developed hybrid system.

5.6 Validation error analysis

To identify the percentage error between the simulation results (x_i) and the experimental results (y_i), the root mean square percentage error (RMSPE) method is applied as follows [35]:

$$RMSPE = \sqrt{\frac{\sum_{i=1}^{N}\left(\left[\frac{y_i - x_i}{x_i}\right]\right)^2}{N}} \times 100 \tag{12}$$

where N is the sample size.

5.7. Environmental cost analysis

Energy generation and consumption have an influence on the environment through the emission of carbon particles. As a result, the cost of carbon emissions is a significant consideration in the environmental evaluation. Environmental cost analysis is a technique used to measure the amount of CO_2 mitigation and the cost associated with it [35]. Environmental cost analysis is also crucial as it indicates the significance of carbon-free renewable energy technologies [34]. The average equivalent CO_2 emission in a coal-fired power generation is estimated to be 960 g CO_2/kWh. It amounts to 2.08 kg CO_2/kWh when transmission and distribution losses are included, as documented by Zuhur et al. [34]. Hence, the reduction of CO_2 emissions from the developed CPV/T-STEG prototype can be calculated based on the methodology adopted by [36]:

$$Q_{CO_2} = \psi_{CO_2} \times \dot{Q}_{th} \tag{13}$$

In this equation Q_{CO_2} is the amount of mitigated CO_2 per hour, ψ_{CO_2} is the average CO_2 emission from a coal-fired power plant (2.08 kg CO_2/kWh) and $\dot{Q}_{th}$ is the total thermal gain of the hybrid system and it can be calculated as follows:

$$E_{th,overall} = E_{HTF} + \frac{P_{total}}{C_{power}} \tag{14}$$

where E_{HTF} is calculated based on Eq. (7). In the Eq. (10) C_{power} is used to calculate the thermal gain from the electrical gain. The value of C_{power} is considered to be 0.38, which is the conversion power of the thermal power plant. This power is determined by the quality of the coal that has the lowest ash ratio [37]. The environmental cost of CO_2 reduction per hour (EC_{CO_2}) is calculated as follows:

$$EC_{CO_2} = Q_{CO_2} \times P_{CO_2} \tag{15}$$

where P_{CO_2} is the carbon price which is considered as 50 €/tCO_2 for the present study [38].

6. Results and discussion

In this subsection, the findings of numerical modelling and experimental analysis of the thermal and electrical output of the CPVT-STEG prototype are presented and analysed in depth. For the transient simulation and experimental analyses of the developed CPVT-STEG prototype, an optimal number of two TEGs for maximum TEG output power and thermal power is considered based on the 1-D steady-state analytical model developed in our previous study [26].

6.1 Environmental Parameters

The measured GHI and DNI values during the field testing of the prototype are plotted in as shown in Fig. 11. During the testing period, the measured GHI values ranged between 571.38 W/m^2 and 1167.134 W/m^2, whereas the measured DNI values ranged between 275.34 W/m^2 and 800.86 W/m^2. In short, the average values of GHI and DNI received by the hybrid system were 1006.22 W/m^2 and 741.34 W/m^2, respectively. Fig. 12 illustrates the fluctuation in ambient temperature, wind speed, and inflow water temperature throughout the observation period. The ambient temperature ranged between 298.01 K and 311.82 K, while the wind speed ranged between 0 and 4.16 m/s. The temperature fluctuation of the inflow water, including the error band, is given in Fig. 12 and varies between 302.44 K and 305.99 K.

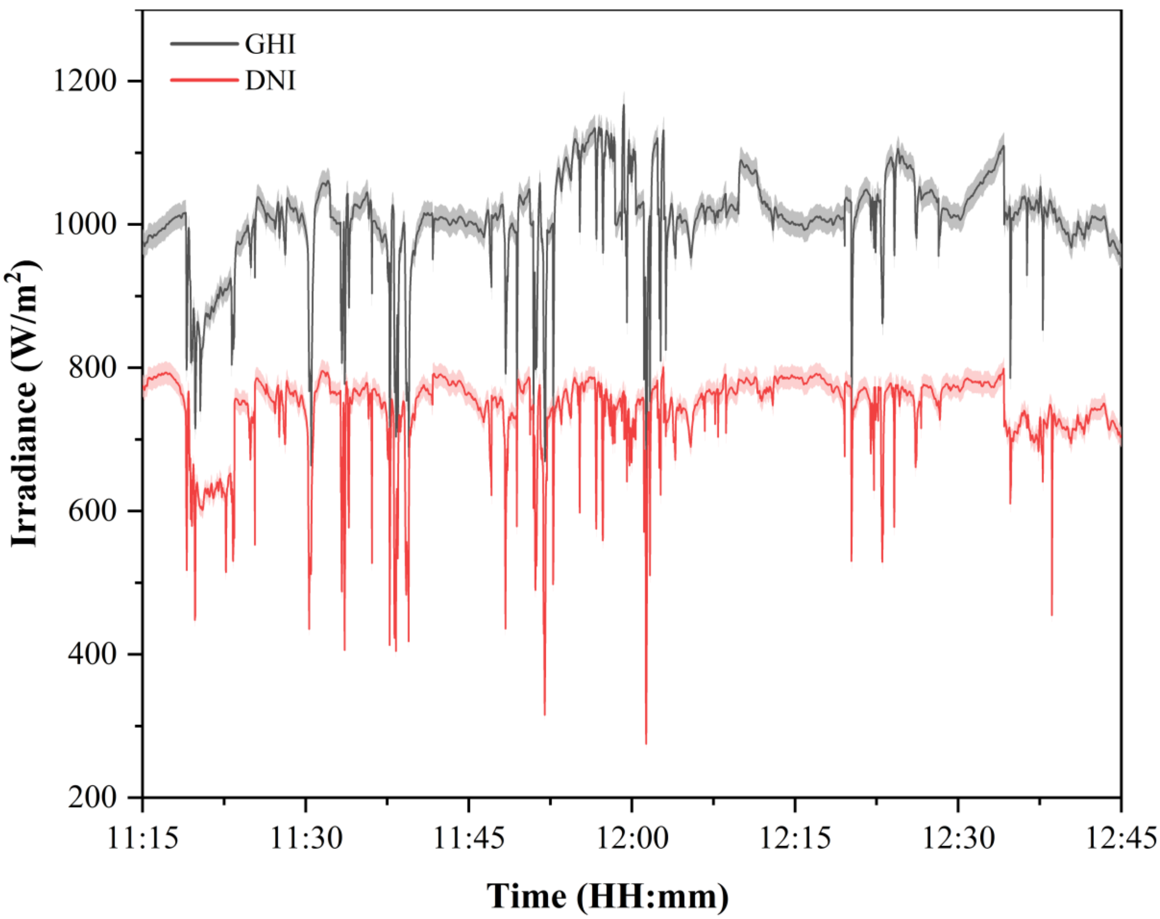

Fig. 11. Variations of GHI and DNI during the period of data collection.

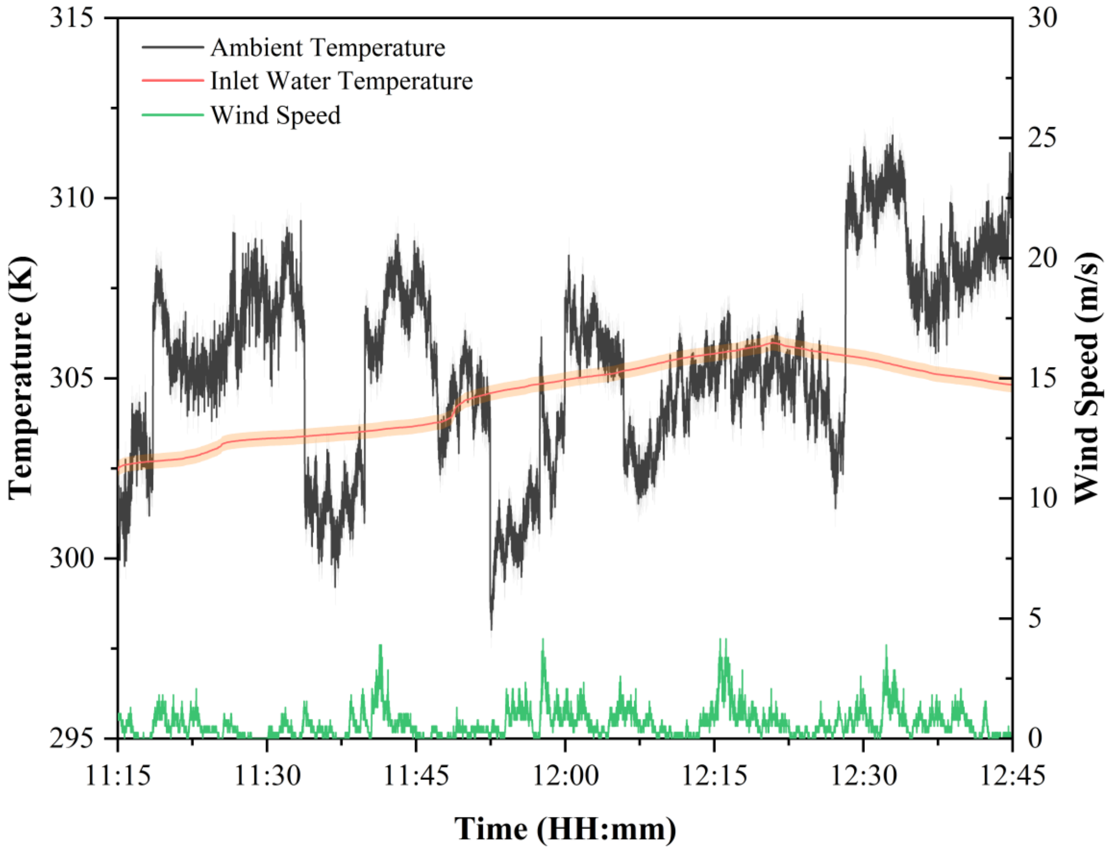

Fig. 12. Variation of ambient temperature, wind speed, and inlet water temperature during the test period.

6.2 PV performance analysis

6.2.1 Temperature of PV cells

The average temperature of the PV cells measured over the course of the test period with the error band for each second is presented in Fig. 13. A maximum temperature of 320.14 K was determined by the measurements for the PV module. Despite being cooled by water at an average inlet temperature of 304.51 K and a flow rate of 3.8 L/min, the average PV temperature over the period of test time was around 318.19 K, which is ~5.6% less as compared to that of a conventional PTC based CPVT-TEG hybrid system [22]. The graph clearly indicates that the temperature of the PV module increases when solar irradiance increases. The same phenomenon is also evident from both Fig. 12 and Fig. 13, where the PV temperature increases proportionally with the water inlet temperature by showing a strong positive correlation. The observed PV temperature was compared to the findings of the transient simulation, and it was found to be in good agreement with a root mean square percent deviation of 1.05 %. The experimental PV temperature is found to be greater than the simulation findings mostly owing to the thermal contact resistance existed between the fluid channel and the PV module, which is caused by the manufacturing faults.

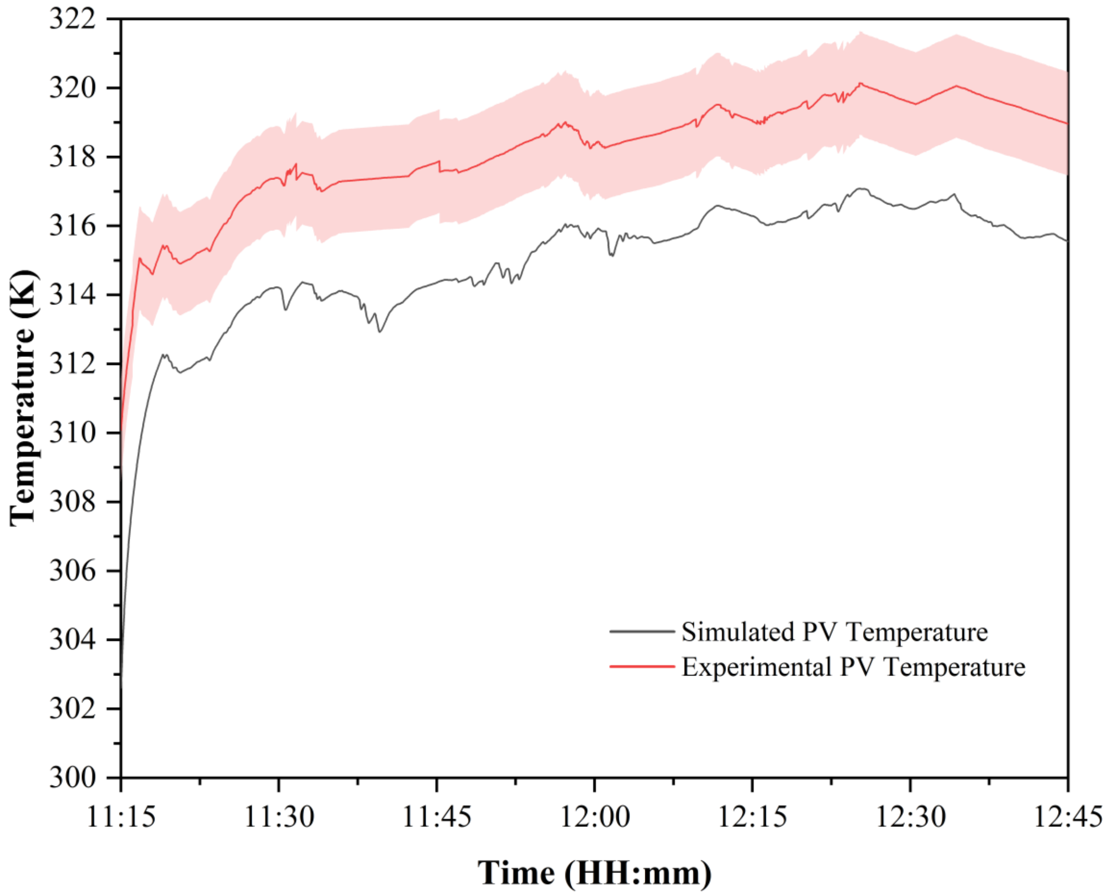

Fig. 13. Simulated and experimental values of PV temperature during the test period.

6.2.2 Current and voltage of the PV module

The maximum values of current and voltage of the PV module are computed using the MATLAB Simulink model based on the measured incident solar irradiance, PV temperature, open-circuit voltage, and short-circuit current. The fluctuation in the maximum output voltage and current of the PV module utilised in the proposed hybrid CPVT-STEG system is depicted in Fig. 14. The graph clearly illustrates that the output current of PV is highly dependent on the GHI values. When the GHI value is 1108.56 W/m^2, the highest PV current recorded is 11.59 A. On the other hand, GHI levels have little effect on the PV voltage. Additionally, as seen in Fig. 14, the PV voltage has a significant inverse relationship with the PV temperature, with a correlation coefficient of -0.92. The observed maximum and minimum output PV voltages are 2.08 V and 1.99 V, respectively.

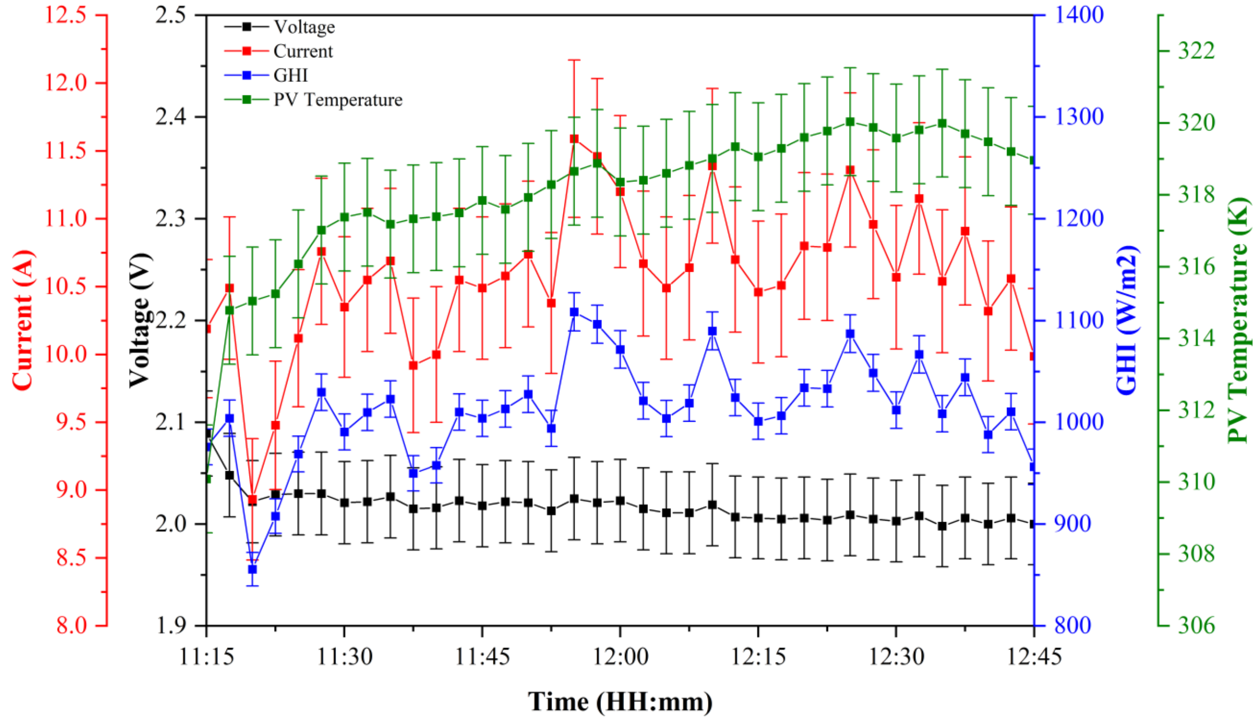

Fig. 14. Experimental variation of current and voltage of the PV during the test period.

6.2.3 I-V and P-V characteristics of PV module

Fig. 15 shows the I-V and P-V characteristic curves of the PV module in the hybrid prototype. The I-V and P-V curves of the PV module are calculated for the maximum DNI value of 800.86 W/m^2 at 12:02:54 pm. The short-circuit current of the PV module increases from 5.40 A to 12.51 A under concentrated sunlight, which is 2.3 times higher than the non-concentrated PV module under STC. The maximum PV output at the DNI of 800.86 W/m^2 is about 24.2 W, which is about 2.1 times higher than the non-concentrated PV module under STC (11.45 W).

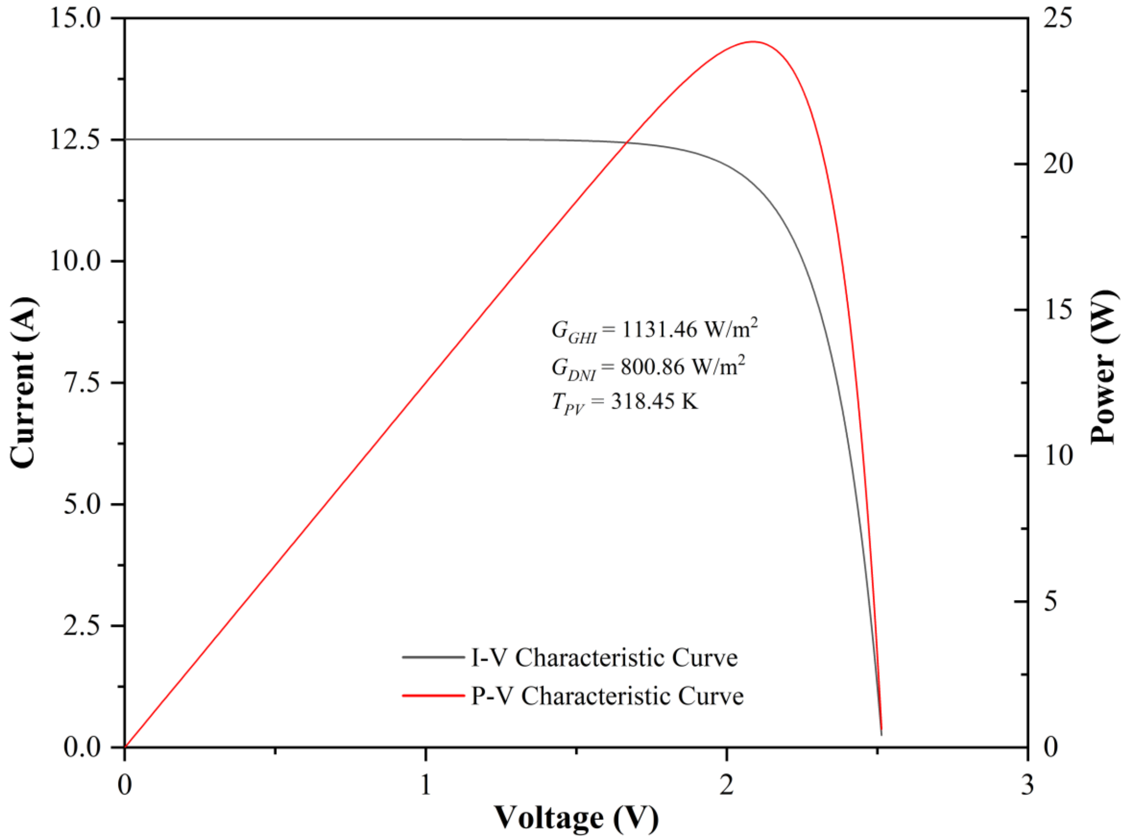

Fig. 15. The I-V and P-V characteristic curves of the PV module in the CPVT-STEG prototype.

6.2.4 PV power and efficiency

Fig. 16 illustrates the variations in PV power and conversion efficiency versus GHI with error bars during the field testing. As both PV power and GHI exhibit the same trend, PV output is directly proportional to input solar irradiance. The maximum simulated photovoltaic power is 25 W. Experimental data shows that PV power ranges from 18.06 W to 24.2 W, with an average of 21.33 W. The experimental results show that the simulation results are quite similar to the experimental data, with a root mean square percent variation of 6.19%.

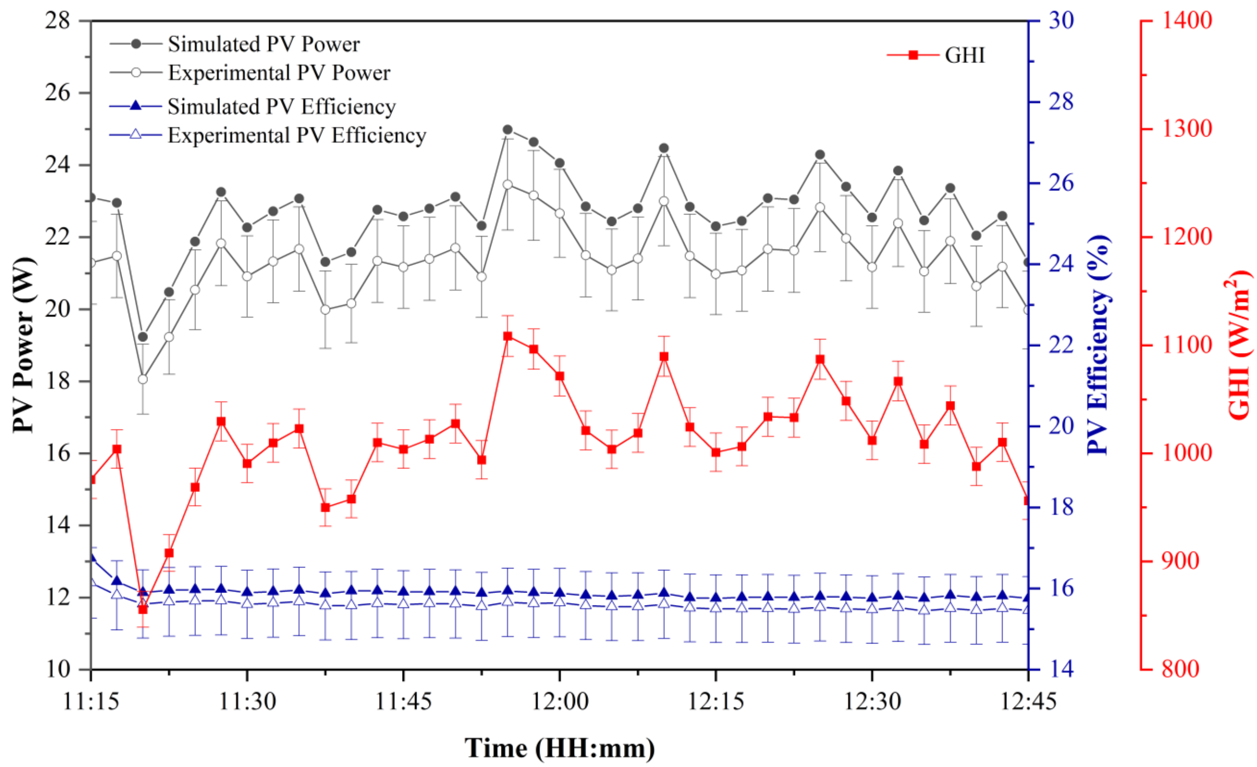

Fig. 16. Simulated and experimental values of PV power and PV efficiency of the CPVT-STEG prototype during the test period.

The highest and average simulated photovoltaic efficiency values are 16.75% and 15.89%, respectively, whereas the maximum and average experimental photovoltaic efficiency values are 16.14% and 15.59% respectively. Correlation analysis showed that there is no strong positive or negative correlation between PV efficiency and GHI. Instead, the PV efficiency has a strong negative correlation with the PV temperature, with a correlation coefficient of -0.9, which means that the PV efficiency decreases as the PV temperature rises. The experimental PV efficiency was satisfactorily confirmed against the simulation results with a root mean square percent variation of 1.89%.

6.3 TEG performance analysis

6.3.1 Temperature across the TEGs

Fig. 17 illustrates the variation of simulated and measured temperatures of the hot and cold sides of the TEGs along with the error band. The hot side temperature of the TEGs depends on the incident DNI values. On the other hand, the cold side temperature of the TEGs depends on the flow rate and temperature of the water at the inlet. The maximum observed hot-side temperature of TEG is 438.53 K and the minimum cold side temperature is 301.03 K. The maximum temperature gradient observed between the TEG hot side and cold side is ΔT=113° C or K, which is 2.8 times greater than the hybrid CPVT-TEG system reported by Riahi et al. [22]. The experimental values of hot side temperature and cold side temperature are well-validated by the simulation results with a root mean square percent error of 1.0% and 1.30%, respectively. The thermal contact resistance generated by the presence of thermocouples in both between the TEG cold side and fluid channel, as well as between the TEG hot side and absorber clamp accounts for the differences between the experimental and simulated TEG temperatures. The optical losses caused by misalignment of the PTC can result in a lower temperature of TEG hot side in the measured results as compared to that of simulation results.

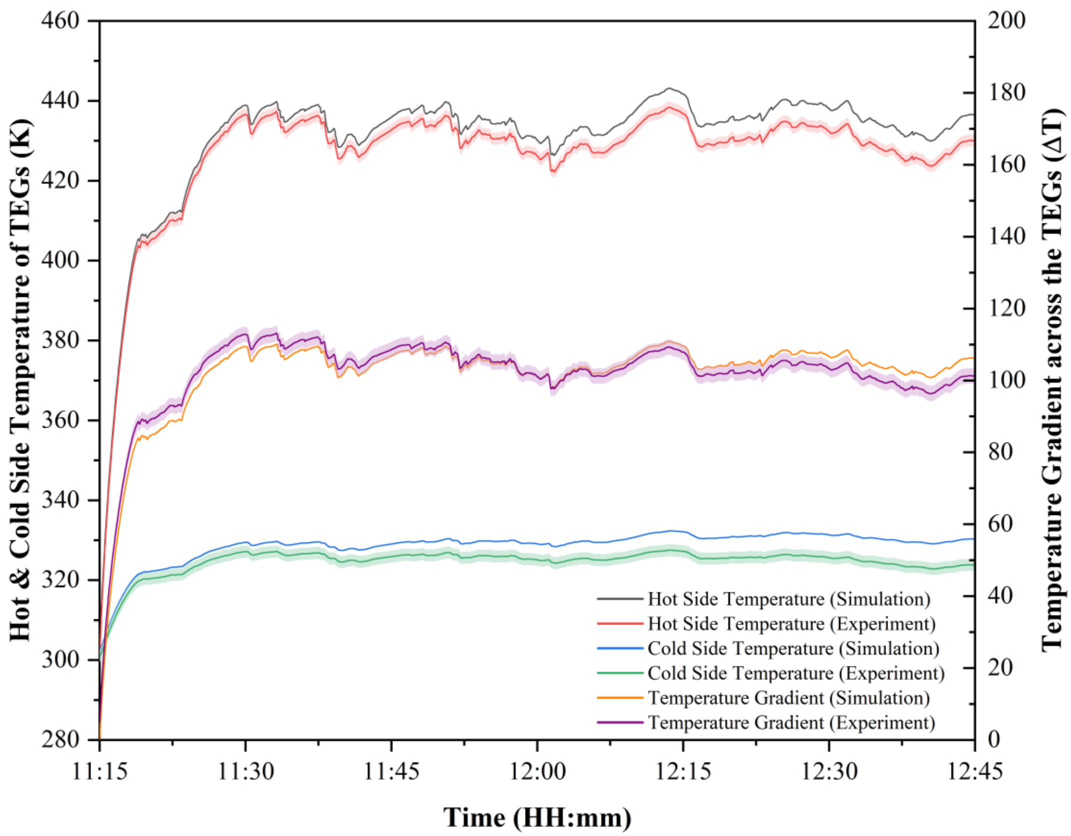

Fig. 17. Simulated and experimental variation of the hot and cold side temperature of TEGs.

6.3.2 Current and voltage of the TEGs

The variations in the measured current and voltage of the TEGs versus local clock time during the test period are depicted in Fig. 18. The experimental results demonstrate that both the measured voltage and current of TEGs are substantially correlated with the temperature gradient of the TEGs, with positive correlation coefficients of 0.99 and 0.98. As a result, more power is generated when the temperature differential across the TEGs is increased. The highest voltage and current detected in the TEGs during the experiment were 5.68 V and 0.63 A, respectively.

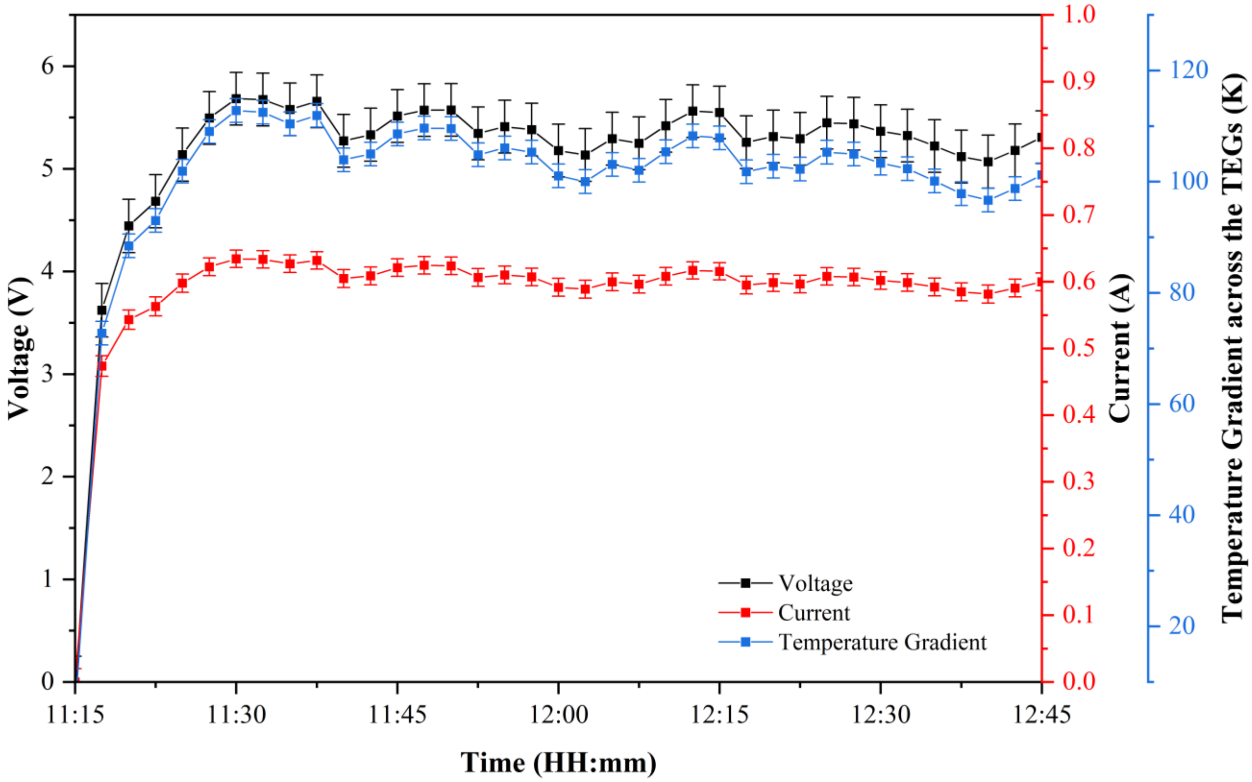

Fig. 18. Experimental variation of measured current and voltage of the TEGs during the test period.

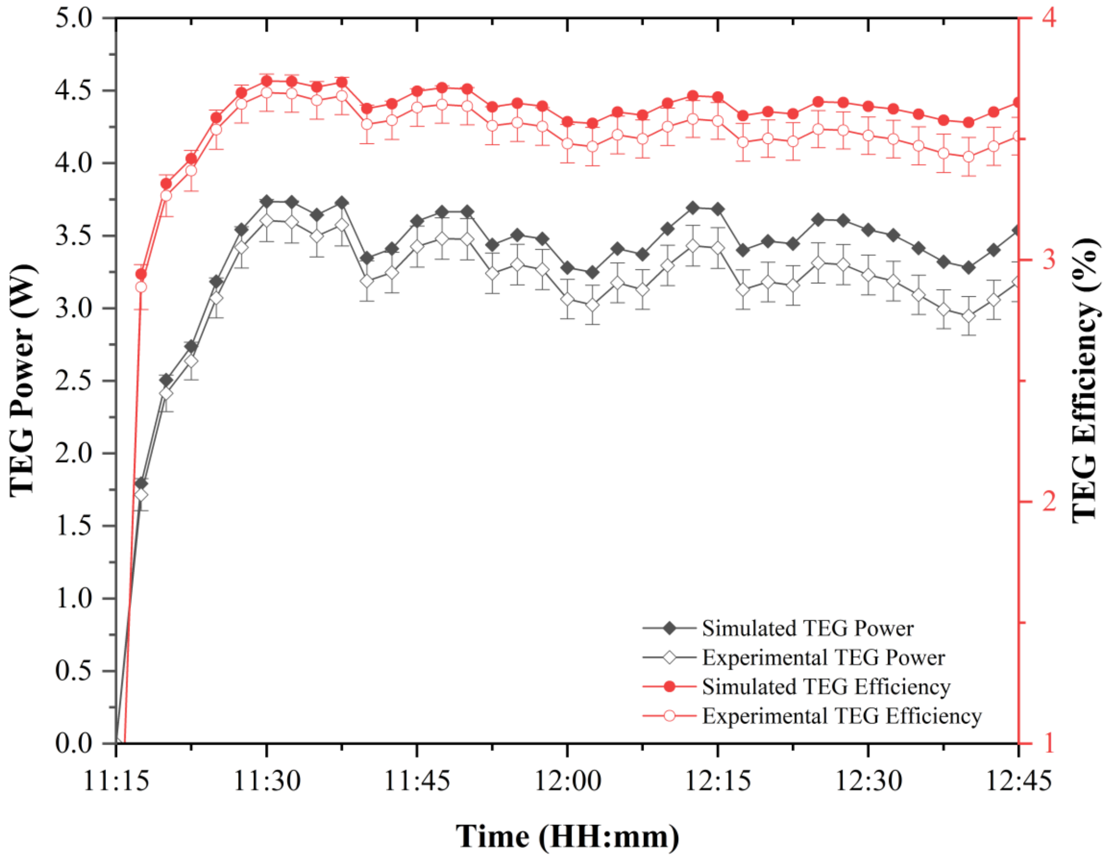

Fig. 19. Simulated and experimental results of TEG power and TEG efficiency during the test period.

As seen in Fig. 19, the TEG efficiency exhibits a similar pattern to the TEG output power. The greatest electrical efficiency of TEG attained through experiments is 3.69 %. The TEG efficiency achieved by transient numerical modelling is also depicted in Fig.19, and it was found to be in good agreement with the experimental data, with a root mean square percent deviation of 2.61%. The maximum TEG efficiency reported in a CPVT-STEG system by Abdo et al. [21] under a 20 sun concentration ratio is 3%, whereas the present hybrid system reached 3.69 % under a solar concentration ratio of 16.6 suns, which is 1.23 times higher.

6.4 Overall electrical and thermal performance of the CPVT-STEG prototype

The simulated and experimental variation of total electrical output power and electrical efficiency with the error bars are depicted in Fig. 20. There were no drastic changes in the net electric power or net electrical efficiency during the test period since the prototype was tracking the sun continuously. The maximum total power obtained during the experimentation is 26.76 W and the average total electrical power is 24.42 W. The maximum electrical efficiency of the hybrid system observed during the test period was 4.86%.

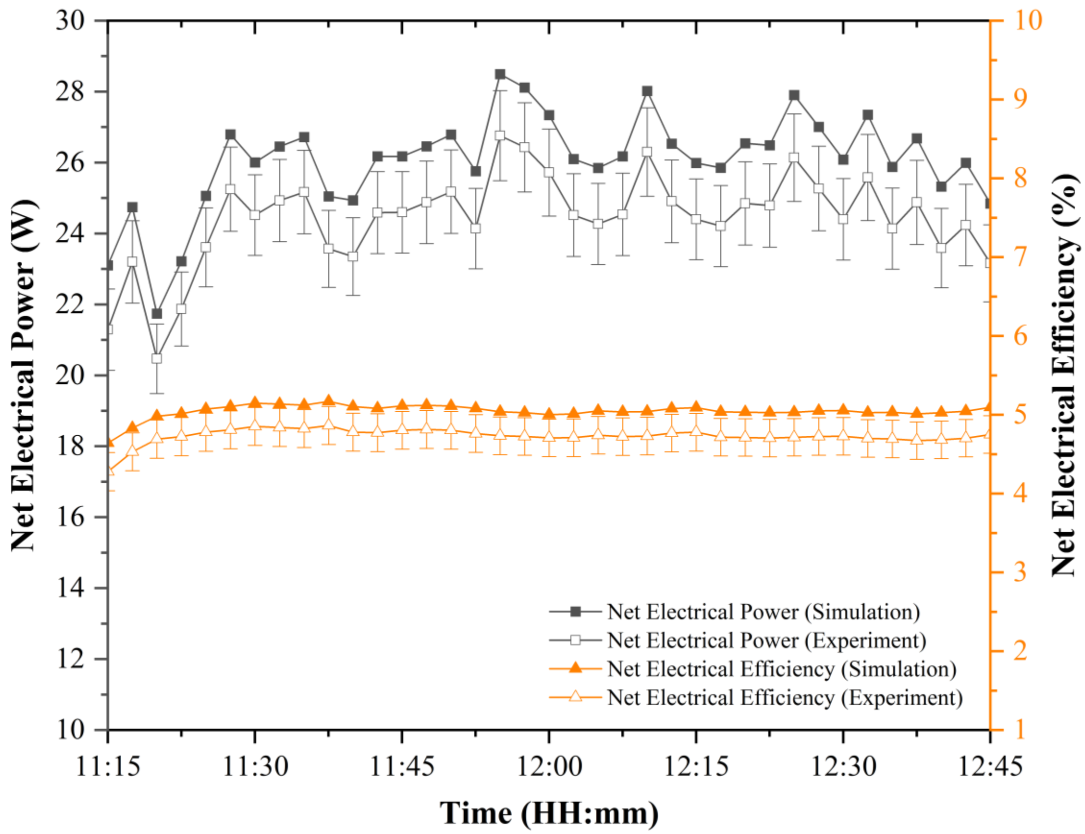

Fig. 20. Simulated and experimental values of overall power and efficiency of the CPVT-STEG prototype during the test period.

Fig. 21 illustrates the fluctuations in the water output temperature and thermal efficiency of the hybrid CPVT-STEG system across the test period with a mass flow rate of 0.0635 kg/s (3.8 L/min). The temperature of the water entering the hybrid system is critical in determining its thermal efficiency. Throughout the test period, the water inflow temperature ranged between 302.44 K and 305.99 K. The peak water temperature measured at the discharge is 306.65 K. Another critical component affecting the thermal efficiency of the system is the temperature rise of the water in the fluid channel. The highest temperature rise obtained in the outlet water is 0.76 K. The increase in water temperature was discovered to have a substantial positive correlation with thermal efficiency, with a correlation value of 0.91. The hybrid system achieved a maximum thermal efficiency of 40% when the solar irradiance is greater than or equal to 1000 W/m^2. The average thermal efficiency of the hybrid system over the course of the trial is about 33.7%. As seen in Fig. 20, the error range for the overall thermal efficiency is slightly larger because of the increased influence of the uncertainty in PT 1000 RTD in detecting the water temperature due to the short distance (540 mm) of the fluid channel. However, the figures of experimental thermal efficiency are corroborated well with the simulated values, with a root mean square percent error of 10.08%. The optical losses caused by slope error and misalignment error in the CPC and PTC also contribute to a lower experimental thermal efficiency as compared to that of the simulation findings.

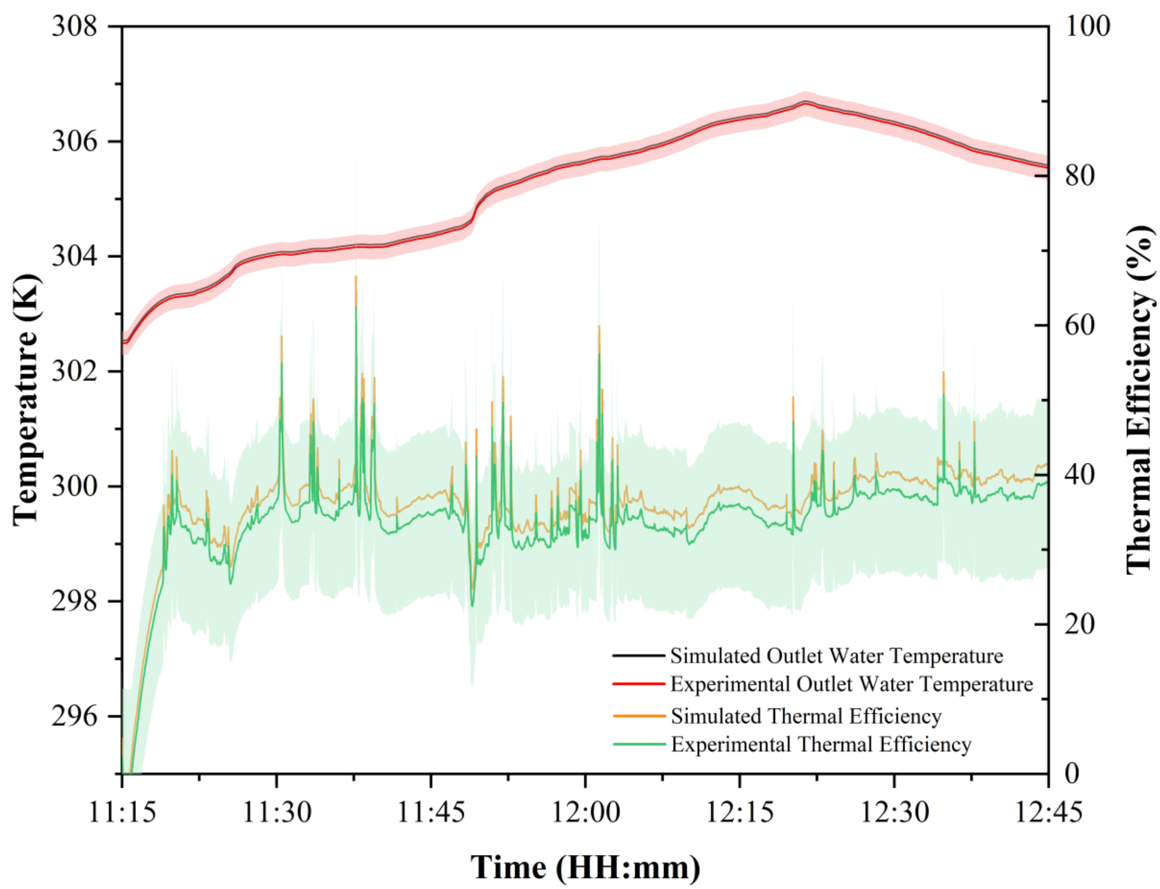

Fig. 21. Simulated and experimental values of water outlet temperature and thermal efficiency during the test period.

A performance comparison between the hybrid CPVT-STEG system and a standalone PV system was performed by considering a 0.51 m^2 mono-crystalline PV module (approx. 32 PV cells) comparable to the aperture area of the hybrid CPVT-STEG prototype. For a 1000 W/m^2 solar irradiance, a standalone PV of 0.51 m^2 area can provide a maximum electric power output of 78.69 W at an efficiency of 15.43% and reach a temperature of 334.4 K (assume: $NOCT = 318.15\ K$; $T_{amb} = 303.15\ K$). On the other hand, the overall power conversion efficiency of the developed hybrid prototype, including electrical and thermal output, is about 4.86% + 40%, which is 3 times higher compared to standalone PV.

The electrical efficiency of the hybrid CPVT-STEG system is 68.5% lower than the standalone PV system. The lower power conversion efficiency of the TEG (3.69%) and the PTC area that is used to focus the sunlight onto the TEG has greatly discounted the overall electrical efficiency of the hybrid system. Nevertheless, the benefits of the hybrid CPVT-STEG system over the standalone PV system are to provide an additional recovery of thermal energy and lower the PV temperature. Besides the direct focused sunlight, the TEG can also harvest the radiative heat from the surrounding environment. The choice between a standalone PV system and a hybrid CPVT-STEG system is determined completely by the specific needs of the application.

A comparison analysis between the developed CPVT-STEG prototype and a similar CPVT-TEG hybrid solar system that uses PTC and mono-crystalline silicon PV cells was performed. The hybrid CPVT-TEG system studied in [22] uses a PTC with a reflectivity 0.89, and the electrical efficiency is estimated as 7.27% if only DNI is considered in the input power. The maximum electrical output of the developed CPVT-STEG prototype can be normalized to 35.5 W at 0.89 reflectivity. The maximum electrical efficiency of the prototype by considering only the DNI (765 W/m^2) in the input is about 9.1% which shows the superiority of the developed CPVT-STEG hybrid system.

6.5 Exergy of the developed CPVT-STEG prototype

The exergy efficiency of the developed prototype during the test period is depicted in Fig. 22. The experimental effectiveness of exergy is between 4.37 % and 5.85 %. The average efficiency of exergy during the test period was found to be 5%. The low exergy efficiency is mostly owing to the small-scale experimental setup, which results in a lower rise in water temperature. Thus, in the case of a large-scale hybrid system with a longer fluid channel and an optimal fluid flow rate, the fluid temperature may be significantly increased, thereby increasing the exergy efficiency. Additionally, research demonstrates that both the numerical simulation and experimental data were well-validated, with a root mean square percent error of 6.3 %.

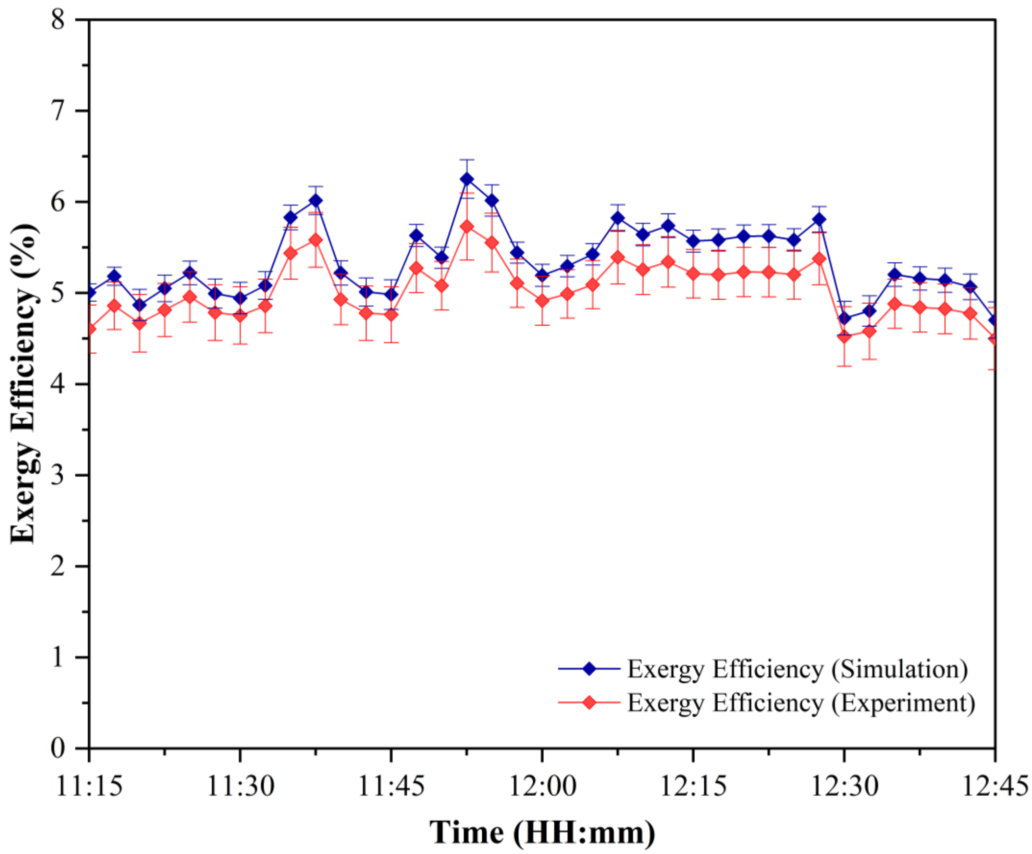

Fig. 22. Simulated and experimental variation of overall exergy efficiency during the test period.

6.6 Repeatability test

In order to ensure the performance repeatability of the developed prototype, the experiments have been repeated five times on different days during the noon time with good DNI and GHI values. Fig. 23 shows the variation in PV temperature, PV performance, TEG performance, and thermal performance measured for five different days with DNI ranging between 764.66 W/m^2 and 800.868 W/m^2. The graphs in Fig. 23 show that the successive measurements of the PV temperature, PV performance, TEG performance, and thermal efficiency are similar under the DNI values of 764.66 W/m^2 to 800.868 W/m^2, thus ensuring the repeatability of the experimental results.

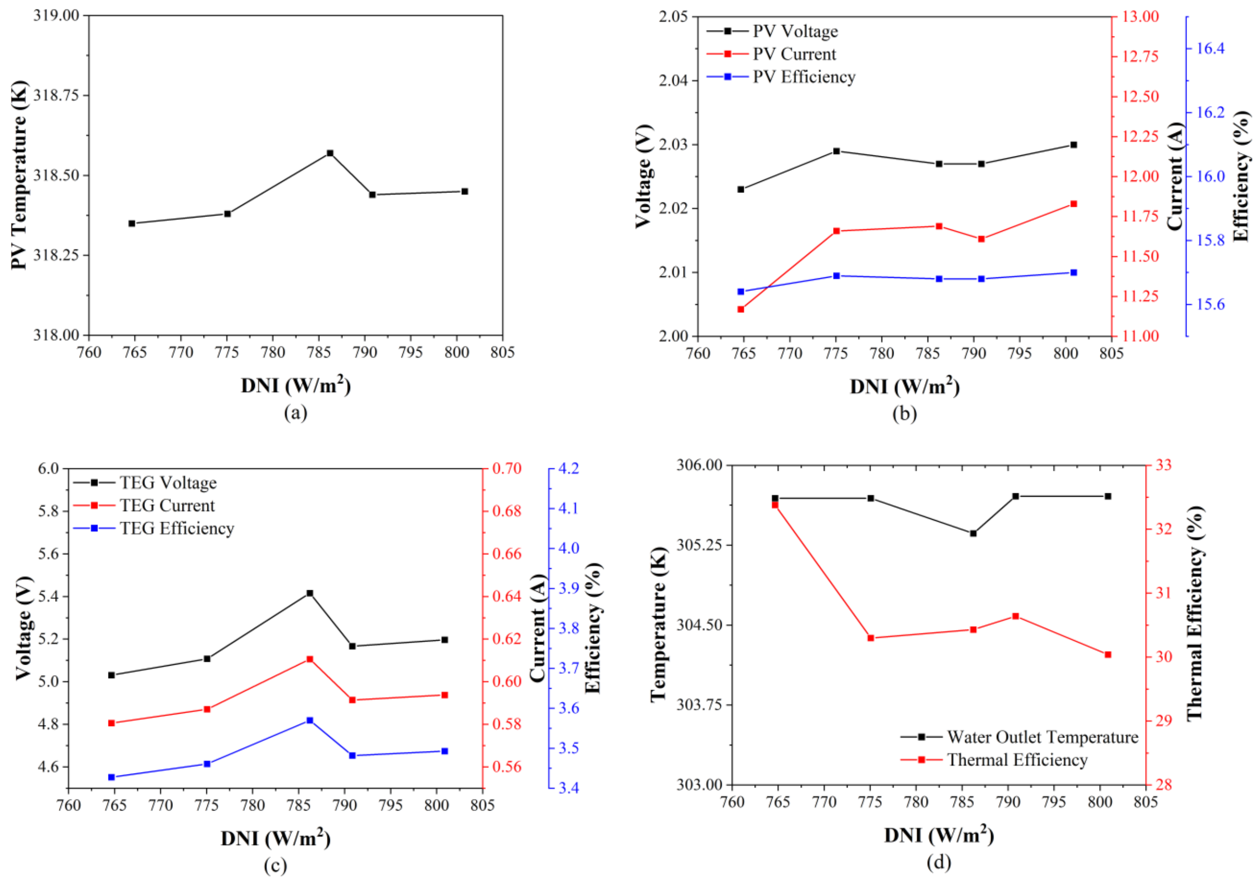

Fig. 23. The experimental results of the CPVT-STEG prototype under DNI from 764.66 W/m^2 to 800.868 W/m^2 for different days in the repeatability tests.

6.7 Environmental cost analysis

The environmental cost analysis in the present study has been done using carbon emissions and carbon pricing. The amount of mitigated carbon emissions during the test period is shown in Fig. 24. The environmental cost savings associated with avoiding CO_2 emissions were estimated using Eq. (15) as shown in Fig. 24. According to the experimentation results, the average CO_2 mitigation during the test period is 0.5 kg/h, and an average environmental cost savings of up to 0.025 €/h has been obtained.

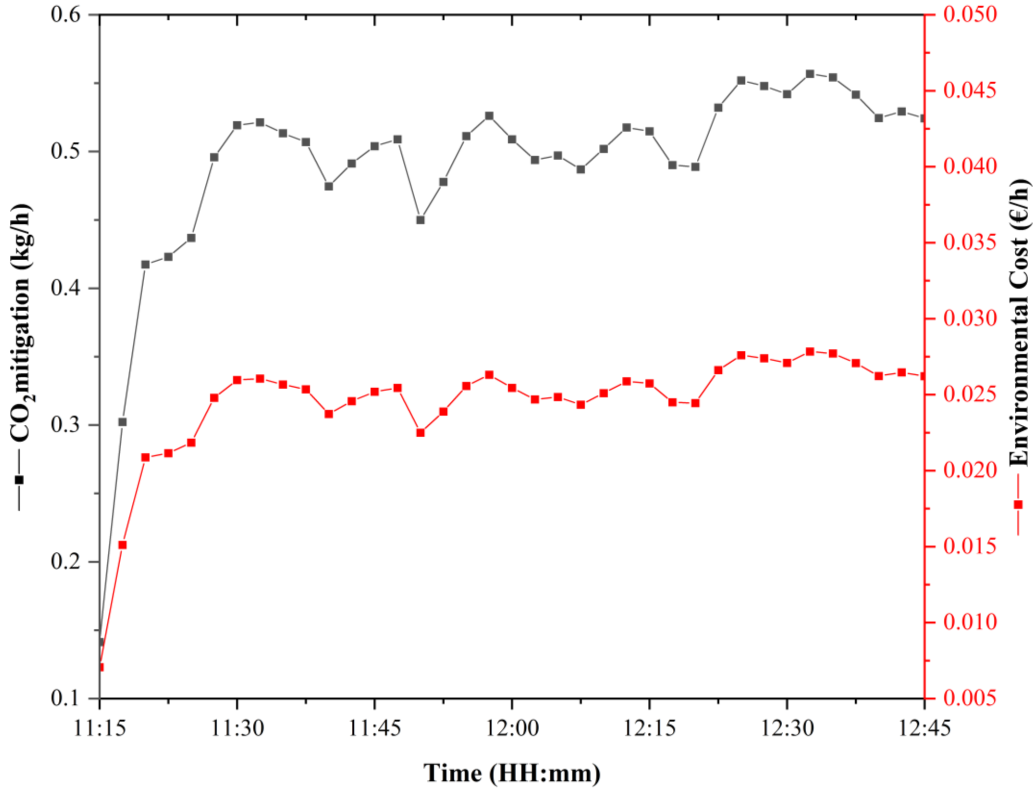

Figure 24. CO_2 reduction and environmental cost saving per hour

6.8 Challenges and Outlook

The efficiency of the developed CPVT-STEG hybrid system is limited by the reflectivity (67%) of the concentrator material used. The electrical and thermal efficiency can be further improved if a reflective material with a reflectivity of more than 90% is used. The electrical efficiency of the CPVT-STEG is also restricted by the number of TEG modules used and its lower efficiency. The optimal number of TEGs used for a maximum power output in a 540 mm long channel is two, and the remaining space is left insulated and unutilised. Hence, solar cells with higher efficiency can replace the TEGs on the rear side of the channel in the prototype to achieve higher overall electrical efficiency. The performance of the CPVT-STEG system can be further enhanced by optimising the design of fluid channels and using highly conductive heat transfer fluids.

In addition to the direct sunlight reflected by PTC, the TEG modules in the prototype can also harvest waste heat from other energy sources through radiation. It is possible if the prototype system is positioned at a geothermal site with hot steam from hot spring water, which can be explored in future work. The developed hybrid structure has the potential to remodel the existing PTC-based solar power plants as CPVT or hybrid CPVT-STEG systems to increase the power production per unit area. Finally, economic and environmental studies can be conducted to evaluate the commercial feasibility of the hybrid prototype. The viability of redesigning existing PTC-based solar power plants requires a comprehensive optimization and techno-economic study of the hybrid prototype.

7. Conclusion

In this research work, we have constructed the prototype of a CPC and PTC based hybrid CPVT-STEG system with an optimal quantity of TEG modules for a maximum TEG output. The performance of prototype was evaluated in terms of thermal and electrical efficiencies. The prototype was tested under outdoor operating conditions during a sunny day where the measured results were compared and validated with transient numerical simulation. The major findings of the experiment can be summarised as follows:

- The average PV temperature during the test period is 318.19 K which is 5.6% less than the PV temperature in the PTC based CPVT-TEG system studied by Riahi et al. [22].
- The maximum TEG efficiency of the hybrid system is 3.69% which is 1.23 times higher as compared with that of the CPVT-STEG system reported by Abdo et al. [21].
- The peak overall efficiency observed during experimentation is 44.86% which is 3 times higher as compared to that of standalone PV system.
- The average exergy efficiency of the hybrid CPVT-STEG prototype during the test period was found to be 5%.
- The proposed hybrid system can reduce carbon emissions by 0.5 kg/h with an associated environmental cost of 0.025 €/h, and thus the idea can contribute to the United Nations Sustainable Development Goals.

Acknowledgement

The authors would like to express gratitude to the Taylor's University Flagship Research Grant (TUFR/2017/001/01) and the Taylor's PhD. Scholarship Program for their support. This research was funded in part by the Fundamental Research Grant Scheme (FRGS/1/2019/TK10/TAYLOR/02/1) from the Ministry of Higher Education, Government of Malaysia.

References

[1] A. Zahedi, Review of modelling details in relation to low-concentration solar concentrating photovoltaic, Renew. Sustain. Energy Rev. 15 (2011) 1609–1614. doi:10.1016/j.rser.2010.11.051.

[2] E. Skoplaki, J.A. Palyvos, Operating temperature of photovoltaic modules: A survey of pertinent correlations, Renew. Energy. 34 (2009) 23–29. doi:10.1016/j.renene.2008.04.009.

[3] S. Manikandan, C. Selvam, N. Poddar, K. Pranjyal, R. Lamba, S.C. Kaushik, Thermal management of low concentrated photovoltaic module with phase change material, J. Clean. Prod. 219 (2019) 359–367. doi:10.1016/j.jclepro.2019.02.086.

[4] O.Z. Sharaf, M.F. Orhan, Concentrated photovoltaic thermal (CPVT) solar collector systems: Part I - Fundamentals, design considerations and current technologies, Renew. Sustain. Energy Rev. 50 (2015) 1500–1565. doi:10.1016/j.rser.2015.05.036.

[5] S. Sripadmanabhan Indira, C.A. Vaithilingam, K.K. Chong, R. Saidur, M. Faizal, S. Abubakar, S. Paiman, A review on various configurations of hybrid concentrator photovoltaic and thermoelectric generator system, Sol. Energy. 201 (2020) 122–148. doi:10.1016/j.solener.2020.02.090.

[6] S. Shittu, G. Li, Y.G. Akhlaghi, X. Ma, X. Zhao, E. Ayodele, Advancements in thermoelectric generators for enhanced hybrid photovoltaic system performance, Renew. Sustain. Energy Rev. 109 (2019) 24–54. doi:10.1016/j.rser.2019.04.023.

[7] C. Babu, P. Ponnambalam, The role of thermoelectric generators in the hybrid PV/T

systems: A review, Energy Convers. Manag. 151 (2017) 368–385. doi:10.1016/j.enconman.2017.08.060.

[8] R. Bjørk, K.K. Nielsen, The performance of a combined solar photovoltaic (PV) and thermoelectric generator (TEG) system, Sol. Energy. 120 (2015) 187–194. doi:10.1016/j.solener.2015.07.035.

[9] T. Cui, Y. Xuan, Q. Li, Design of a novel concentrating photovoltaic-thermoelectric system incorporated with phase change materials, Energy Convers. Manag. 112 (2016) 49–60. doi:10.1016/j.enconman.2016.01.008.

[10] A. Rezania, D. Sera, L.A. Rosendahl, Coupled thermal model of photovoltaic-thermoelectric hybrid panel for sample cities in Europe, Renew. Energy. 99 (2016) 127–135. doi:10.1016/j.renene.2016.06.045.

[11] W. Lin, T.M. Shih, J.C. Zheng, Y. Zhang, J. Chen, Coupling of temperatures and power outputs in hybrid photovoltaic and thermoelectric modules, Int. J. Heat Mass Transf. 74 (2014) 121–127. doi:10.1016/j.ijheatmasstransfer.2014.02.075.

[12] E. Yin, Q. Li, Y. Xuan, Thermal resistance analysis and optimization of photovoltaic-thermoelectric hybrid system, Energy Convers. Manag. 143 (2017) 188–202. doi:10.1016/j.enconman.2017.04.004.

[13] S. Su, T. Liu, Y. Wang, X. Chen, J. Wang, J. Chen, Performance optimization analyses and parametric design criteria of a dye-sensitized solar cell thermoelectric hybrid device, Appl. Energy. 120 (2014) 16–22. doi:10.1016/j.apenergy.2014.01.048.

[14] T. Cui, Y. Xuan, E. Yin, Q. Li, D. Li, Experimental investigation on potential of a concentrated photovoltaic-thermoelectric system with phase change materials, Energy. 122 (2017) 94–102. doi:10.1016/j.energy.2017.01.087.

[15] E. Yin, Q. Li, D. Li, Y. Xuan, Experimental investigation on effects of thermal resistances on a photovoltaic-thermoelectric system integrated with phase change materials, Energy. 169 (2019) 172–185. doi:10.1016/j.energy.2018.12.035.

[16] J. Zhang, H. Zhai, Z. Wu, Y. Wang, H. Xie, M. Zhang, Enhanced performance of photovoltaic–thermoelectric coupling devices with thermal interface materials, Energy

Rep. 6 (2020) 116–122. doi:10.1016/j.egyr.2019.12.001.

[17] A. Lekbir, S. Hassani, M.R. Ab Ghani, C.K. Gan, S. Mekhilef, R. Saidur, Improved energy conversion performance of a novel design of concentrated photovoltaic system combined with thermoelectric generator with advance cooling system, Energy Convers. Manag. 177 (2018) 19–29. doi:10.1016/j.enconman.2018.09.053.

[18] S. Soltani, A. Kasaeian, T. Sokhansefat, M.B. Shafii, Performance investigation of a hybrid photovoltaic/thermoelectric system integrated with parabolic trough collector, Energy Convers. Manag. 159 (2018) 371–380. doi:10.1016/j.enconman.2017.12.091.

[19] M. Mohsenzadeh, M.B. Shafii, H. Jafari mosleh, A novel concentrating photovoltaic/thermal solar system combined with thermoelectric module in an integrated design, Renew. Energy. 113 (2017) 822–834. doi:10.1016/j.renene.2017.06.047.

[20] E. Yin, Q. Li, Y. Xuan, Experimental optimization of operating conditions for concentrating photovoltaic-thermoelectric hybrid system, J. Power Sources. 422 (2019) 25–32. doi:10.1016/j.jpowsour.2019.03.034.

[21] A. Abdo, S. Ookawara, M. Ahmed, Performance evaluation of a new design of concentrator photovoltaic and solar thermoelectric generator hybrid system, Energy Convers. Manag. 195 (2019) 1382–1401. doi:10.1016/j.enconman.2019.04.093.

[22] A. Riahi, A. Ben Haj Ali, A. Fadhel, A. Guizani, M. Balghouthi, Performance investigation of a concentrating photovoltaic thermal hybrid solar system combined with thermoelectric generators, Energy Convers. Manag. 205 (2020). doi:10.1016/j.enconman.2019.112377.

[23] S. Shittu, G. Li, X. Zhao, X. Ma, Y.G. Akhlaghi, Y. Fan, Comprehensive study and optimization of concentrated photovoltaic-thermoelectric considering all contact resistances, Energy Convers. Manag. 205 (2020) 112422. doi:10.1016/j.enconman.2019.112422.

[24] O. Rejeb, S. Shittu, C. Ghenai, G. Li, X. Zhao, M. Bettayeb, Optimization and performance analysis of a solar concentrated photovoltaic-thermoelectric (CPV-TE) hybrid system, Renew. Energy. 152 (2020) 1342–1353. doi:10.1016/j.renene.2020.02.007.

[25] S. Sripadmanabhan Indira, C.A. Vaithilingam, R. Sivasubramanian, K.K. Chong, R. Saidur, K. Narasingamurthi, Optical performance of a hybrid compound parabolic concentrator and parabolic trough concentrator system for dual concentration, Sustain. Energy Technol. Assessments. 47 (2021) 101538. doi:10.1016/j.seta.2021.101538.

[26] S. Sripadmanabhan Indira, C.A. Vaithilingam, K. Narasingamurthi, R. Sivasubramanian, K.-K. Chong, R. Saidur, Mathematical modelling , performance evaluation and exergy analysis of a hybrid photovoltaic / thermal-solar thermoelectric system integrated with compound parabolic concentrator and parabolic trough concentrator, Appl. Energy. 320 (2022) 119294. doi:10.1016/j.apenergy.2022.119294.

[27] J. Macedo-Valencia, J. Ramírez-Ávila, R. Acosta, O.A. Jaramillo, J.O. Aguilar, Design, construction and evaluation of parabolic trough collector as demonstrative prototype, Energy Procedia. 57 (2014) 989–998. doi:10.1016/j.egypro.2014.10.082.

[28] D. Yadav, P. Azad, R. Vaish, Solar Energy Harvesting using Candle- Soot- Coated Thermoelectric Materials, Glob. Challenges. 4 (2020) 1900080. doi:10.1002/gch2.201900080.

[29] K.K. Chong, T.K. Yew, C.W. Wong, M.H. Tan, W.C. Tan, B.H. Lim, Dense-array concentrator photovoltaic prototype using non-imaging dish concentrator and an array of cross compound parabolic concentrators, Appl. Energy. 204 (2017) 898–911. doi:10.1016/j.apenergy.2017.03.108.

[30] A. Montecucco, J. Siviter, A.R. Knox, The effect of temperature mismatch on thermoelectric generators electrically connected in series and parallel, Appl. Energy. 123 (2014) 47–54. doi:10.1016/j.apenergy.2014.02.030.

[31] N.A. Bakhari, N.A. Hamid, A.R. Syafeeza, Y.C. Wong, M. Ibrahim, Simulation and analysis of flexible TEG using polymer based and pyroelectric material for microdevice energy harvesting, J. Phys. Conf. Ser. 1502 (2020). doi:10.1088/1742-6596/1502/1/012022.

[32] C. Haiping, L. Haowen, Z. Heng, L. Kai, G. Xinxin, Y. Boran, Numerical simulation and experimental analysis of an LCPV/T system under real operating conditions, J. Clean.

Prod. 209 (2019) 903–915. doi:10.1016/j.jclepro.2018.10.256.

[33] M. Valizadeh, F. Sarhaddi, Mahdavi Adeli, Exergy performance assessment of a linear parabolic trough photovoltaic thermal collector, Renew. Energy. 138 (2019) 1028–1041. doi:10.1016/j.renene.2019.02.039.

[34] S. Zuhur, İ. Ceylan, A. Ergün, Energy, exergy and environmental impact analysis of concentrated PV/cooling system in Turkey, Sol. Energy. 180 (2019) 567–574. doi:10.1016/j.solener.2019.01.060.

[35] N. Gakkhar, M.K. Soni, S. Jakhar, Experimental and theoretical analysis of hybrid concentrated photovoltaic/thermal system using parabolic trough collector, Appl. Therm. Eng. 171 (2020) 115069. doi:10.1016/j.applthermaleng.2020.115069.

[36] R. Tripathi, G.N. Tiwari, V.K. Dwivedi, Overall energy, exergy and carbon credit analysis of N partially covered Photovoltaic Thermal (PVT) concentrating collector connected in series, Sol. Energy. 136 (2016) 260–267. doi:10.1016/j.solener.2016.07.002.

[37] I. Ceylan, A.E. Gürel, A. Ergün, A. Tabak, Performance analysis of a concentrated photovoltaic and thermal system, Sol. Energy. 129 (2016) 217–223. doi:10.1016/j.solener.2016.02.010.

[38] Value of Carbon Market Update 2021, Carbon Credit Cap. (n.d.). https://carboncreditcapital.com/value-of-carbon-market-update-2021-2/ (accessed March 6, 2022).

Prototype of a novel hybrid concentrator photovoltaic/thermal and solar thermoelectric generator system for outdoor study

Sridhar Sripadmanabhan Indira[1*], Chockalingam Aravind Vaithilingam[1*], Ramsundar Sivasubramanian[1], Kok-Keong Chong[2], Kulasekharan Narasingamurthi[3], R. Saidur [4,5]

[1] School of Engineering, Faculty of Innovation and Technology, Taylor's University Lakeside Campus, No. 1, Jalan Taylor's, 47500 Subang Jaya, Selangor, Malaysia.
[2] Lee Kong Chian Faculty of Engineering and Science, Universiti Tunku Abdul Rahman, Bandar Sungai Long, 43000 Kajang, Selangor, Malaysia.
[3] Metier Technical Leader, Valeo India Private Limited, No. 63, Rajiv Gandhi Salai, Navallur, Chennai – 600130, India.
[4] Research Centre for Nano-Materials and Energy Technology (RCNMET), School of Engineering and Technology, Sunway University, 47500 Subang Jaya, Malaysia.
[5] Department of Engineering, Lancaster University, Lancaster LA1 4YW, UK.

*Corresponding authors.

E-mail addresses: sridharsripadmanabhannadarindira@sd.taylors.edu.my, sibisri819@gmail.com (S. S Indira), chockalingamaravind.vaithilingam@taylors.edu.my, aravindcv@ieee.org (C.A. Vaithilingam).

Abstract

In this study, a novel prototype of a hybrid concentrator photovoltaic/thermal and solar thermoelectric generator system has been designed and constructed for combined heat and power production. In the developed hybrid system, both the solar cells and thermoelectric modules that share a common heat transfer medium are exposed to concentrated irradiance via a compound parabolic concentrator and a parabolic trough concentrator, respectively. To assess the performance of the hybrid system, a prototype of the hybrid system was built and tested under outdoor operating conditions, and the findings were compared with those of a transient numerical simulation conducted using ANSYS Fluent. The average PV temperature obtained during the test period at a flow rate of 3.8 L/min is 318.19 K which is ~5.6 % lesser compared with a conventional hybrid CPVT-TEG system. The outdoor trials show maximum electrical efficiency of 4.86 % and thermal efficiency of 40% when the solar irradiance is greater than or equal to 1000 W/m^2. The overall power conversion efficiency of the developed prototype is 3 times higher compared to a standalone PV system. The hybrid system helps to reduce carbon emission by 0.5 kg/h, with an associated environmental cost of 0.025 €/h.

Keywords: Thermoelectric generator; Concentrator photovoltaic/thermal; Hybrid system; Prototype development; Experimental analysis; Transient simulation

Nomenclature

A	area
C_p	specific heat capacity
D_h	hydraulic diameter
E	thermal energy (W)
EC	environmental cost
$\dot{E}x$	Exergy rate
f	friction coefficient
G	solar radiation
I	current
L	length
m	mass flow rate
N	sample size
P_{CO_2}	carbon price
Re	Reynolds number
T	temperature
T_h	hot side temperature of TEG
T_c	cold side temperature of TEG
T_{Sun}	surface temperature of sun
V	velocity / voltage

Greek Symbols

η	efficiency
ϱ_f	density of HTF
ψ_{CO_2}	average CO_2 emission

Subscripts

amb	ambient
DNI	direct normal irradiance
ex	exergy
el	electrical
GHI	global horizontal irradiance
in	inlet/input
m	maximum
oc	open-circuit
out	outlet/output

sc	short-circuit
th	thermal

Abbreviations

CPV	Concentrator Photovoltaics
CPVT	Concentrator Photovoltaic/Thermal
EMR	Eliminating Multiple Reflections
HTF	Heat Transfer Fluid
NOCT	Nominal Operating Cell Temperature
PV	Photovoltaic
PCM	Phase Changing Material
STEG	Solar Thermoelectric Generator
TEC	Thermoelectric Cooler
TEG	Thermoelectric Generator

1. Introduction

Solar photovoltaic (PV) technology has advanced rapidly in recent decades due to the increased global demand for renewable energy to reduce greenhouse gas emissions. The PV technology requires a large land area to compensate for the moderate power conversion efficiency of the commercial silicon solar cells. Concentrator photovoltaics (CPV) is a new generation of PV technology with the idea of using cost-effective reflective mirrors or concentrating lenses to enhance the yield intensity of commercial solar cells [1]. The solar cell's efficiency drops by 0.2 % to 0.5 % for every 1°C rise in temperature, making CPV technology vulnerable to high temperatures [2]. A temperature gradient in the CPV cell can lead to hotspots which degrade the performance of the CPV at high rates [3]. Therefore, various hybrid systems, including PV-TEG, CPVT, CPV-TEG, and CPVT-TEG have been proposed to increase the performance by boosting the power production via converting the excess heat into electricity and useful thermal energy. The CPVT system can resolve the inherent drawbacks of high temperature issue in CPVs and low thermal energy in PVTs by harnessing the unutilized excess heat [4]. In hybrid CPV-TEG and CPV/T-TEG systems, the TEGs are introduced to transform the surplus heat from the PV into electric power. Several studies suggest that the overall power output of PV-TEG, CPV-TEG, and CPVT-TEG systems have increased in comparison to a standalone PV system [5].

The purpose of introducing the TEG on the rear side of the PV is to compensate the power loss in PV attributed to high operating temperature [6]. In comparison to standalone PV, solar TEG, and PV/T systems, the amount of power produced by hybrid PV-TEG systems is much greater [7]. However, there are a few studies that have reported negative results in a combination of TEG and PV. With the poor conversion efficiency of TEG, the reduction of PV performance with increasing temperature was reported to be faster than the increase in power generated by TEG [8]. It was discovered that the overall efficiency of hybrid CPV-TEG decreases with an increase in temperature, regardless of the ZT of TEG [9]. In most of the existing hybrid systems, the TEG is positioned between the PV and the heat sink, which leads to a competing relationship between the PV cells and TEGs because the PV cell requires a lower temperature for a better efficiency, whereas the hot side of the TEGs requires a higher temperature for a higher temperature gradient [10]. According to Lin et al. [11], a higher efficiency of PV-TEG is only possible if TEG has a low thermal conductivity and a high Seebeck coefficient. Yin et al. [12] included the thermal resistance concept into the theoretical model of a CPV-TEG hybrid system with different types of PV cells and cooling technologies to optimise the performance of the hybrid system. The results demonstrated that the water-cooled hybrid system consisting of an amorphous silicon PV cell or a polymer PV cell and a TEG with increased thermal resistance is superior in performance.

Su et al. [13] and Cui et al. [9] discovered an ideal operating temperature at which the TEG output equals the reduced power output of the PV and thus it can lead to the improved overall efficiency of the hybrid system. Later, Cui et al. [14] introduced PCM in between the PV and TEG in a hybrid CPV-TEG system to maintain the optimal working temperature for improving efficiency. Nevertheless, the thermal contact resistance at the interface and the low thermal conductivity of the PCM can result in large temperature differences between the PV, the PCM, and the TEG, which impacts the efficiency of the hybrid system. In another work, Yin et al. [15] employed PCM to manage the operational temperature of a CPV-TEG hybrid system and reported a 23.52 % increase in output power. Zhang et al. [16] employed thermal interface materials between PV and TEG to reduce the thermal contact resistance, resulting in a 14 % increase in PV production and a 60 % increase in TEG output.

Lekbir et al. [17] in their theoretical study of the hybrid CPVT-TEG system suggest that using nanofluid as a heat transfer medium can improve the electrical and thermal efficiency in comparison to conventional cooling methods. The effects of thermal contact resistance and thermal resistance of the TEG were not considered in their study. Soltani et al. [18] modelled a PTC based CPVT-TEG in which the PV cells are arranged on the lateral side of the absorber tube with the TEGs on their back side. In their analysis, the non-uniform PV illumination induced by PTC, as well as the impacts of thermal contact resistance and thermal resistance of TEG, were not considered. Mohsenzadeh et al. [19] designed an experimental prototype of a PTC-based CPVT-TEG system with a triangular channel covered with PV cells and TEGs at the back of the PV to generate both electrical and thermal energy. It was discovered that the hybrid system performed better than that of the PV alone system. Yin et al. [20] optimised the effects of PV voltage and TEG load resistance on the temperature and output power of a water-cooled CPV-TEG hybrid system in their experimental study. The optimised output performance of the CPV-TEG outperforms the CPV alone system.

Abdo et al. [21] developed a new configuration of PV and TEG hybrid systems that are not thermally connected. Both the PV and TEG are combined with a microchannel heat sink between them, and they are exposed to high intensity solar irradiance using a Fresnel lens. Numerical evaluation reveals that the efficiency of the hybrid concentrator photovoltaic/thermal-solar thermoelectric generator (CPVT-STEG) system configuration is more efficient than the traditional hybrid CPVT-TEG system configuration. An experimental prototype of a PTC-based hybrid CPVT-TEG system was described by Riahi et al. [22]. The findings revealed that the CPVT-TEG performed better than a CPVT system. Nevertheless, the PV temperature in the CPV/T-TEG system was found to be higher when compared to the CPVT system, and this is due to the higher thermal resistance of the TEG. Shittu et al. [23] carried out a three-dimensional (3-D) numerical simulation of a hybrid CPV-TEG system by considering all the contact resistances and discovered that ignoring the contact resistances causes the total power output and efficiency to be overestimated by 7.6 % and 7.4 % respectively. In the study conducted by Rejeb et al. [24], the numerical simulation results of the CPV-TEG system were analysed using a statistical tool to determine the significance of solar radiation, solar concentration ratio, ambient temperature, height of TEG leg, and external load resistance on the electrical efficiency, as well as how to optimise these parameters for maximum electrical efficiency.

Most of the CPV-TEG and CPVT-TEG studies in the existing literature are limited to either conceptual models without any practical prototype or small-scale setups tested under laboratory conditions. Although the idea of combining CPV and TEG has been explored in many studies, this type of hybrid system is still far from reaching a commercialization stage due to a lack of field testing under transient environmental conditions. In the majority of the hybrid CPV and TEG experimental investigations, the TECs are employed instead of TEGs, despite the fact that the TEC's working temperature limit is not suitable to work under high concentration solar collectors such as PTC and Fresnel lenses. Furthermore, the effect of the working temperature limit and the quantity of TEG modules on the electrical output of the hybrid system are often overlooked in the modelling and experimental studies. Increasing the number of TEG modules in a hybrid system where TEGs are thermally coupled to PV cells may reduce the thermal gradient and electrical output of TEG. Hence, the required quantity of TEG modules should be optimised based on the PV temperature as well as the overall output power of the PV and TEG modules.

Although several hybrid CPV-TEG and CPVT-TEG experiments have been reported, the studies on the outdoor performance of such hybrid systems are limited. Hence, the outdoor performance of a prototype of our proposed hybrid CPVT and STEG system is presented in this study. In our prior work the optical and mathematical modelling have been carried out to analyse the electrical and thermal performance of the CPVT-STEG system under steady-state conditions [25,26]. Using the steady-state model developed in our previous study [26], the final design of a CPVT-STEG prototype with the optimal number of TEGs have been determined and fabricated for field testing to evaluate the transient effects of environmental parameters on its performance. Since the TEGs are not thermally connected to the PV cells in the developed CPVT-STEG system, the number of TEGs is optimised for obtaining a maximum TEG output power. In the present study, a transient 3-D numerical simulation of the CPVT-STEG system was conducted using ANSYS Fluent, and the results are compared with the experimental results obtained from the prototype. Despite the limitations and challenges in evaluating the effectiveness of the CPVT-STEG prototype, this study seeks to be a significant benchmark in investigating the CPVT-STEG system under outdoor operating conditions.

2. Prototype description

In the present study, a hybrid CPVT-STEG receiver is integrated between the solar concentrators of CPC and PTC as shown in Fig. 1. Both the PV cells and TEG modules share a common cooling channel, which is designed for harnessing thermal energy from excess heat. The working principle of the hybrid CPVT-STEG receiver is clearly illustrated in the schematic diagram as shown in Fig. 1. In the proposed hybrid system, commercial mono-crystalline PV cells with a dimension of 125 mm × 125 mm each from Allmejores and a high temperature graphite plated TEG (TEG1-1263-4.3) composed of bismuth telluride with a dimension of 30 mm × 30 mm are used in the hybrid receiver for energy conversion. TEGs with high thermal conductive graphite coatings are preferred to minimize the thermal contact resistance. The geometrical parameters of the hybrid CPVT-STEG prototype are listed in Table 1. The characteristics of both the PV and TEG modules used in the prototype are listed in Table 2 and Table 3, respectively.

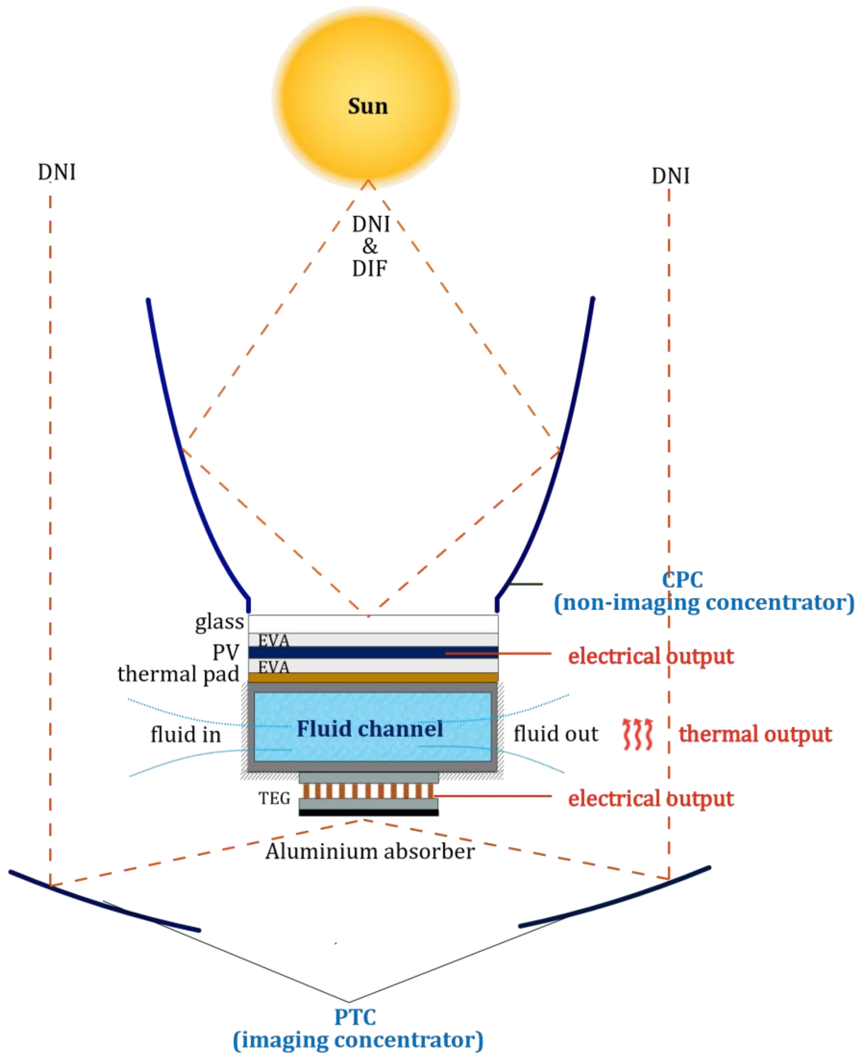

Fig. 1. Schematic diagram of the working principle of hybrid CPVT-STEG prototype.

Table 1. Geometrical parameters of different components in the hybrid CPVT-STEG prototype [26].

Components	Width, mm	Length, mm	Thickness, mm
	PV panel		
Glass layer	130	540	5
EVA layer	130	540	0.5
Silicon wafer	125	540	0.2
Thermal pad	130	540	0.5
	TEG module		
Graphite layer	30	30	0.13
Ceramic layer	30	30	0.8
Copper strips	1.08	2.7	0.15
P-N legs	1.08	1.08	1.5
Aluminium absorber clamp	30	540	2
	Rectangular Channel		
Fluid domain	124	540	30
Wall thickness	-	-	3
Full channel	130	540	36

Table 2. The characteristics of the PV module in the hybrid CPVT-STEG prototype [26].

Parameters	Value
Optical parameters	
Absorptivity of glass	0.018
Transmissivity of glass	0.92
Emissivity of glass	0.85
Absorptivity of EVA	0.08
Emissivity of EVA	0.9
Transmissivity of EVA	0.9
Absorptivity of silicon wafer	0.9
Absorptivity of thermal pad	0.5
Thermal parameters	
Thermal conductivity of glass	2 W/m.K
Thermal conductivity of EVA	0.35 W/m.K
Thermal conductivity of silicon wafer	148 W/m.K
Thermal conductivity of thermal pad	2.8 W/m.K
Electrical parameters	
No. of PV cells connected in series (mono-Si)	4 cells (125 mm x 125 mm each)
Open circuit voltage of a cell	0.635 V
Short circuit current of a cell	5.744 A
Maximum voltage of a cell	0.530 V
Maximum current of a cell	5.401 A
PV efficiency at STC	18.6 %
Temperature coefficient of power	-0.47 % / °C

Table 3. The characteristics of the TEG module in the hybrid CPVT-STEG prototype [26].

Parameters	Value
Pairs of PN legs	126
Max. TEG hot side temperature limit	613.15 K
Max. TEG cold side temperature limit	463.15 K
Thermal conductivity of graphite	10 W/m.K
Thermal conductivity of ceramic	18 W/m.K
Seebeck coefficient of p leg	$\alpha_p(T)$ = -8.105 x 10^{-14} T^3 -1.45838 x 10^{-9} T^2 + 9.2444677 x 10^{-7} T + 7.417 x 10^{-5}
Seebeck coefficient of n leg	$\alpha_n(T)$ = 1.7324623 x 10^{-13} T^3 – 1.147783 x 10^{-9} T^2 + 5.90568332 x 10^{-7} T + 1.4392165 x 10^{-4}
Electrical resistivity of p leg	$\rho_p(T)$ = 6.21731 x 10^{-15} T^4 – 1.085722 x 10^{-11} T^3 + 6.857354 x 10^{-9} T^2 – 1.797597 x 10^{-6} T + 1.73549 x 10^{-4}
Electrical resistivity of n leg	$\rho_n(T)$ = 1.18538 x 10^{-15} T^4 - 2.301947 x 10^{-12} T^3 + 1.5708605 x 10^{-9} T^2 – 4.125723 x 10^{-7} T + 4.42835937 x 10^{-5}
Thermal conductivity of p leg	$k_p(T)$ = - 6.0097596 x 10^{-8} T^3 + 9.0134323 x 10^{-5} T^2 - 3.7380241 x 10^{-2} T + 6.1921321
Thermal conductivity of n leg	$k_n(T)$ = - 3.38062 x 10^{-8} T^3 + 6.22422 x 10^{-5} T^2 - 2.95477835 x 10^{-2} T + 5.7041796
Figure of merit of p leg	$ZT_p(T)$ = -1.68766 x 10^{-8} T^3 + 3.2614 x 10^{-5} T^2 - 2.2459 x 10^{-2} T + 5.424505
Figure of merit of n leg	$ZT_n(T)$ = 2.85296 x 10^{-8} T^{-3} - 3.5168 x 10^{-5} T^2 + 1.0560 x 10^{-2} T + 0.3213
Thermal conductivity of Copper strips	385 W/m.K
Thermal conductivity of Aluminium	202.4 W/m.K
Absorptivity of aluminium absorber clamp	0.9
Emissivity of aluminium absorber clamp	0.15

The supporting frame of the prototype was fabricated as illustrated in Fig. 2, where the size of the primary base structure is 1.10 m × 1.12 m. The primary base structure has a single vertical shaft at the centre that joins the base structure to the secondary base structure. The main shaft has two upper hinges and a lower hinge. The upper hinges allow pivoting movement of the entire secondary base in the east-west direction, while the lower hinge allows pivoting movement of the entire secondary base in the north-south direction. Both the CPC and PTC are mounted on the secondary base, and the upper and lower hinges in the primary shaft are actuated by a pair of linear actuators as shown in Fig. 2(a) to adjust the cardinal orientation of the secondary base based on the direction of solar irradiance from the sun as detected by the light sensor. The width of the secondary base is equivalent to or larger than the aperture width of the CPC. The secondary base has four pairs of vertical shafts to hold the receiver of the hybrid system. The vertical shafts include linear guide rails and rollers to adjust the focal position of the receiver (see Fig. 2(b)). The second set of linear actuators is used to actuate the rollers to adjust the position of the receiver to its focal point.

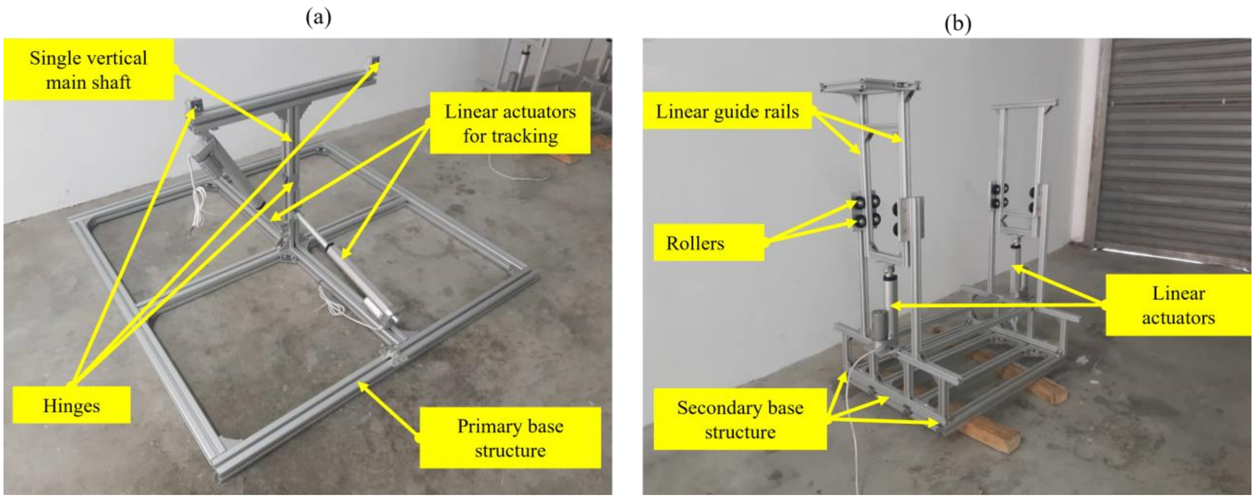

Fig. 2. Fabrication of support structure: (a) primary base and (b) secondary base

Based on our previous optical study, our design for the hybrid CPVT-STEG prototype includes a HEMR CPC ($CR = 4\, suns$, $\theta_c = 10.61°$) paired with a PTC ($CR = 16.6\, suns$, $\varphi_r = 45°$) [25]. The CPC and PTC profiles were built using laser-cut aluminium ribs. Mirror-polished stainless-steel sheets with a reflectivity of 67 % were screwed onto aluminium ribs to construct the HEMR CPC and PTC, as shown in Fig. 3. Flat reflectors are added on the bottom side of the CPC to characterize it as a HEMR CPC, resulting in uniform illumination on the CPC receiver. In Fig. 4, four pieces of mono-crystalline silicon cells are connected in series and sandwiched between the glass cover and EVA layers in an aluminium frame to form a complete PV module. The rear side of the PV module is backed with a 0.5 mm thick silicone thermal pad that acts as a thermal interface material between the PV module and the fluid channel, which allows for efficient heat transfer.

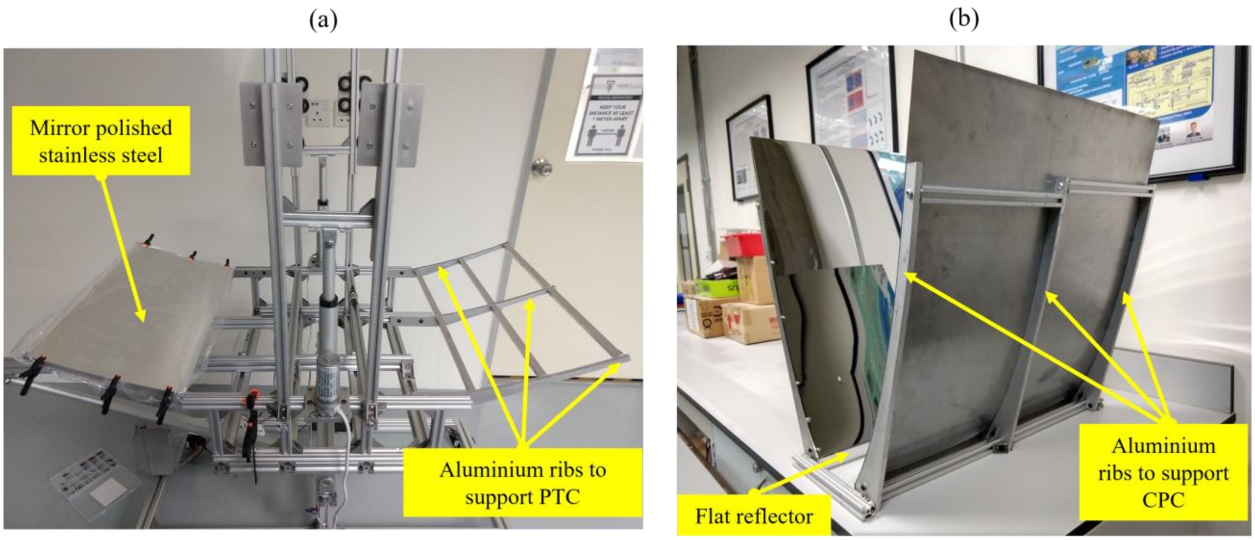

Fig. 3. Fabrication of solar concentrators: (a) PTC, and (b) CPC

As seen in Fig. 5(a), the fluid channel is an enclosed rectangular aluminium tube with an inlet and outlet pipe. The channel is manufactured with thermowell at the inlet and outlet to accommodate thermocouples for measuring the temperature of the water at the inlet and outlet (see Fig. 5(b)). To avoid any fluid channel leakage, the thermowells were sealed with an anti-leakage sealant. On the backside of the fluid channel TEGs are installed and fastened together using an aluminium absorber clamp. Fibreglass was used to insulate the empty area outside of the contact zone between the channel and the TEGs. Additionally, the sidewalls and non-contact parts of the fluid channel were insulated with fibreglass to prevent heat loss (see Fig. 6). In order to increase the absorptivity of the aluminium clamp, it is coated with candle soot [27]. The average absorbance of the candle soot in the spectral range of 150 – 1500 nm is 0.86 [28].

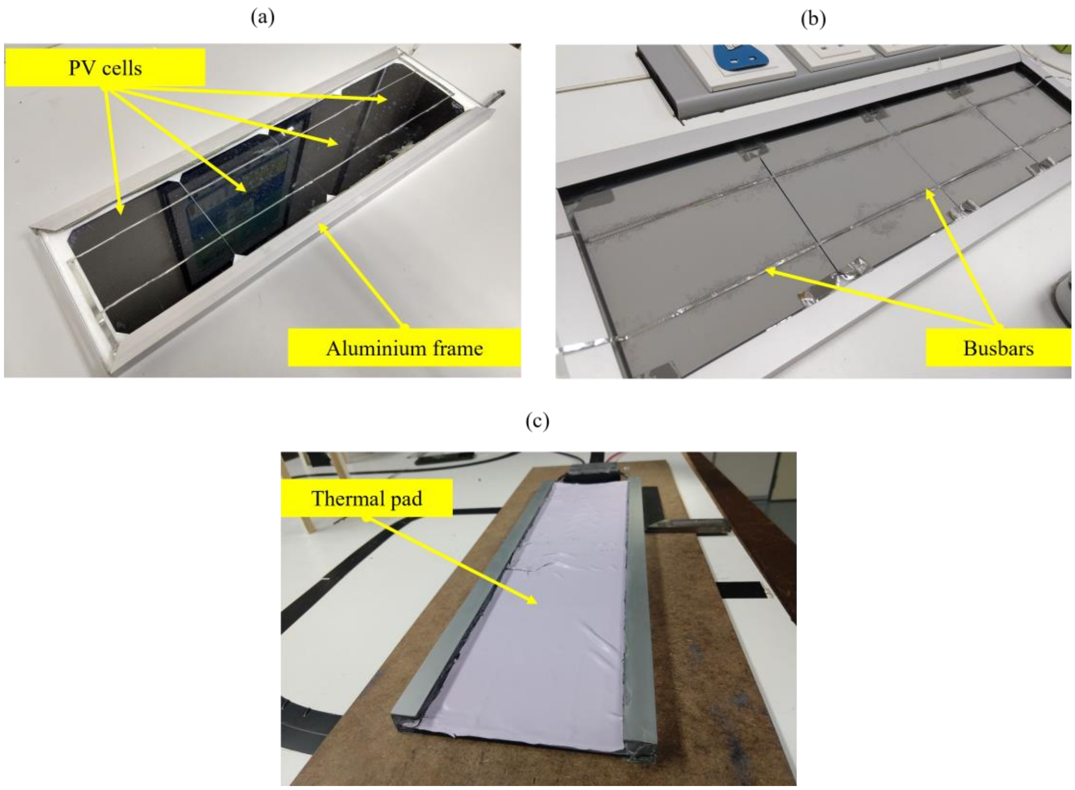

Fig. 4. Fabrication of PV module: (a) PV front side, (b) PV rear side, and (c) PV rear side with thermal pad.

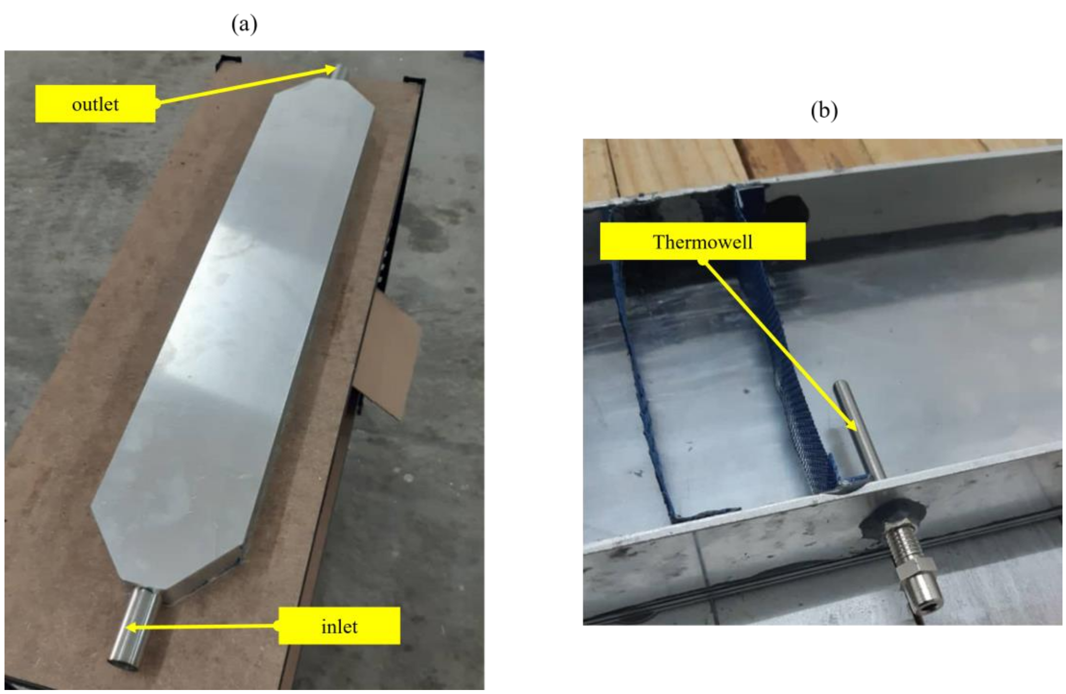

Fig. 5. Fabrication of fluid channel.

(a)

(b)

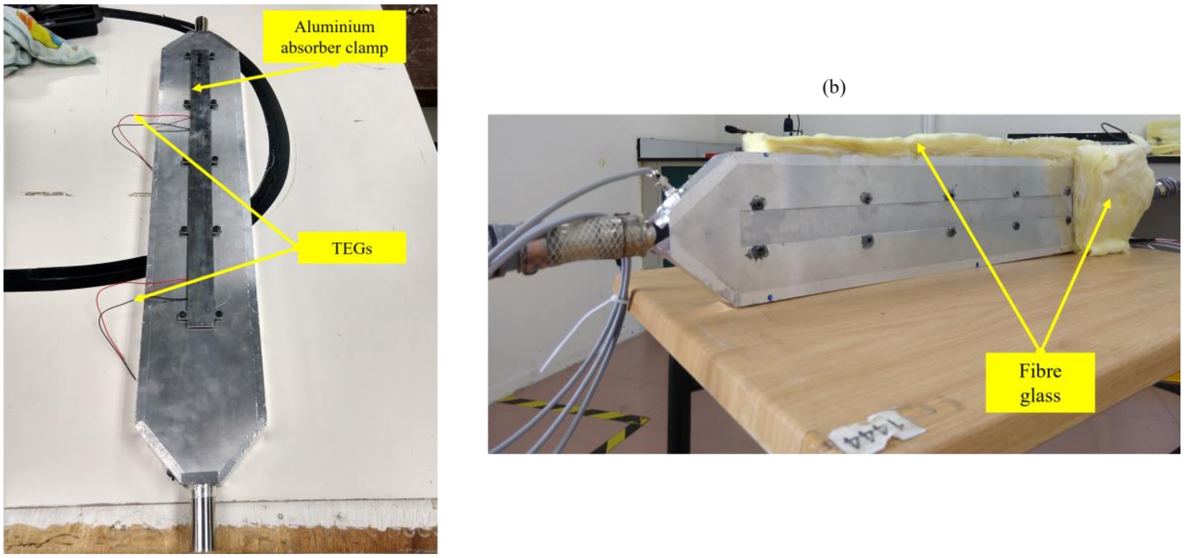

Fig. 6. (a) Integration of TEG modules with fluid channel (b) insulation of fluid channel with fiberglass.

3. Experimental setup and measuring equipment

The experimental prototype was built at the Taylor's University campus, Malaysia (3.0626° 101.6168° E). The constructed prototype was evaluated to assess its electrical and thermal performance under transient outdoor conditions. The schematic diagram of the prototype to show numerous components and thermocouple locations is illustrated in Fig. 7. Table 4 shows the specifications of the measurement devices used throughout the experiment, including their respective measurement ranges and accuracies. The constructed hybrid concentrator structure is equipped with a sun tracking mechanism in both east-west and north-south directions. The receiver of the hybrid system is aligned along the polar north-south axis with the latitude-dependent tilt angle, and a microcontroller with an LED sensor-based sun-tracking system is used to track the aperture of the hybrid system from east to west. The receiver of the hybrid system is fixed at the focal point by adjusting the linear guide rails using the linear actuators. Two units of K-type thermocouples were installed on both sides of the PV module without casting any shadow on the PV cells, which were then connected to the datalogger for monitoring the surface temperatures of the PV module.

Table 4. List of measuring instruments used for the experimental study.

Instruments	Measuring range	Accuracy
Pyranometer (Hukseflux SR05-D1A3	0 – 2000 W/m^2	+/- 1.8 %
Pyrheliometer (Delta Ohm LP Pyrhe 16)	0 – 2000 W/m^2	+/- 2 %
Basic wind speed sensor (Lambrecht meteo)	0.7 – 50 m/s	+/- 2 %
PT 1000 RTD	-20 to 100 ° C	0.15 + 0.002 (° C)
RS PRO Type K Thermocouple	-50 to 1000 ° C	+/- 1.5 ° C
Kimo Type-T thermocouple	-40 to 350 ° C	+/- 0.5 ° C
Proskit multimeter for current measurement	20 Amps Max.	+/- 0.5 %
Techgear multimeter for current measurement	60 mV – 1000 V	+/- 0.2 %
Flow meter hall effect sensor (YF-S201)	1 – 30 L/min	+/- 10 %
INA 219	26 V / 3.2 Amps Max.	1 %

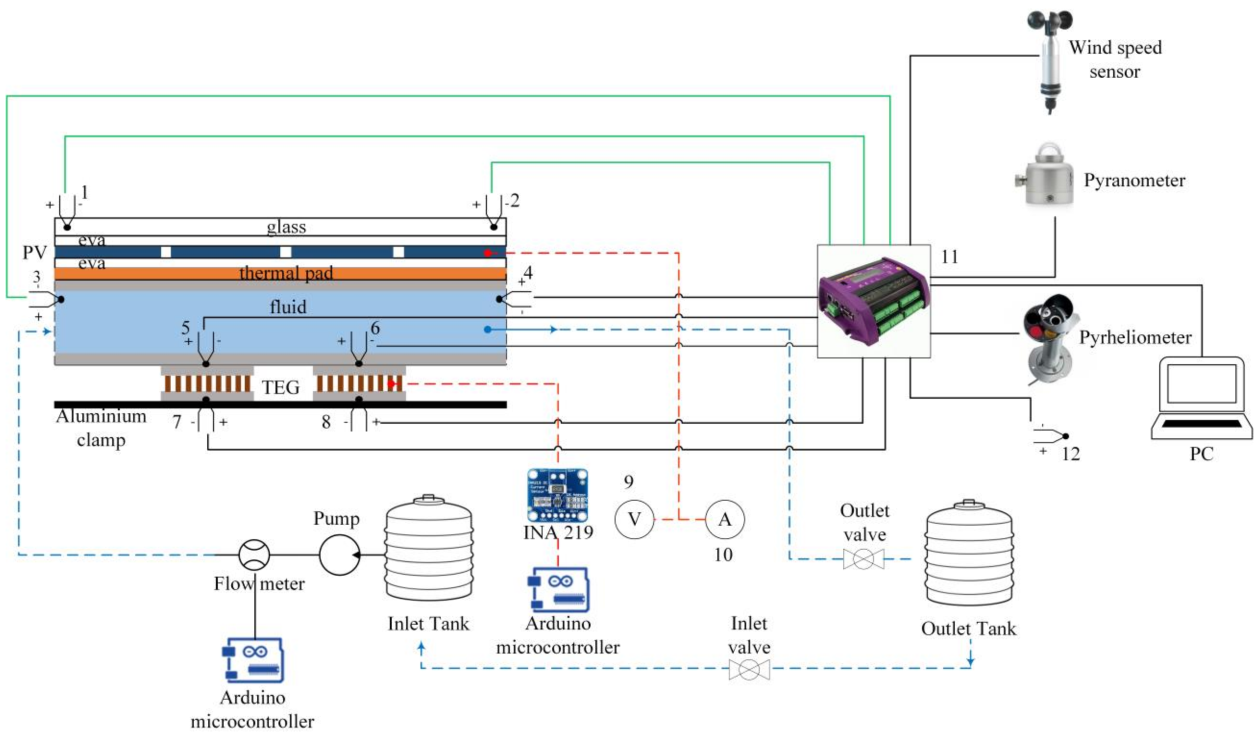

Fig. 7. Schematic of hybrid CPVT-STEG experimental setup: (1 & 2) PV temperature sensor location, (3) and (4) fluid inlet and outlet temperature sensor location, (5) and (6) TEG cold side temperature sensor location, (7) & (8) TEG hot side temperature sensor location, (9 & 10) Multimeter, (11) data logger and (12) ambient temperature sensor location.

Two units of K-type thermocouples were attached between the bottom part of the fluid channel and the cold side of TEGs to measure the cold side temperature of the TEGs. Another two units of K-type thermocouples were attached between the aluminium absorber clamp and the hot side of the TEGs to measure the hot side temperature of the TEGs. The four thermocouples from the TEGs were routed along the fluid channel walls without casting any shade on the bottom part of the PTC, in which all the thermocouples were linked to the data-logger for continuous recording of temperatures throughout the experiment. Additionally, a T-type thermocouple was used to record the ambient temperature during the experiment. Moreover, instruments such as a pyranometer, pyrheliometer, and wind speed sensor were connected to the data-logger for monitoring and recording direct normal irradiance, global horizontal irradiance, and wind speed, respectively, during the field testing. Two units of platinum resistance temperature detectors were fixed in the fluid channel via a tiny hole in the thermowell to monitor the water temperature at the inlet and outlet of the fluid channel. The experimental setup consisted of one inlet tank connected to the inlet of the fluid channel and one outlet tank connected to the outlet of the fluid channel. The water was pumped from the inlet tank using a diaphragm water pump at a constant flow rate. The fluid channel and the inlet pipe from the inlet tank were completely insulated by using fibreglass to avoid the heat losses from the hybrid system.

The CPVT-STEG system was tested on the rooftop of a building on the campus of Taylor's University on a sunny day, October 26, 2021, as depicted in Fig. 8. The water flow rate inside the fluid channel is tuned to achieve a constant rate of 3.8 L/min. To obtain a stable test condition, the fluid outlet was closed so that the water filled the channel without any air gaps and achieved a uniform flow. Once the water flow in the channel was uniform, the outlet was opened so that the prototype was exposed to direct sunlight for power production. The wind speed, ambient temperature, GHI, DNI, PV temperature, TEG temperature, fluid inlet and outlet temperature, voltage, and current were recorded for a period of 1 hour and 30 minutes, from 11:15 am to 12:45 pm (peak sun hours). Due to the frequent rainfall in the test location, the period of data collection was constrained since neither the prototype nor the data acquisition system employed were designed to withstand the rigours of wet conditions. The environmental and operating parameters were recorded every second via an automated data acquisition system. The open-circuit and short-circuit current of both the PV and TEGs were monitored and recorded every 5 minutes using digital multimeters and INA 219 sensor, respectively.

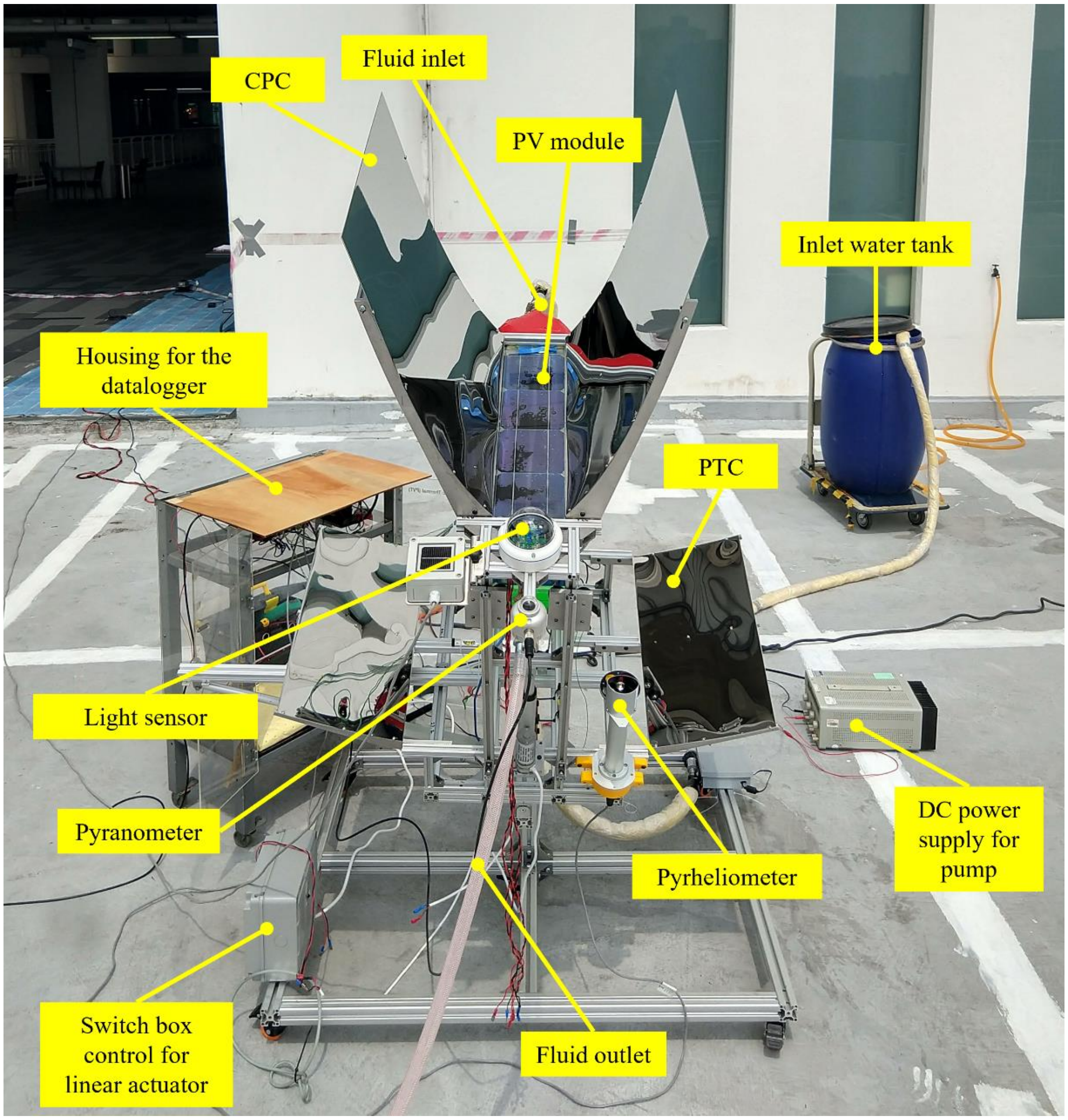

Fig. 8. Outdoor experimental setup for testing the prototype.

4. Numerical simulation

Real-time transient simulation is critical because real-time transient situations can happen in an unpredictable and fast manner in the real world. The intermittency of weather conditions, particularly in partially cloudy climes, can influence the output power and conversion efficiency of the hybrid system, which are significant factors in stabilising the electrical response of hybrid system. The ideal quantity of TEG modules for producing a maximum TEG output in the hybrid system was determined using the steady-state heat transfer model from our previous work [26]. For the transient simulation, the numerical model of the CPVT-STEG system with the optimal number of TEGs (2 units of TEG) is considered. The transient response of the hybrid system was modelled using ANSYS Fluent.

The flowchart to show the methodology of transient numerical simulation and experimental study is indicated in Fig. 9. Based on our previous study, the number mesh elements used is 8.386×10^6 [26]. For transient simulation, the input boundary conditions are based on the measured solar radiation and ambient conditions on the day of measurement. The input solar irradiance is processed based on the optical efficiency, and it is imported to ANSYS Fluent as a volumetric heat source.

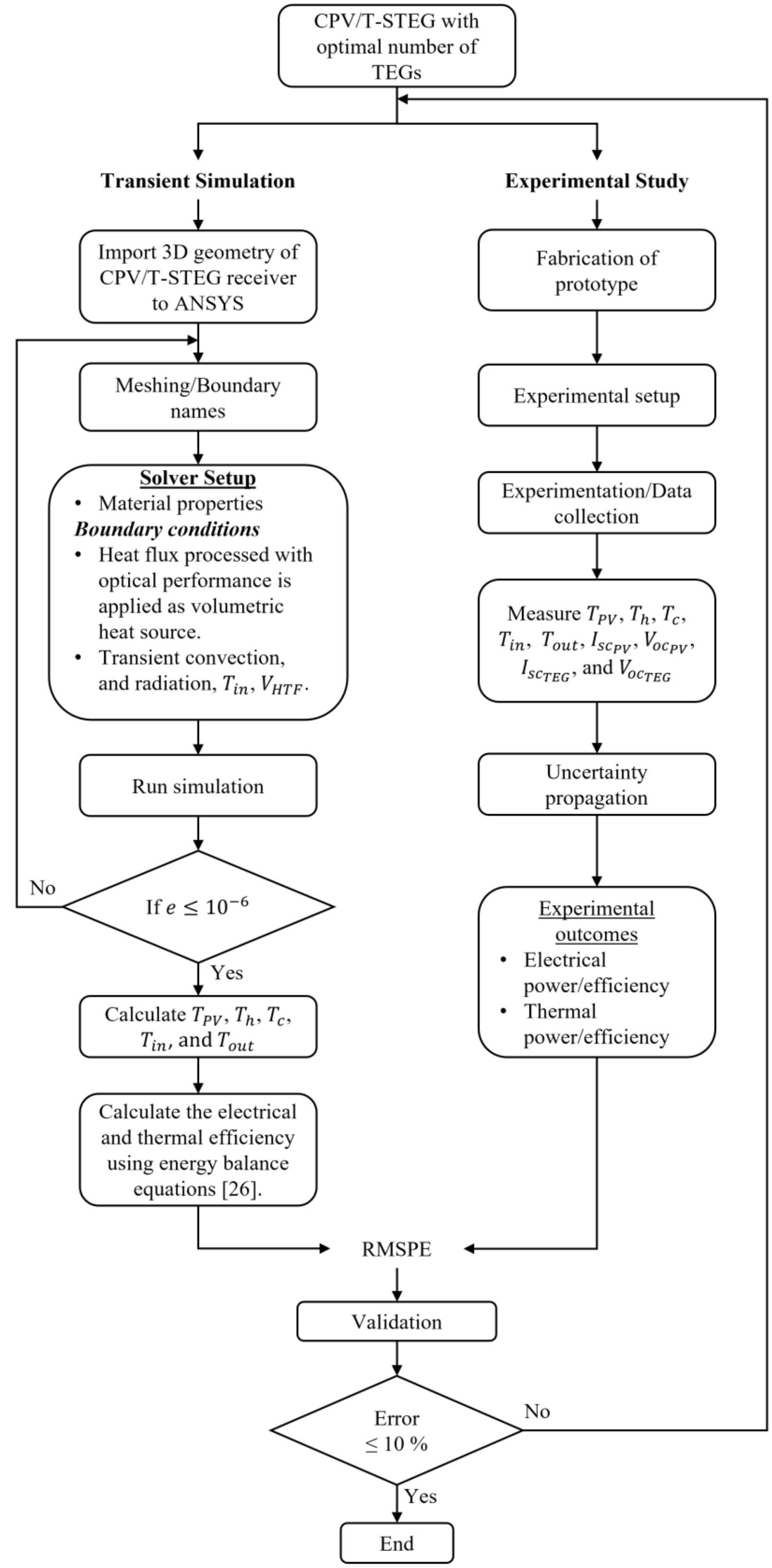

Figure 9. Flowchart of transient numerical simulation and experimental study

5. Computational method

5.1 Photovoltaic module measurements

Since the experimental prototype employs only four silicon PV cells in series, the overall open-circuit voltage is around 2.54 V, which is too low to be measured directly using any commercially available I-V tracer. Electric power generated by any PV module can be estimated using Simulink provided that open-circuit voltage and short-circuit current are added to the modelled circuit [29]. In this investigation, the I-V and P-V curves of the PV module in the hybrid system were simulated using Simulink in MATLAB (see Fig. 10) based on the open-circuit and short-circuit current measured via multimeters. Given the open-circuit voltage, short-circuit current, and temperature of PV module, we can compute the maximum PV voltage, maximum PV current, and the maximum power of the PV module.

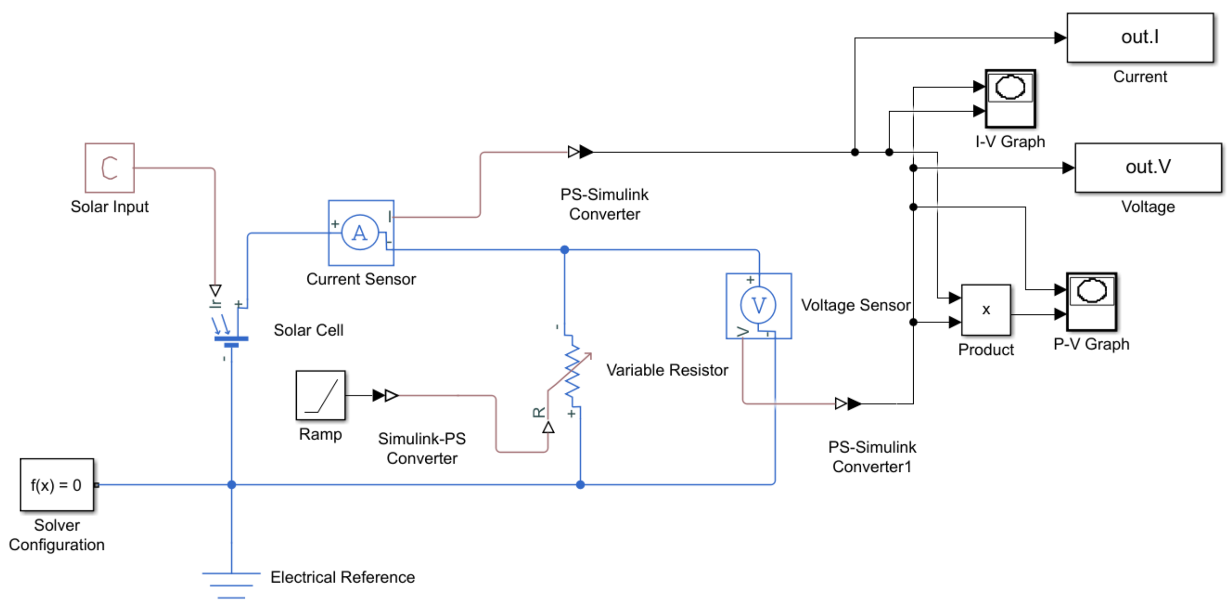

Fig. 10 Simulink circuit model used for I-V and P-V curve calculation.

5.2 Thermoelectric generator measurements

The prototype has two TEGs connected in series, where the output terminals are connected to an INA 219 sensor and an Arduino microcontroller for monitoring the short-circuit current ($I_{sc_{TEG}}$) and open-circuit voltage ($V_{oc_{TEG}}$). The maximum power point (MPP), at which the TEG provides the highest feasible power ($P_{m_{TEG}}$) to the external load at a given temperature, is expressed as the following [30] [31]:

$$P_{m_{TEG}} = \frac{V_{oc_{TEG}}}{2} \times \frac{I_{sc_{TEG}}}{2} \tag{1}$$

5.3 Net efficiency of CPVT-STEG prototype

The net electrical efficiency of the developed CPVT-STEG prototype can be calculated as [26]:

$$\eta_{el} = \frac{P_{m_{PV}} + P_{m_{TEG}} - P_{pump}}{A_{PTC} G_{GHI}} = \frac{P_{total}}{A_{PTC} G_{GHI}} \tag{2}$$

where P_{pump} is the required pump power, A_{PTC} is the aperture area of the PTC, and G_{GHI} is the total solar irradiance falling on the hybrid system. The following equation is used to figure out how much power the pump needs:

$$P_{pump} = \dot{V}_{HTF} f \frac{L}{D_h} \frac{\varrho_{HTF} V_{HTF}^2}{2} \tag{3}$$

where $\dot{V}_{HTF}$ is the volumetric flow rate, f is the friction coefficient, L is the length of the channel, D_h is the hydraulic diameter, ϱ_{HTF} is the density of the HTF, and V_{HTF} is the velocity of the HTF, which can be calculated using Eq. (4):

$$\dot{V}_{HTF} = V_{HTF} A_{cross} \tag{4}$$

$$f = \frac{72.92}{Re} \tag{5}$$

where A_{cross} is the cross-sectional area of the fluid channel and Re is the Reynold's number.

The net thermal efficiency of the hybrid system is computed using the following equation (6):

$$\eta_{th} = \frac{E_{HTF}}{A_{PTC} G_{GHI}} \tag{6}$$

where E_{HTF} is the excess heat transmitted to the HTF from PV cells and TEGs which can be determined by the following equation (7) [32]:

$$E_{HTF} = m_{HTF} C_p (T_{out} - T_{in}) \tag{7}$$

where m_{HTF} is the mass flow rate of HTF, C_p is the specific heat capacity of HTF, T_{in} and T_{out} are the inlet and outlet temperatures of HTF, respectively.

The exergy efficiency (η_{ex}) of the developed prototype is calculated using the following equation [33]:

$$\eta_{ex} = \frac{\dot{E}x_{out}}{\dot{E}x_{in}} \tag{8}$$

where exergy output $\dot{E}x_{out}$ is the total of thermal and electrical exergies. The exergy of incident solar irradiance ($\dot{E}x_{in}$) is calculated using Petela model [34], as given in Eq. (10):

$$\dot{E}x_{out} = \dot{E}x_{th} + \dot{E}x_{el} \tag{9}$$

$$\dot{E}x_{in} = G_{GHI} A_{PTC} \left[1 - \frac{4}{3}\frac{T_{amb}}{T_{Sun}} + \frac{1}{3}\left(\frac{T_{amb}}{T_{Sun}}\right)^4\right] \tag{10}$$

where $\dot{E}x_{el}$ is the total electrical output of the hybrid system. The thermal exergy ($\dot{E}x_{th}$) is determined using the Eq. (11) [33]:

$$\dot{E}x_{th} = mC_p(T_{out} - T_{in}) - mC_p T_{amb} \ln\left[\frac{T_{out}}{T_{in}}\right] \tag{11}$$

5.4 Uncertainty analysis of experimental results

The experimental data are variables measured through equipment with some uncertainties. The uncertainty of experimental measurements can be readily calculated by collecting a sample and acquiring the error percentage of the instruments from the datasheets. The Engineering

Equation Solver (EES) automates the process of uncertainty analysis internally using the root sum square (RSS) method [33]. Based on the energy balance concept, the uncertainty assessment was conducted on both thermal and electrical efficiencies using EES. The error percentage values can be assigned to measured variables such as G_{GHI}, G_{DNI}, V_{air}, T_{amb}, T_{PV}, T_h, T_c, V_{HTF}, T_{in}, T_{out}, $I_{sc_{PV}}$, $V_{oc_{PV}}$, $I_{sc_{TEG}}$, and $V_{oc_{TEG}}$. EES uses these values of uncertainty to automatically compute the associated uncertainty in the thermal and electrical efficiencies of the developed hybrid system.

5.6 Validation error analysis

To identify the percentage error between the simulation results (x_i) and the experimental results (y_i), the root mean square percentage error (RMSPE) method is applied as follows [35]:

$$RMSPE = \sqrt{\frac{\sum_{i=1}^{N}\left(\left[\frac{y_i - x_i}{x_i}\right]\right)^2}{N}} \times 100 \tag{12}$$

where N is the sample size.

5.7. Environmental cost analysis

Energy generation and consumption have an influence on the environment through the emission of carbon particles. As a result, the cost of carbon emissions is a significant consideration in the environmental evaluation. Environmental cost analysis is a technique used to measure the amount of CO_2 mitigation and the cost associated with it [35]. Environmental cost analysis is also crucial as it indicates the significance of carbon-free renewable energy technologies [34]. The average equivalent CO_2 emission in a coal-fired power generation is estimated to be 960 g CO_2/kWh. It amounts to 2.08 kg CO_2/kWh when transmission and distribution losses are included, as documented by Zuhur et al. [34]. Hence, the reduction of CO_2 emissions from the developed CPV/T-STEG prototype can be calculated based on the methodology adopted by [36]:

$$Q_{CO_2} = \psi_{CO_2} \times \dot{Q}_{th} \tag{13}$$

In this equation Q_{CO_2} is the amount of mitigated CO_2 per hour, ψ_{CO_2} is the average CO_2 emission from a coal-fired power plant (2.08 kg CO_2/kWh) and $\dot{Q}_{th}$ is the total thermal gain of the hybrid system and it can be calculated as follows:

$$E_{th,overall} = E_{HTF} + \frac{P_{total}}{C_{power}} \tag{14}$$

where E_{HTF} is calculated based on Eq. (7). In the Eq. (10) C_{power} is used to calculate the thermal gain from the electrical gain. The value of $C_{power}$is considered to be 0.38, which is the conversion power of the thermal power plant. This power is determined by the quality of the coal that has the lowest ash ratio [37]. The environmental cost of CO_2 reduction per hour (EC_{CO_2}) is calculated as follows:

$$EC_{CO_2} = Q_{CO_2} \times P_{CO_2} \tag{15}$$

where P_{CO_2} is the carbon price which is considered as 50 €/tCO_2 for the present study [38].

6. Results and discussion

In this subsection, the findings of numerical modelling and experimental analysis of the thermal and electrical output of the CPVT-STEG prototype are presented and analysed in depth. For the transient simulation and experimental analyses of the developed CPVT-STEG prototype, an optimal number of two TEGs for maximum TEG output power and thermal power is considered based on the 1-D steady-state analytical model developed in our previous study [26].

6.1 Environmental Parameters

The measured GHI and DNI values during the field testing of the prototype are plotted in as shown in Fig. 11. During the testing period, the measured GHI values ranged between 571.38 W/m^2 and 1167.134 W/m^2, whereas the measured DNI values ranged between 275.34 W/m^2 and 800.86 W/m^2. In short, the average values of GHI and DNI received by the hybrid system were 1006.22 W/m^2 and 741.34 W/m^2, respectively. Fig. 12 illustrates the fluctuation in ambient temperature, wind speed, and inflow water temperature throughout the observation period. The ambient temperature ranged between 298.01 K and 311.82 K, while the wind speed ranged between 0 and 4.16 m/s. The temperature fluctuation of the inflow water, including the error band, is given in Fig. 12 and varies between 302.44 K and 305.99 K.

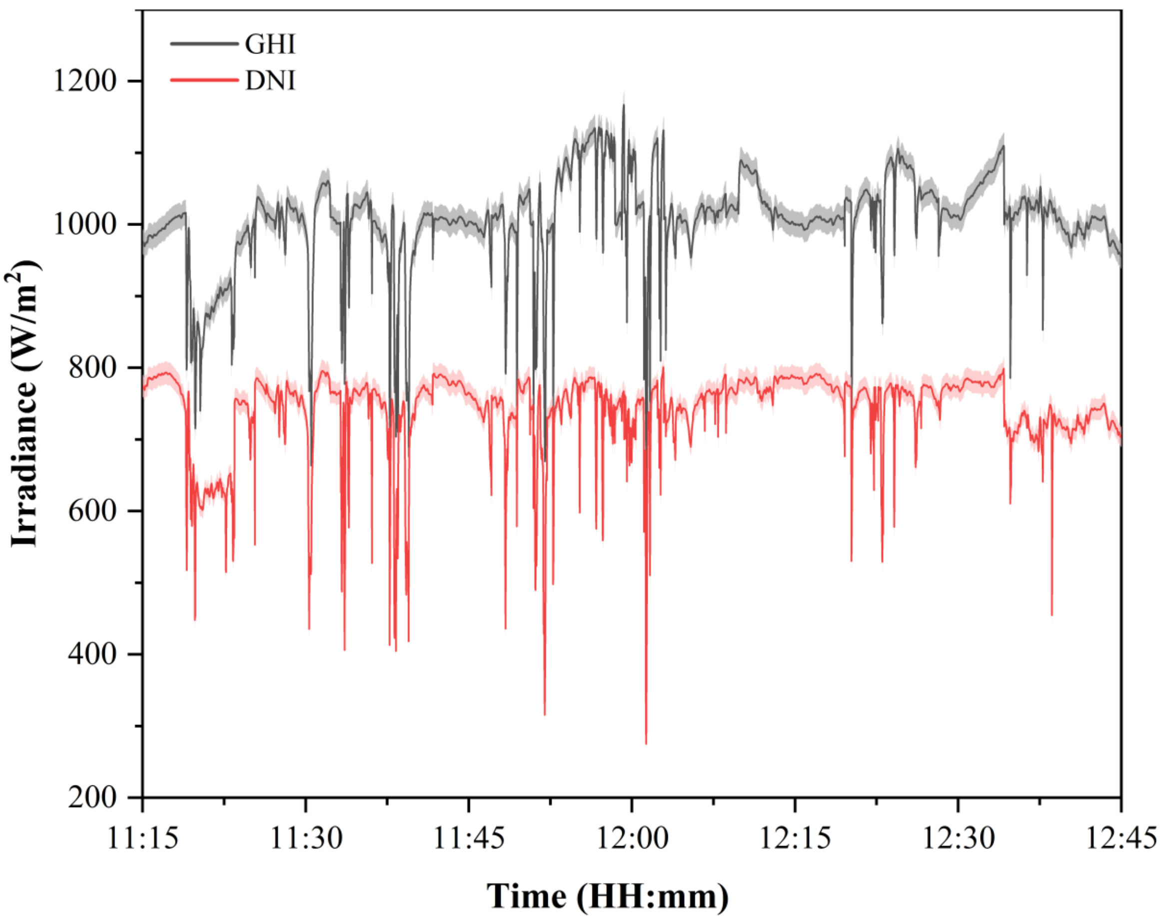

454 Fig. 11. Variations of GHI and DNI during the period of data collection.

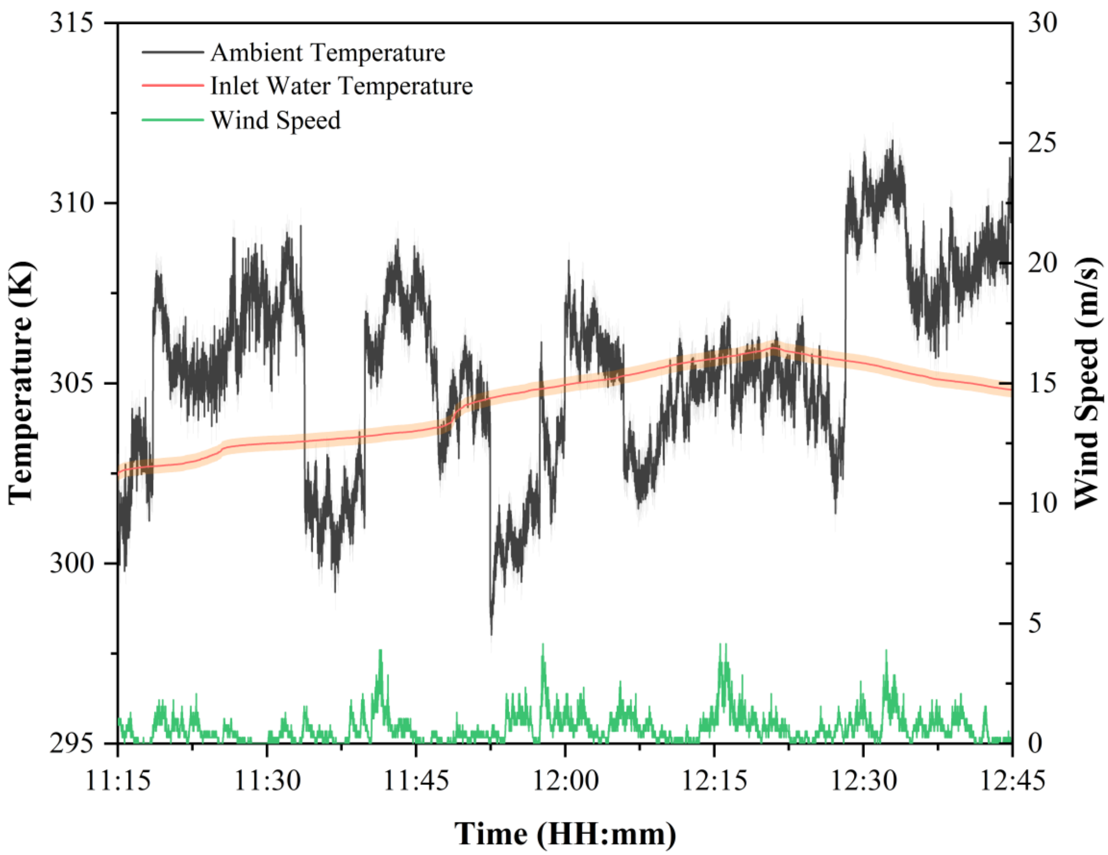

Fig. 12. Variation of ambient temperature, wind speed, and inlet water temperature during the test period.

6.2 PV performance analysis

6.2.1 Temperature of PV cells

The average temperature of the PV cells measured over the course of the test period with the error band for each second is presented in Fig. 13. A maximum temperature of 320.14 K was determined by the measurements for the PV module. Despite being cooled by water at an average inlet temperature of 304.51 K and a flow rate of 3.8 L/min, the average PV temperature over the period of test time was around 318.19 K, which is ~5.6% less as compared to that of a conventional PTC based CPVT-TEG hybrid system [22]. The graph clearly indicates that the temperature of the PV module increases when solar irradiance increases. The same phenomenon is also evident from both Fig. 12 and Fig. 13, where the PV temperature increases proportionally with the water inlet temperature by showing a strong positive correlation. The observed PV temperature was compared to the findings of the transient simulation, and it was found to be in good agreement with a root mean square percent deviation of 1.05 %. The experimental PV temperature is found to be greater than the simulation findings mostly owing to the thermal contact resistance existed between the fluid channel and the PV module, which is caused by the manufacturing faults.

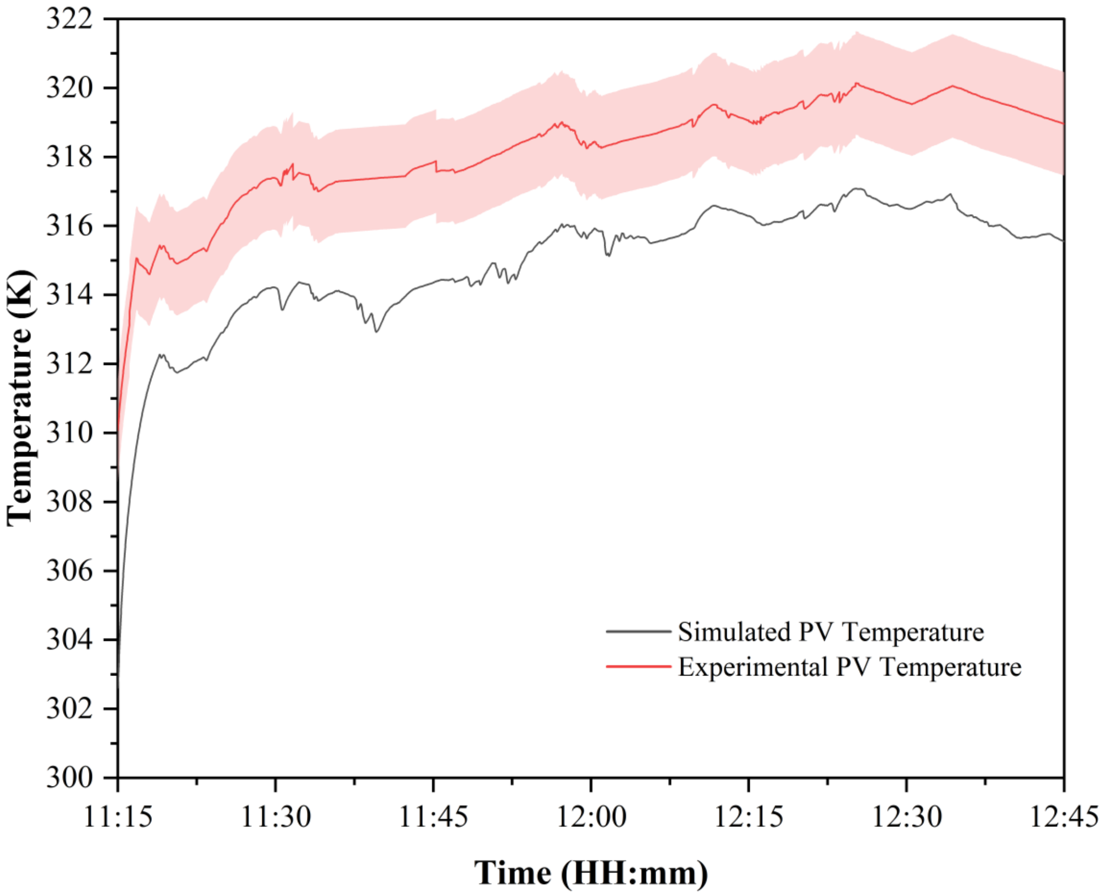

Fig. 13. Simulated and experimental values of PV temperature during the test period.

6.2.2 Current and voltage of the PV module

The maximum values of current and voltage of the PV module are computed using the MATLAB Simulink model based on the measured incident solar irradiance, PV temperature, open-circuit voltage, and short-circuit current. The fluctuation in the maximum output voltage and current of the PV module utilised in the proposed hybrid CPVT-STEG system is depicted in Fig. 14. The graph clearly illustrates that the output current of PV is highly dependent on the GHI values. When the GHI value is 1108.56 W/m^2, the highest PV current recorded is 11.59 A. On the other hand, GHI levels have little effect on the PV voltage. Additionally, as seen in Fig. 14, the PV voltage has a significant inverse relationship with the PV temperature, with a correlation coefficient of -0.92. The observed maximum and minimum output PV voltages are 2.08 V and 1.99 V, respectively.

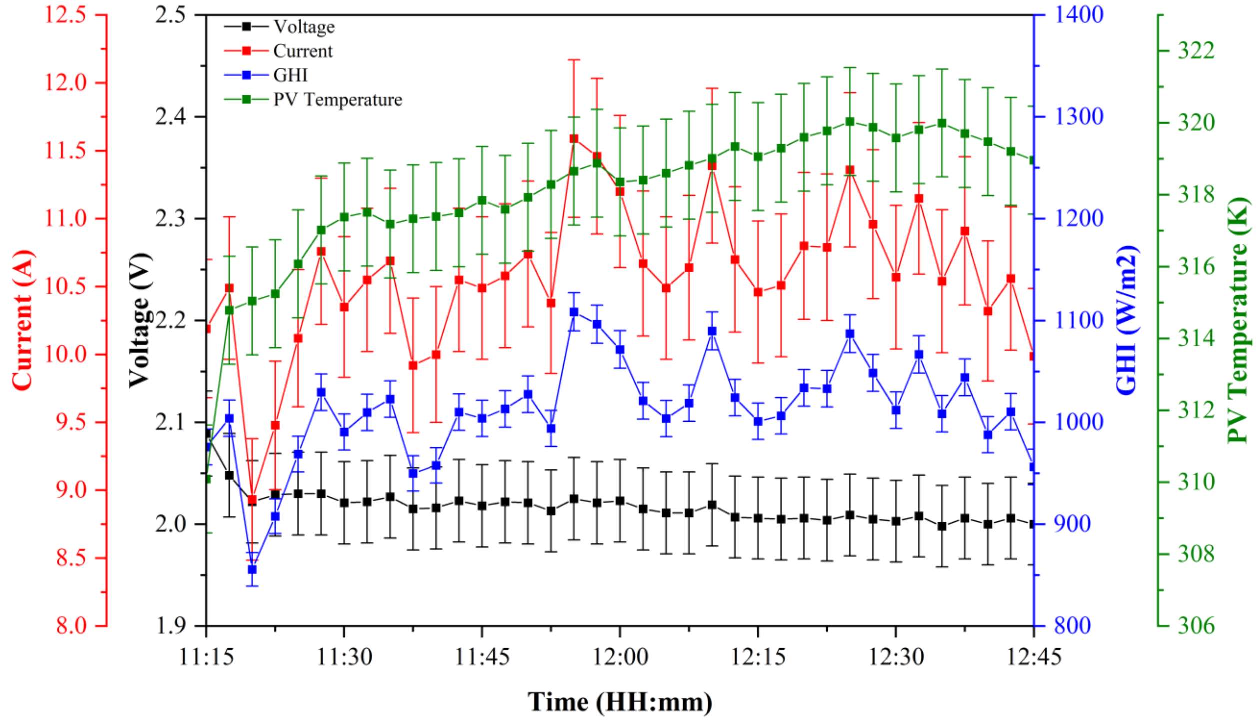

Fig. 14. Experimental variation of current and voltage of the PV during the test period.

6.2.3 I-V and P-V characteristics of PV module

Fig. 15 shows the I-V and P-V characteristic curves of the PV module in the hybrid prototype. The I-V and P-V curves of the PV module are calculated for the maximum DNI value of 800.86 W/m^2 at 12:02:54 pm. The short-circuit current of the PV module increases from 5.40 A to 12.51 A under concentrated sunlight, which is 2.3 times higher than the non-concentrated PV module under STC. The maximum PV output at the DNI of 800.86 W/m^2 is about 24.2 W, which is about 2.1 times higher than the non-concentrated PV module under STC (11.45 W).

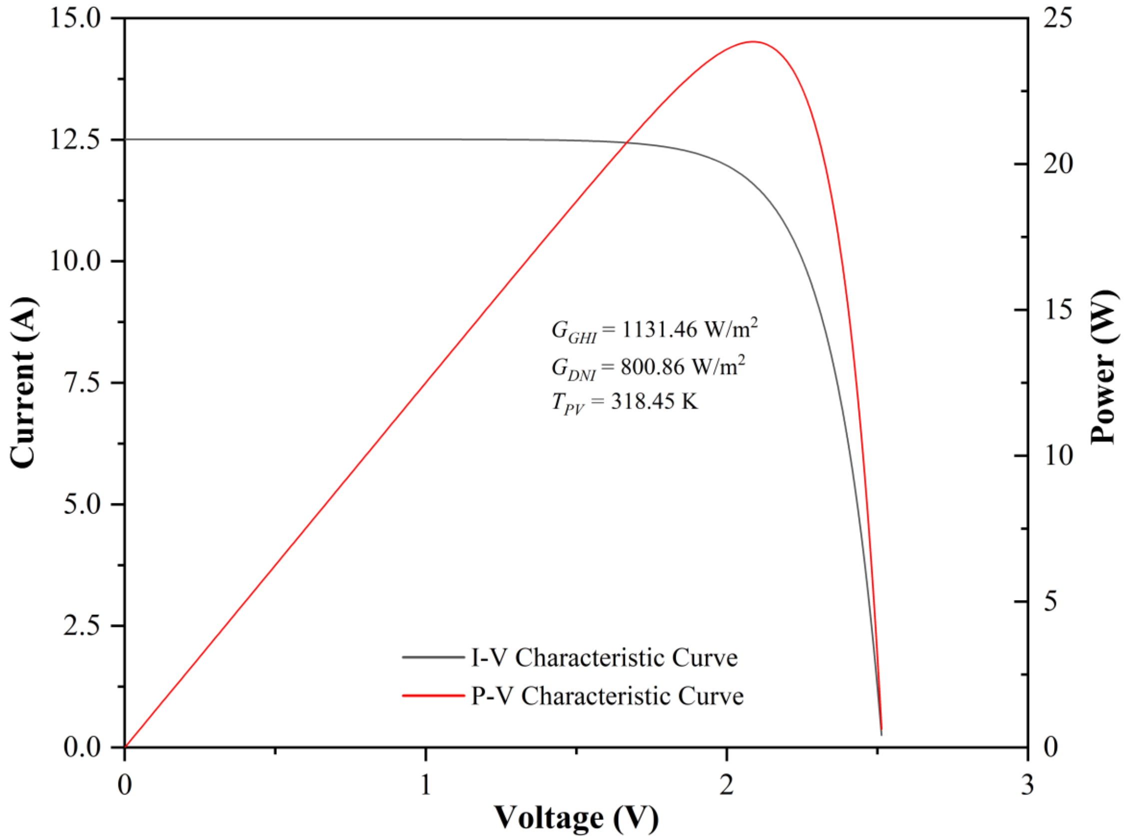

Fig. 15. The I-V and P-V characteristic curves of the PV module in the CPVT-STEG prototype.

6.2.4 PV power and efficiency

Fig. 16 illustrates the variations in PV power and conversion efficiency versus GHI with error bars during the field testing. As both PV power and GHI exhibit the same trend, PV output is directly proportional to input solar irradiance. The maximum simulated photovoltaic power is 25 W. Experimental data shows that PV power ranges from 18.06 W to 24.2 W, with an average of 21.33 W. The experimental results show that the simulation results are quite similar to the experimental data, with a root mean square percent variation of 6.19%.

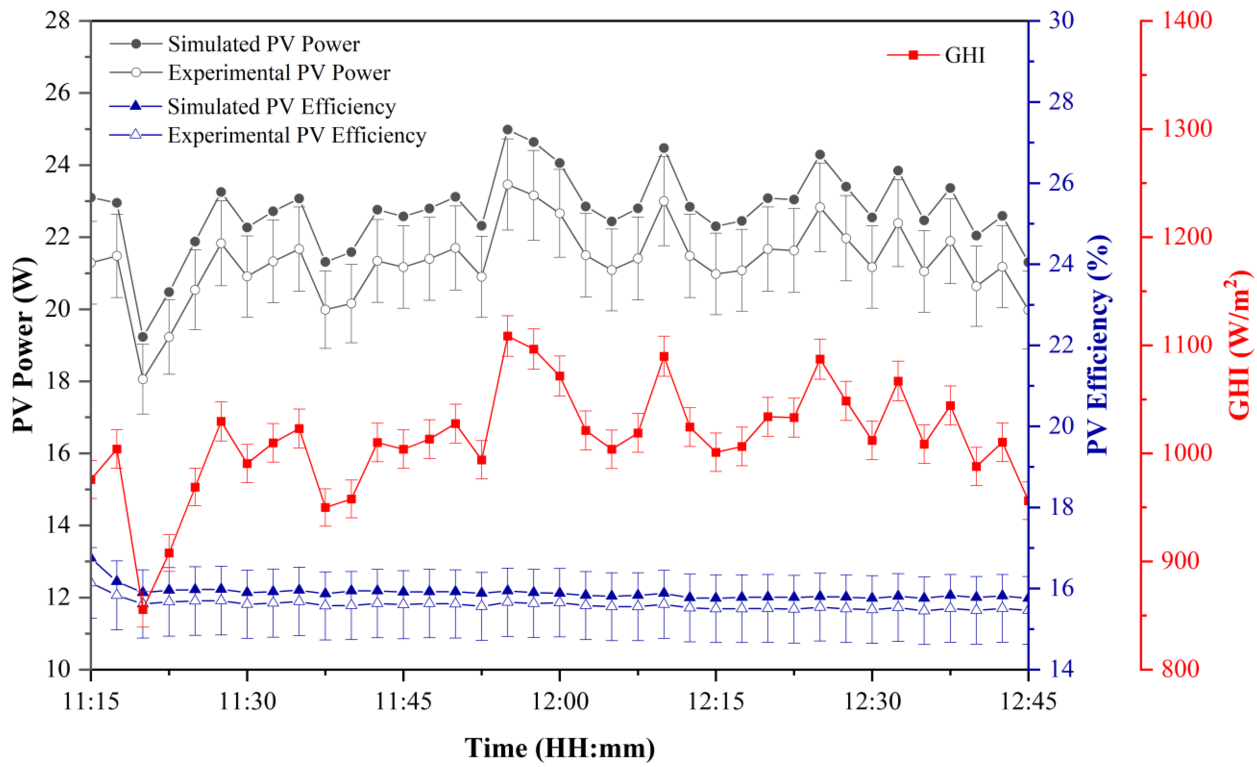

Fig. 16. Simulated and experimental values of PV power and PV efficiency of the CPVT-STEG prototype during the test period.

The highest and average simulated photovoltaic efficiency values are 16.75% and 15.89%, respectively, whereas the maximum and average experimental photovoltaic efficiency values are 16.14% and 15.59% respectively. Correlation analysis showed that there is no strong positive or negative correlation between PV efficiency and GHI. Instead, the PV efficiency has a strong negative correlation with the PV temperature, with a correlation coefficient of -0.9, which means that the PV efficiency decreases as the PV temperature rises. The experimental PV efficiency was satisfactorily confirmed against the simulation results with a root mean square percent variation of 1.89%.

6.3 TEG performance analysis

6.3.1 Temperature across the TEGs

Fig. 17 illustrates the variation of simulated and measured temperatures of the hot and cold sides of the TEGs along with the error band. The hot side temperature of the TEGs depends on the incident DNI values. On the other hand, the cold side temperature of the TEGs depends on the flow rate and temperature of the water at the inlet. The maximum observed hot-side temperature of TEG is 438.53 K and the minimum cold side temperature is 301.03 K. The maximum temperature gradient observed between the TEG hot side and cold side is ΔT=113° C or K, which is 2.8 times greater than the hybrid CPVT-TEG system reported by Riahi et al. [22]. The experimental values of hot side temperature and cold side temperature are well-validated by the simulation results with a root mean square percent error of 1.0% and 1.30%, respectively. The thermal contact resistance generated by the presence of thermocouples in both between the TEG cold side and fluid channel, as well as between the TEG hot side and absorber clamp accounts for the differences between the experimental and simulated TEG temperatures. The optical losses caused by misalignment of the PTC can result in a lower temperature of TEG hot side in the measured results as compared to that of simulation results.

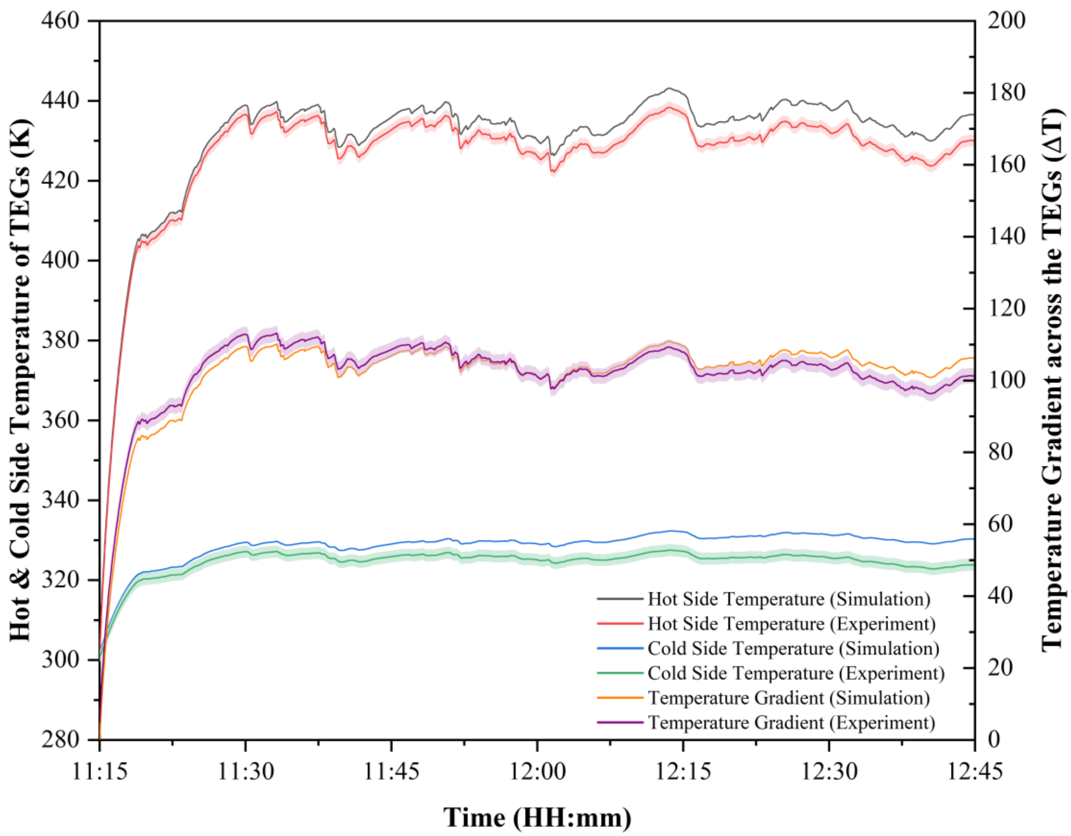

Fig. 17. Simulated and experimental variation of the hot and cold side temperature of TEGs.

6.3.2 Current and voltage of the TEGs

The variations in the measured current and voltage of the TEGs versus local clock time during the test period are depicted in Fig. 18. The experimental results demonstrate that both the measured voltage and current of TEGs are substantially correlated with the temperature gradient of the TEGs, with positive correlation coefficients of 0.99 and 0.98. As a result, more power is generated when the temperature differential across the TEGs is increased. The highest voltage and current detected in the TEGs during the experiment were 5.68 V and 0.63 A, respectively.

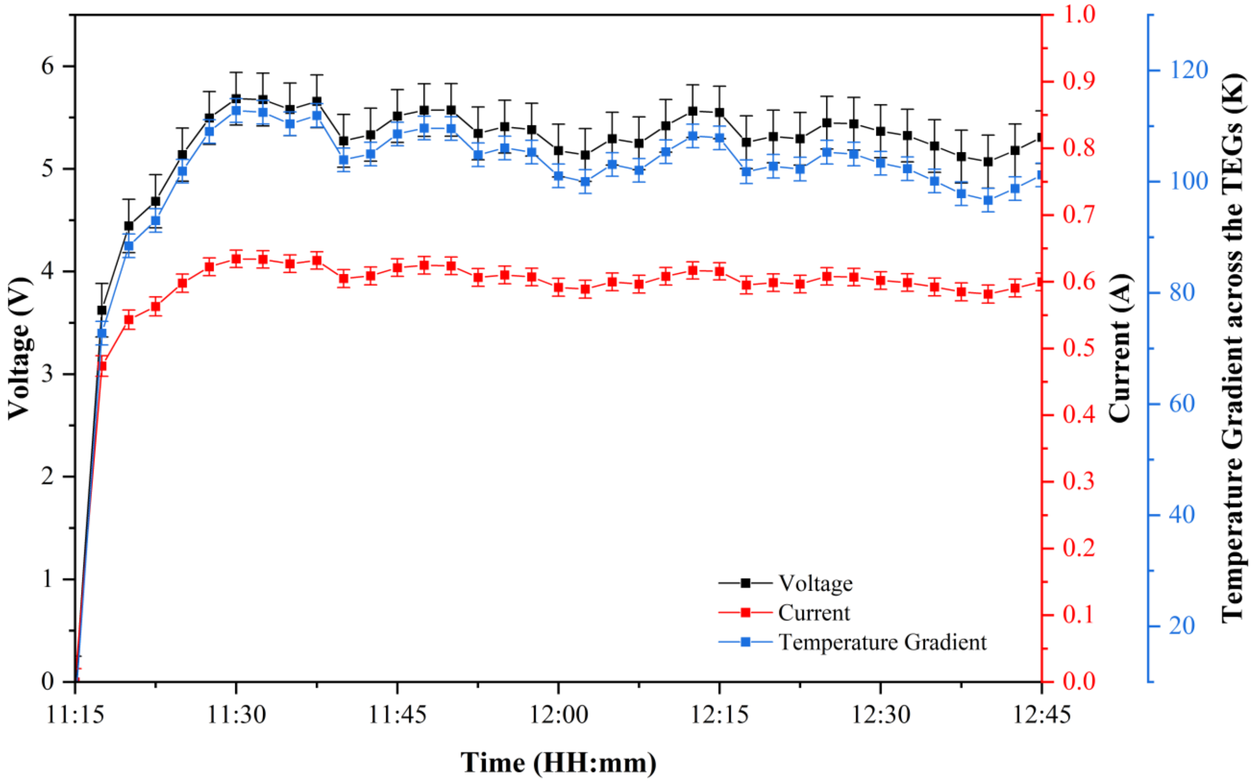

Fig. 18. Experimental variation of measured current and voltage of the TEGs during the test period.

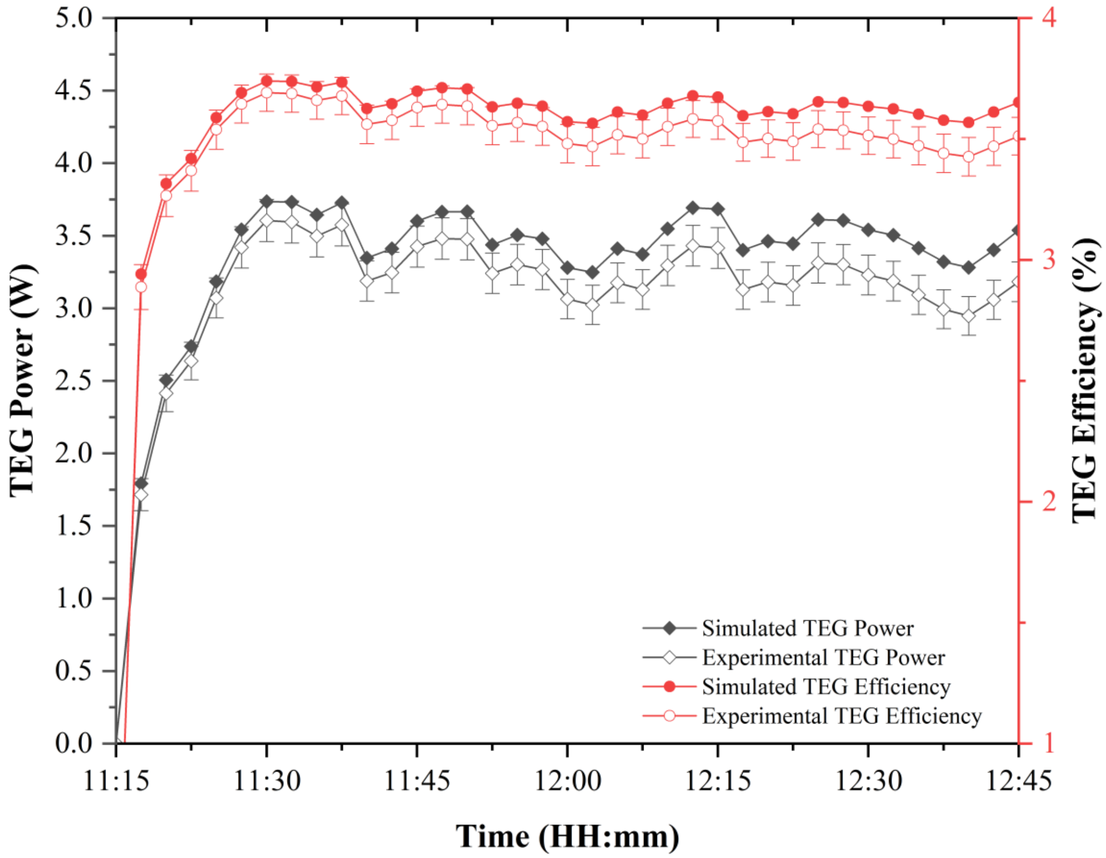

Fig. 19. Simulated and experimental results of TEG power and TEG efficiency during the test period.

As seen in Fig. 19, the TEG efficiency exhibits a similar pattern to the TEG output power. The greatest electrical efficiency of TEG attained through experiments is 3.69 %. The TEG efficiency achieved by transient numerical modelling is also depicted in Fig.19, and it was found to be in good agreement with the experimental data, with a root mean square percent deviation of 2.61%. The maximum TEG efficiency reported in a CPVT-STEG system by Abdo et al. [21] under a 20 sun concentration ratio is 3%, whereas the present hybrid system reached 3.69 % under a solar concentration ratio of 16.6 suns, which is 1.23 times higher.

6.4 Overall electrical and thermal performance of the CPVT-STEG prototype

The simulated and experimental variation of total electrical output power and electrical efficiency with the error bars are depicted in Fig. 20. There were no drastic changes in the net electric power or net electrical efficiency during the test period since the prototype was tracking the sun continuously. The maximum total power obtained during the experimentation is 26.76 W and the average total electrical power is 24.42 W. The maximum electrical efficiency of the hybrid system observed during the test period was 4.86%.

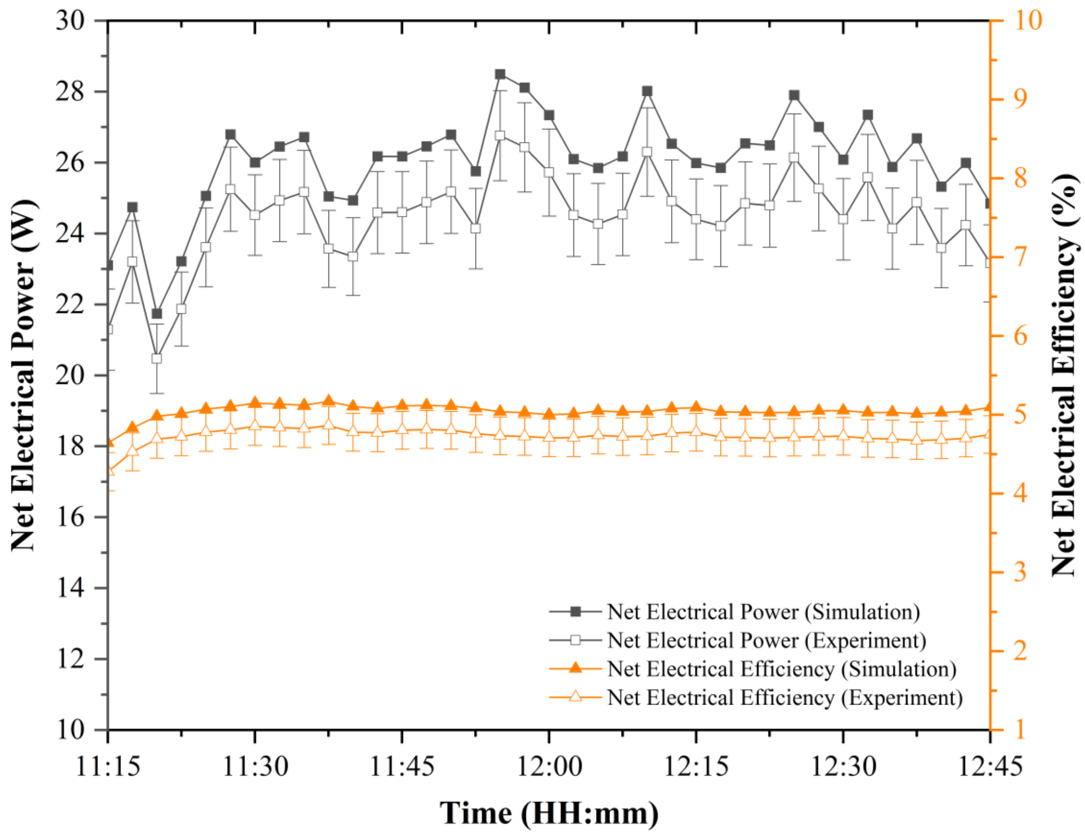

Fig. 20. Simulated and experimental values of overall power and efficiency of the CPVT-STEG prototype during the test period.

Fig. 21 illustrates the fluctuations in the water output temperature and thermal efficiency of the hybrid CPVT-STEG system across the test period with a mass flow rate of 0.0635 kg/s (3.8 L/min). The temperature of the water entering the hybrid system is critical in determining its thermal efficiency. Throughout the test period, the water inflow temperature ranged between 302.44 K and 305.99 K. The peak water temperature measured at the discharge is 306.65 K. Another critical component affecting the thermal efficiency of the system is the temperature rise of the water in the fluid channel. The highest temperature rise obtained in the outlet water is 0.76 K. The increase in water temperature was discovered to have a substantial positive correlation with thermal efficiency, with a correlation value of 0.91. The hybrid system achieved a maximum thermal efficiency of 40% when the solar irradiance is greater than or equal to 1000 W/m^2. The average thermal efficiency of the hybrid system over the course of the trial is about 33.7%. As seen in Fig. 20, the error range for the overall thermal efficiency is slightly larger because of the increased influence of the uncertainty in PT 1000 RTD in detecting the water temperature due to the short distance (540 mm) of the fluid channel. However, the figures of experimental thermal efficiency are corroborated well with the simulated values, with a root mean square percent error of 10.08%. The optical losses caused by slope error and misalignment error in the CPC and PTC also contribute to a lower experimental thermal efficiency as compared to that of the simulation findings.

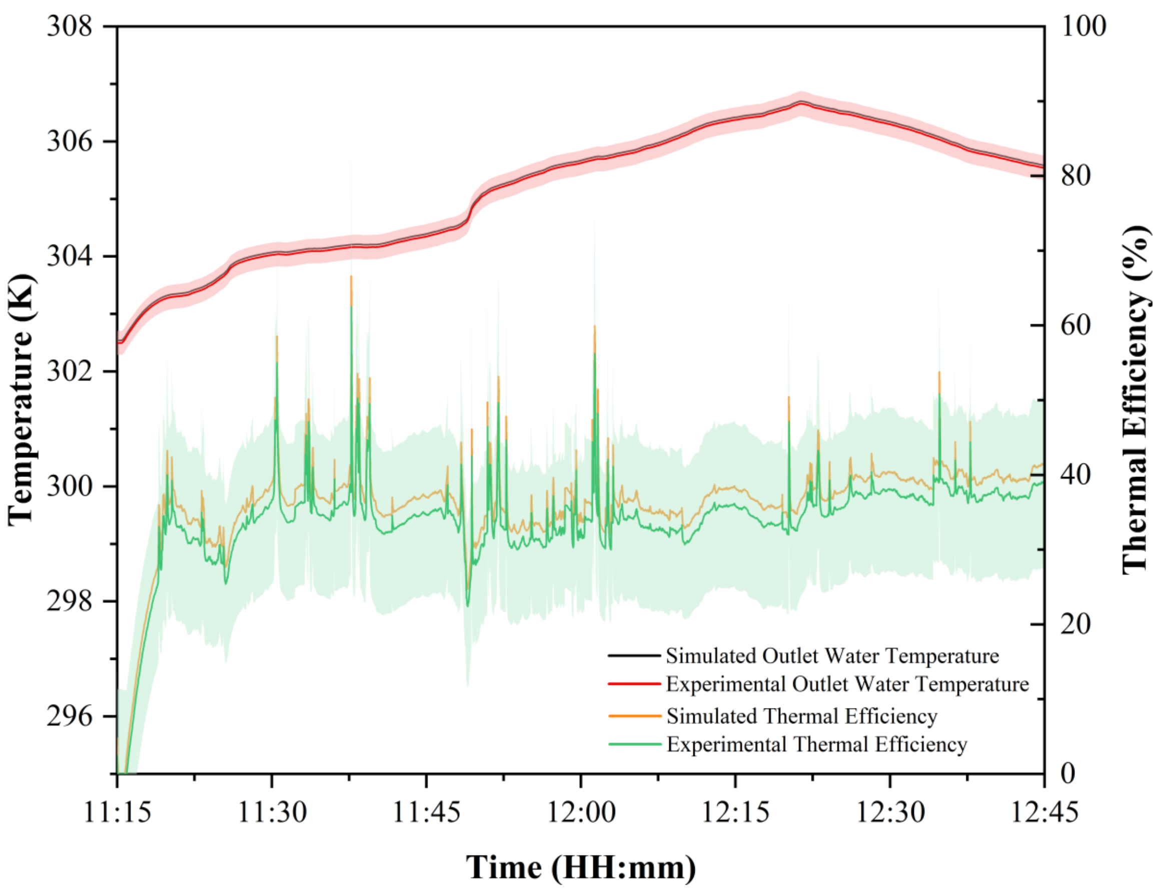

Fig. 21. Simulated and experimental values of water outlet temperature and thermal efficiency during the test period.

A performance comparison between the hybrid CPVT-STEG system and a standalone PV system was performed by considering a 0.51 m^2 mono-crystalline PV module (approx. 32 PV cells) comparable to the aperture area of the hybrid CPVT-STEG prototype. For a 1000 W/m^2 solar irradiance, a standalone PV of 0.51 m^2 area can provide a maximum electric power output of 78.69 W at an efficiency of 15.43% and reach a temperature of 334.4 K (assume: $NOCT = 318.15\ K$; $T_{amb} = 303.15\ K$). On the other hand, the overall power conversion efficiency of the developed hybrid prototype, including electrical and thermal output, is about 4.86% + 40%, which is 3 times higher compared to standalone PV.

The electrical efficiency of the hybrid CPVT-STEG system is 68.5% lower than the standalone PV system. The lower power conversion efficiency of the TEG (3.69%) and the PTC area that is used to focus the sunlight onto the TEG has greatly discounted the overall electrical efficiency of the hybrid system. Nevertheless, the benefits of the hybrid CPVT-STEG system over the standalone PV system are to provide an additional recovery of thermal energy and lower the PV temperature. Besides the direct focused sunlight, the TEG can also harvest the radiative heat from the surrounding environment. The choice between a standalone PV system and a hybrid CPVT-STEG system is determined completely by the specific needs of the application.

A comparison analysis between the developed CPVT-STEG prototype and a similar CPVT-TEG hybrid solar system that uses PTC and mono-crystalline silicon PV cells was performed. The hybrid CPVT-TEG system studied in [22] uses a PTC with a reflectivity 0.89, and the electrical efficiency is estimated as 7.27% if only DNI is considered in the input power. The maximum electrical output of the developed CPVT-STEG prototype can be normalized to 35.5 W at 0.89 reflectivity. The maximum electrical efficiency of the prototype by considering only the DNI (765 W/m^2) in the input is about 9.1% which shows the superiority of the developed CPVT-STEG hybrid system.

6.5 Exergy of the developed CPVT-STEG prototype

The exergy efficiency of the developed prototype during the test period is depicted in Fig. 22. The experimental effectiveness of exergy is between 4.37 % and 5.85 %. The average efficiency of exergy during the test period was found to be 5%. The low exergy efficiency is mostly owing to the small-scale experimental setup, which results in a lower rise in water temperature. Thus, in the case of a large-scale hybrid system with a longer fluid channel and an optimal fluid flow rate, the fluid temperature may be significantly increased, thereby increasing the exergy efficiency. Additionally, research demonstrates that both the numerical simulation and experimental data were well-validated, with a root mean square percent error of 6.3 %.

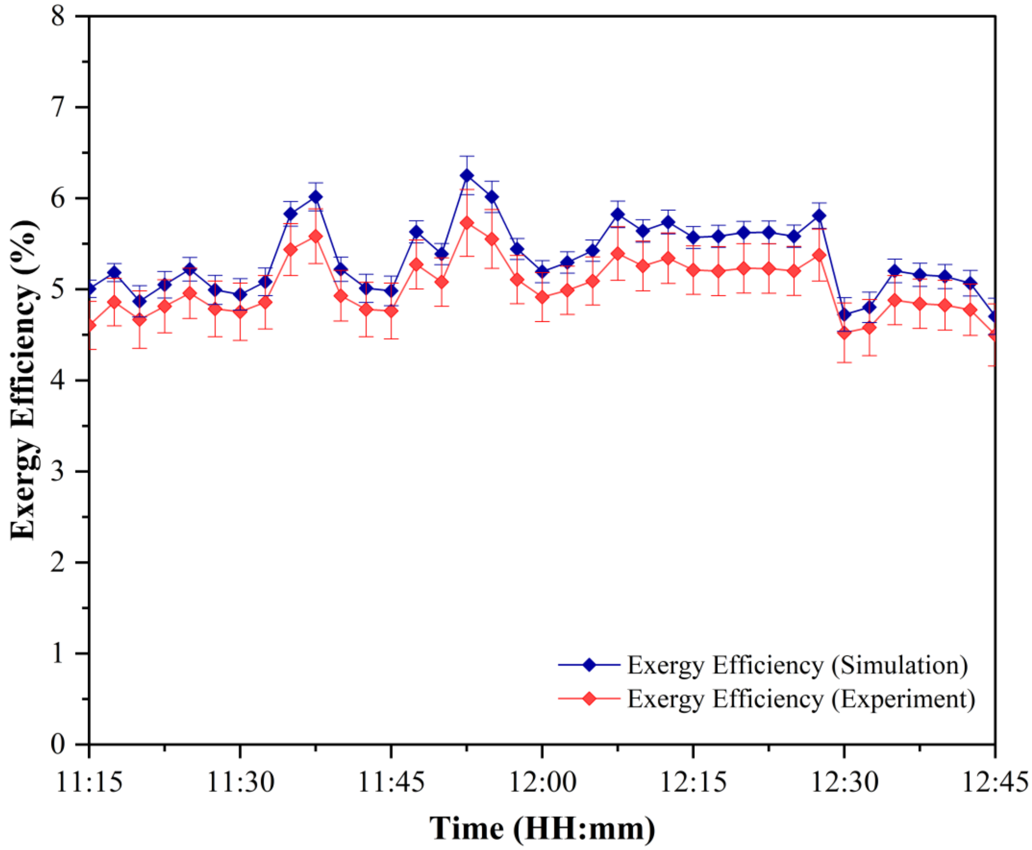

Fig. 22. Simulated and experimental variation of overall exergy efficiency during the test period.

6.6 Repeatability test

In order to ensure the performance repeatability of the developed prototype, the experiments have been repeated five times on different days during the noon time with good DNI and GHI values. Fig. 23 shows the variation in PV temperature, PV performance, TEG performance, and thermal performance measured for five different days with DNI ranging between 764.66 W/m^2 and 800.868 W/m^2. The graphs in Fig. 23 show that the successive measurements of the PV temperature, PV performance, TEG performance, and thermal efficiency are similar under the DNI values of 764.66 W/m^2 to 800.868 W/m^2, thus ensuring the repeatability of the experimental results.

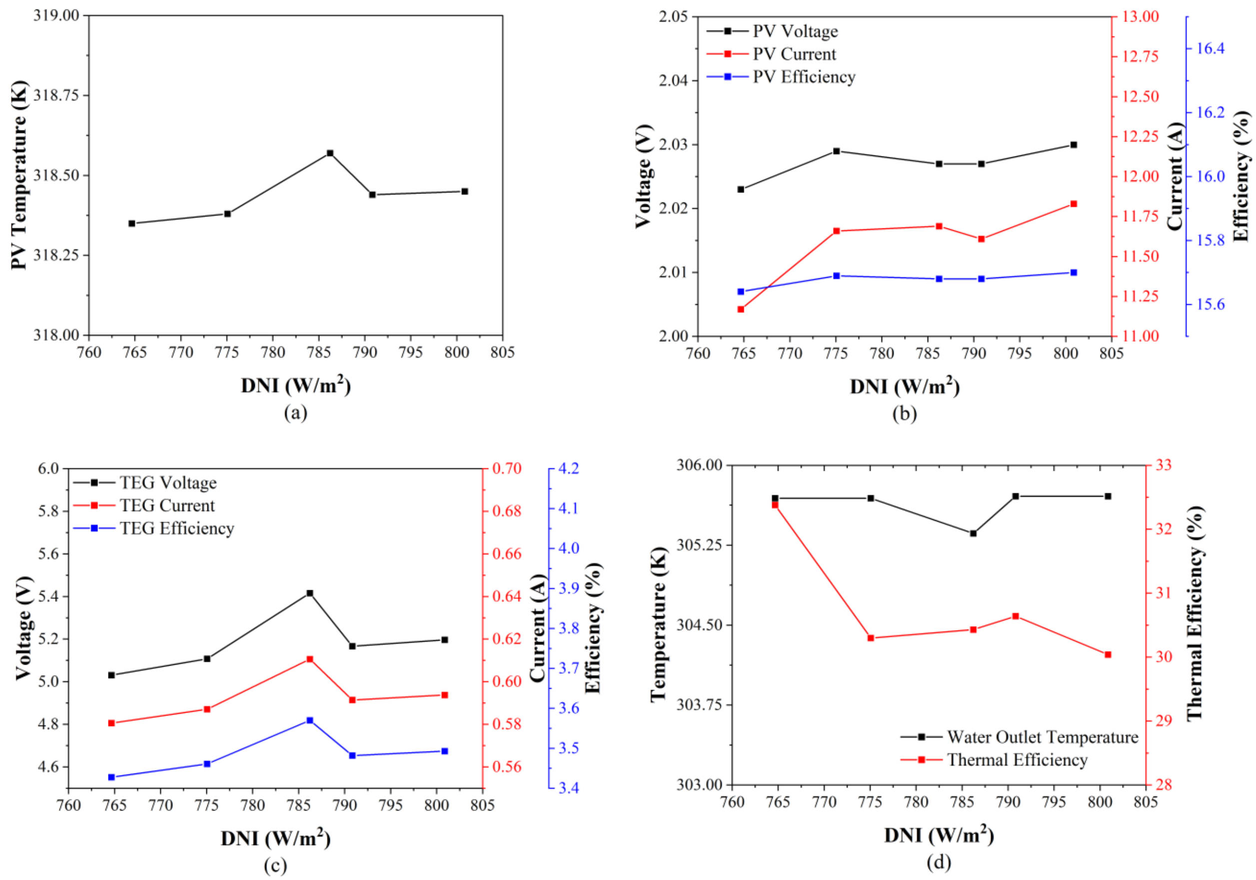

Fig. 23. The experimental results of the CPVT-STEG prototype under DNI from 764.66 W/m^2 to 800.868 W/m^2 for different days in the repeatability tests.

6.7 Environmental cost analysis

The environmental cost analysis in the present study has been done using carbon emissions and carbon pricing. The amount of mitigated carbon emissions during the test period is shown in Fig. 24. The environmental cost savings associated with avoiding CO_2 emissions were estimated using Eq. (15) as shown in Fig. 24. According to the experimentation results, the average CO_2 mitigation during the test period is 0.5 kg/h, and an average environmental cost savings of up to 0.025 €/h has been obtained.

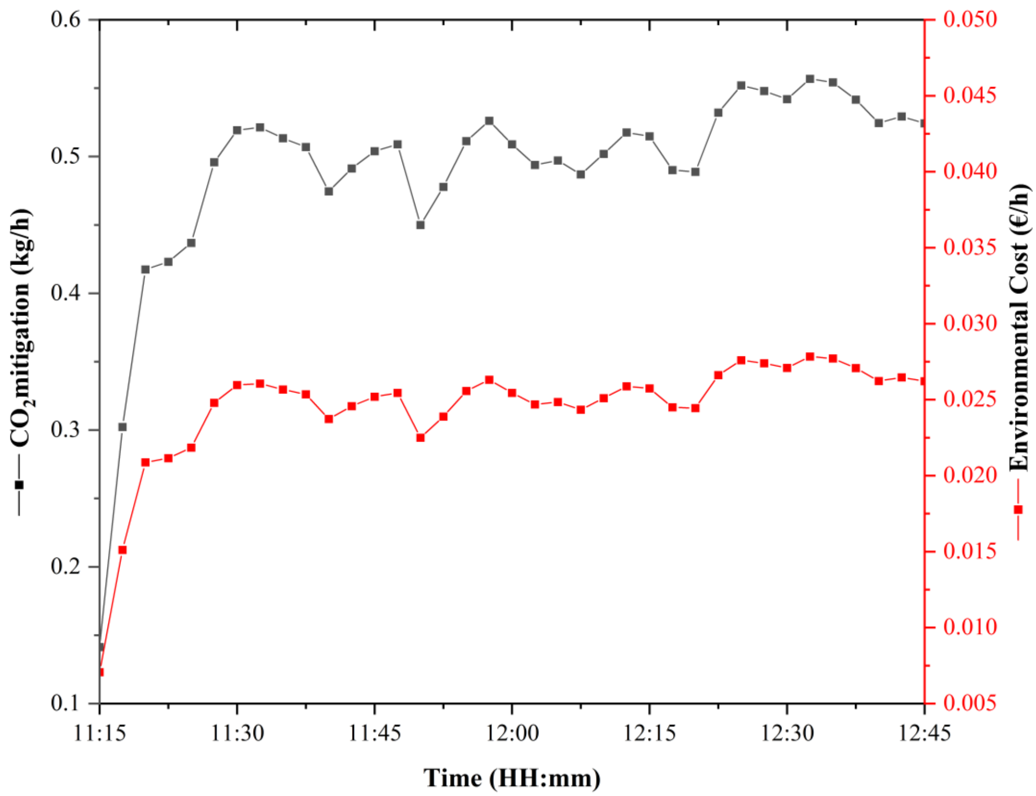

Figure 24. CO_2 reduction and environmental cost saving per hour

6.8 Challenges and Outlook

The efficiency of the developed CPVT-STEG hybrid system is limited by the reflectivity (67%) of the concentrator material used. The electrical and thermal efficiency can be further improved if a reflective material with a reflectivity of more than 90% is used. The electrical efficiency of the CPVT-STEG is also restricted by the number of TEG modules used and its lower efficiency. The optimal number of TEGs used for a maximum power output in a 540 mm long channel is two, and the remaining space is left insulated and unutilised. Hence, solar cells with higher efficiency can replace the TEGs on the rear side of the channel in the prototype to achieve higher overall electrical efficiency. The performance of the CPVT-STEG system can be further enhanced by optimising the design of fluid channels and using highly conductive heat transfer fluids.

In addition to the direct sunlight reflected by PTC, the TEG modules in the prototype can also harvest waste heat from other energy sources through radiation. It is possible if the prototype system is positioned at a geothermal site with hot steam from hot spring water, which can be explored in future work. The developed hybrid structure has the potential to remodel the existing PTC-based solar power plants as CPVT or hybrid CPVT-STEG systems to increase the power production per unit area. Finally, economic and environmental studies can be conducted to evaluate the commercial feasibility of the hybrid prototype. The viability of redesigning existing PTC-based solar power plants requires a comprehensive optimization and techno-economic study of the hybrid prototype.

7. Conclusion

In this research work, we have constructed the prototype of a CPC and PTC based hybrid CPVT-STEG system with an optimal quantity of TEG modules for a maximum TEG output. The performance of prototype was evaluated in terms of thermal and electrical efficiencies. The prototype was tested under outdoor operating conditions during a sunny day where the measured results were compared and validated with transient numerical simulation. The major findings of the experiment can be summarised as follows:

- The average PV temperature during the test period is 318.19 K which is 5.6% less than the PV temperature in the PTC based CPVT-TEG system studied by Riahi et al. [22].
- The maximum TEG efficiency of the hybrid system is 3.69% which is 1.23 times higher as compared with that of the CPVT-STEG system reported by Abdo et al. [21].
- The peak overall efficiency observed during experimentation is 44.86% which is 3 times higher as compared to that of standalone PV system.
- The average exergy efficiency of the hybrid CPVT-STEG prototype during the test period was found to be 5%.
- The proposed hybrid system can reduce carbon emissions by 0.5 kg/h with an associated environmental cost of 0.025 €/h, and thus the idea can contribute to the United Nations Sustainable Development Goals.

Acknowledgement

The authors would like to express gratitude to the Taylor's University Flagship Research Grant (TUFR/2017/001/01) and the Taylor's PhD. Scholarship Program for their support. This research was funded in part by the Fundamental Research Grant Scheme (FRGS/1/2019/TK10/TAYLOR/02/1) from the Ministry of Higher Education, Government of Malaysia.

References

[1] A. Zahedi, Review of modelling details in relation to low-concentration solar concentrating photovoltaic, Renew. Sustain. Energy Rev. 15 (2011) 1609–1614. doi:10.1016/j.rser.2010.11.051.

[2] E. Skoplaki, J.A. Palyvos, Operating temperature of photovoltaic modules: A survey of pertinent correlations, Renew. Energy. 34 (2009) 23–29. doi:10.1016/j.renene.2008.04.009.

[3] S. Manikandan, C. Selvam, N. Poddar, K. Pranjyal, R. Lamba, S.C. Kaushik, Thermal management of low concentrated photovoltaic module with phase change material, J. Clean. Prod. 219 (2019) 359–367. doi:10.1016/j.jclepro.2019.02.086.

[4] O.Z. Sharaf, M.F. Orhan, Concentrated photovoltaic thermal (CPVT) solar collector systems: Part I - Fundamentals, design considerations and current technologies, Renew. Sustain. Energy Rev. 50 (2015) 1500–1565. doi:10.1016/j.rser.2015.05.036.

[5] S. Sripadmanabhan Indira, C.A. Vaithilingam, K.K. Chong, R. Saidur, M. Faizal, S. Abubakar, S. Paiman, A review on various configurations of hybrid concentrator photovoltaic and thermoelectric generator system, Sol. Energy. 201 (2020) 122–148. doi:10.1016/j.solener.2020.02.090.

[6] S. Shittu, G. Li, Y.G. Akhlaghi, X. Ma, X. Zhao, E. Ayodele, Advancements in thermoelectric generators for enhanced hybrid photovoltaic system performance, Renew. Sustain. Energy Rev. 109 (2019) 24–54. doi:10.1016/j.rser.2019.04.023.

[7] C. Babu, P. Ponnambalam, The role of thermoelectric generators in the hybrid PV/T

systems: A review, Energy Convers. Manag. 151 (2017) 368–385. doi:10.1016/j.enconman.2017.08.060.

[8] R. Bjørk, K.K. Nielsen, The performance of a combined solar photovoltaic (PV) and thermoelectric generator (TEG) system, Sol. Energy. 120 (2015) 187–194. doi:10.1016/j.solener.2015.07.035.

[9] T. Cui, Y. Xuan, Q. Li, Design of a novel concentrating photovoltaic-thermoelectric system incorporated with phase change materials, Energy Convers. Manag. 112 (2016) 49–60. doi:10.1016/j.enconman.2016.01.008.

[10] A. Rezania, D. Sera, L.A. Rosendahl, Coupled thermal model of photovoltaic-thermoelectric hybrid panel for sample cities in Europe, Renew. Energy. 99 (2016) 127–135. doi:10.1016/j.renene.2016.06.045.

[11] W. Lin, T.M. Shih, J.C. Zheng, Y. Zhang, J. Chen, Coupling of temperatures and power outputs in hybrid photovoltaic and thermoelectric modules, Int. J. Heat Mass Transf. 74 (2014) 121–127. doi:10.1016/j.ijheatmasstransfer.2014.02.075.

[12] E. Yin, Q. Li, Y. Xuan, Thermal resistance analysis and optimization of photovoltaic-thermoelectric hybrid system, Energy Convers. Manag. 143 (2017) 188–202. doi:10.1016/j.enconman.2017.04.004.

[13] S. Su, T. Liu, Y. Wang, X. Chen, J. Wang, J. Chen, Performance optimization analyses and parametric design criteria of a dye-sensitized solar cell thermoelectric hybrid device, Appl. Energy. 120 (2014) 16–22. doi:10.1016/j.apenergy.2014.01.048.

[14] T. Cui, Y. Xuan, E. Yin, Q. Li, D. Li, Experimental investigation on potential of a concentrated photovoltaic-thermoelectric system with phase change materials, Energy. 122 (2017) 94–102. doi:10.1016/j.energy.2017.01.087.

[15] E. Yin, Q. Li, D. Li, Y. Xuan, Experimental investigation on effects of thermal resistances on a photovoltaic-thermoelectric system integrated with phase change materials, Energy. 169 (2019) 172–185. doi:10.1016/j.energy.2018.12.035.

[16] J. Zhang, H. Zhai, Z. Wu, Y. Wang, H. Xie, M. Zhang, Enhanced performance of photovoltaic–thermoelectric coupling devices with thermal interface materials, Energy

Rep. 6 (2020) 116–122. doi:10.1016/j.egyr.2019.12.001.

[17] A. Lekbir, S. Hassani, M.R. Ab Ghani, C.K. Gan, S. Mekhilef, R. Saidur, Improved energy conversion performance of a novel design of concentrated photovoltaic system combined with thermoelectric generator with advance cooling system, Energy Convers. Manag. 177 (2018) 19–29. doi:10.1016/j.enconman.2018.09.053.

[18] S. Soltani, A. Kasaeian, T. Sokhansefat, M.B. Shafii, Performance investigation of a hybrid photovoltaic/thermoelectric system integrated with parabolic trough collector, Energy Convers. Manag. 159 (2018) 371–380. doi:10.1016/j.enconman.2017.12.091.

[19] M. Mohsenzadeh, M.B. Shafii, H. Jafari mosleh, A novel concentrating photovoltaic/thermal solar system combined with thermoelectric module in an integrated design, Renew. Energy. 113 (2017) 822–834. doi:10.1016/j.renene.2017.06.047.

[20] E. Yin, Q. Li, Y. Xuan, Experimental optimization of operating conditions for concentrating photovoltaic-thermoelectric hybrid system, J. Power Sources. 422 (2019) 25–32. doi:10.1016/j.jpowsour.2019.03.034.

[21] A. Abdo, S. Ookawara, M. Ahmed, Performance evaluation of a new design of concentrator photovoltaic and solar thermoelectric generator hybrid system, Energy Convers. Manag. 195 (2019) 1382–1401. doi:10.1016/j.enconman.2019.04.093.

[22] A. Riahi, A. Ben Haj Ali, A. Fadhel, A. Guizani, M. Balghouthi, Performance investigation of a concentrating photovoltaic thermal hybrid solar system combined with thermoelectric generators, Energy Convers. Manag. 205 (2020). doi:10.1016/j.enconman.2019.112377.

[23] S. Shittu, G. Li, X. Zhao, X. Ma, Y.G. Akhlaghi, Y. Fan, Comprehensive study and optimization of concentrated photovoltaic-thermoelectric considering all contact resistances, Energy Convers. Manag. 205 (2020) 112422. doi:10.1016/j.enconman.2019.112422.

[24] O. Rejeb, S. Shittu, C. Ghenai, G. Li, X. Zhao, M. Bettayeb, Optimization and performance analysis of a solar concentrated photovoltaic-thermoelectric (CPV-TE) hybrid system, Renew. Energy. 152 (2020) 1342–1353. doi:10.1016/j.renene.2020.02.007.

[25] S. Sripadmanabhan Indira, C.A. Vaithilingam, R. Sivasubramanian, K.K. Chong, R. Saidur, K. Narasingamurthi, Optical performance of a hybrid compound parabolic concentrator and parabolic trough concentrator system for dual concentration, Sustain. Energy Technol. Assessments. 47 (2021) 101538. doi:10.1016/j.seta.2021.101538.

[26] S. Sripadmanabhan Indira, C.A. Vaithilingam, K. Narasingamurthi, R. Sivasubramanian, K.-K. Chong, R. Saidur, Mathematical modelling , performance evaluation and exergy analysis of a hybrid photovoltaic / thermal-solar thermoelectric system integrated with compound parabolic concentrator and parabolic trough concentrator, Appl. Energy. 320 (2022) 119294. doi:10.1016/j.apenergy.2022.119294.

[27] J. Macedo-Valencia, J. Ramírez-Ávila, R. Acosta, O.A. Jaramillo, J.O. Aguilar, Design, construction and evaluation of parabolic trough collector as demonstrative prototype, Energy Procedia. 57 (2014) 989–998. doi:10.1016/j.egypro.2014.10.082.

[28] D. Yadav, P. Azad, R. Vaish, Solar Energy Harvesting using Candle- Soot- Coated Thermoelectric Materials, Glob. Challenges. 4 (2020) 1900080. doi:10.1002/gch2.201900080.

[29] K.K. Chong, T.K. Yew, C.W. Wong, M.H. Tan, W.C. Tan, B.H. Lim, Dense-array concentrator photovoltaic prototype using non-imaging dish concentrator and an array of cross compound parabolic concentrators, Appl. Energy. 204 (2017) 898–911. doi:10.1016/j.apenergy.2017.03.108.

[30] A. Montecucco, J. Siviter, A.R. Knox, The effect of temperature mismatch on thermoelectric generators electrically connected in series and parallel, Appl. Energy. 123 (2014) 47–54. doi:10.1016/j.apenergy.2014.02.030.

[31] N.A. Bakhari, N.A. Hamid, A.R. Syafeeza, Y.C. Wong, M. Ibrahim, Simulation and analysis of flexible TEG using polymer based and pyroelectric material for microdevice energy harvesting, J. Phys. Conf. Ser. 1502 (2020). doi:10.1088/1742-6596/1502/1/012022.

[32] C. Haiping, L. Haowen, Z. Heng, L. Kai, G. Xinxin, Y. Boran, Numerical simulation and experimental analysis of an LCPV/T system under real operating conditions, J. Clean.

Prod. 209 (2019) 903–915. doi:10.1016/j.jclepro.2018.10.256.

[33] M. Valizadeh, F. Sarhaddi, Mahdavi Adeli, Exergy performance assessment of a linear parabolic trough photovoltaic thermal collector, Renew. Energy. 138 (2019) 1028–1041. doi:10.1016/j.renene.2019.02.039.

[34] S. Zuhur, İ. Ceylan, A. Ergün, Energy, exergy and environmental impact analysis of concentrated PV/cooling system in Turkey, Sol. Energy. 180 (2019) 567–574. doi:10.1016/j.solener.2019.01.060.

[35] N. Gakkhar, M.K. Soni, S. Jakhar, Experimental and theoretical analysis of hybrid concentrated photovoltaic/thermal system using parabolic trough collector, Appl. Therm. Eng. 171 (2020) 115069. doi:10.1016/j.applthermaleng.2020.115069.

[36] R. Tripathi, G.N. Tiwari, V.K. Dwivedi, Overall energy, exergy and carbon credit analysis of N partially covered Photovoltaic Thermal (PVT) concentrating collector connected in series, Sol. Energy. 136 (2016) 260–267. doi:10.1016/j.solener.2016.07.002.

[37] I. Ceylan, A.E. Gürel, A. Ergün, A. Tabak, Performance analysis of a concentrated photovoltaic and thermal system, Sol. Energy. 129 (2016) 217–223. doi:10.1016/j.solener.2016.02.010.

[38] Value of Carbon Market Update 2021, Carbon Credit Cap. (n.d.). https://carboncreditcapital.com/value-of-carbon-market-update-2021-2/ (accessed March 6, 2022).

Declaration of interests

☒ The authors declare that they have no known competing financial interests or personal relationships that could have appeared to influence the work reported in this paper.

☐The authors declare the following financial interests/personal relationships which may be considered as potential competing interests:

Credit Author Statement:

Sridhar Sripadmanabhan Indira: Conceptualization, Methodology, Investigation, Software, Formal Analysis, Validation, Visualization, Writing – Original Draft.: **Chockalingam Aravind Vaithilingam:** Formal Analysis, Writing – Review and Editing, Supervision.: **Ramsundar Sivasubramanian:** Investigation, Writing – Review & Editing.: **Kok-Keong Chong:** Writing – Review & Editing.: **Kulasekharan Narasingamurthi:** Software, Writing – Review & Editing.: **R. Saidur:** Writing – Review & Editing, Supervision.